



Norwegian University of
Science and Technology

Bearing Capacity Analysis Over Mudmat Foundations Under Multidimensional Loading

GHAZALEH HERAVI

Geotechnics and Geohazards

Submission date: July 2018

Supervisor: Gudmund Reidar Eiksund, IBM

Co-supervisor: Seyed Ali Ghoreishian Amiri, IBM

Norwegian University of Science and Technology
Department of Civil and Environmental Engineering

GHAZALEH HERAVI

Bearing Capacity Analysis Over Mudmat Foundations Under Multidimensional Loading

Trondheim, July 2018

PROJECT THESIS: TBA4510

Main supervisor: Professor Gudmund Reidar Eiksund, IBM

Co-supervisor: Dr. Seyed Ali Ghoreishian Amiri, IBM

Department of Civil and Transport Engineering

Norwegian University of Science and Technology (NTNU)



NTNU – Trondheim
Norwegian University of
Science and Technology



Report Title: Bearing Capacity Analysis Over Mudmat Foundations Under Multidimensional Loading	Dato: 11.07.2018
	Number of pages(Including Appendix): 106
	Master Thesis x
Name: GHAZALEH HERAVI	
Professor in charge/supervisor: Professor Gudmund Reidar Eiksund, IBM	
Other external professional contacts/supervisors: Dr. Seyed Ali Ghoreishian Amiri, IBM	

Abstract:

The ultimate bearing capacity is at its maximum when the foundation is under pure vertical loading. In the field, pure vertical loading is the least likely load combination to happen but, it is mostly combined loading condition applying on a foundation which causes a bearing capacity reduction. The offshore condition is where a structure faces more various load combination of vertical, horizontal and moment loads in different directions. This report determines the ultimate bearing capacity for different load combinations by using PLAXIS 3D which is a finite element(FE) software. Also, several hand calculations based on a method proposed by DNV is executed. The main idea of this thesis is to compare the results of analyses from PLAXIS or hand calculation. The foundation is a rectangular mudmat foundation. It has outer skirts embedded for one meter in the soil and no inner skirts are modelled. The soil is assumed as soft clay which has its shear strength increasing with depth. The foundation plates are set elastic and rigid, so it won't fail under loading. Knowing that the plates and soil have interactions, so the interfaces are fully bounded therefore there will be no gap between the plate and soil due to loads on it. The transiently uplifting loads could be resisted by negative pore pressure due to the gap and it might compromise the assumption of untrained condition assumed in this case study. The vertical bearing capacity of mudmat foundation resulted from PLAXIS 3D and hand calculation with the DNV method with a good approximation is the same. However, the horizontal bearing capacity differs slightly which seems to be due to the meshing system on PLAXIS which would lead to a more accurate answer if the mesh is finer. Also, assumption of roughness ratio as zero on hand calculation could be another reason. Second reason could be that PLAXIS 3D is modelling a three-dimensional environment while DNV method is based on a review through Hansen and Davis & Booker methods which are plane strain methods. Analysing the model on PLAXIS is time taking. Having a proper computer with high analysing properties is a must to work in 3D environment. Generally, the results from FE software are more accurate when it is generated by elements which are smaller in length but more in number. The assumption for hand calculation was not to have any tension loading though PLAXIS involves tension in the calculation. It is possible to use tension cut-off option on PLAXIS model as well. The model presented in this paper is having this condition to have comparable results. Hence, the failure path for moment loading in hand calculation and FEM results are expected to match. The results are closer when the moment is acting on the shorter edge than the longer one which is because of some forces on the 3D environment having influence on the results which are not seen in hand calculation. Further studies over torsional and cyclic loading is recommended.

Keywords:

1. Bearing Capacity
2. Mudmat Foundations
3. Offshore
4.

Preface

This report is written as a Master Thesis at the Norwegian University of Science and Technology as part of the MSc in Geotechnics and Geohazards, it was carried out during spring semester of 2018. The idea for this project was brought up by the geotechnical group at NTNU.

The subject of this master thesis is bearing capacity analysis of mudmat foundations under multidimensional loading. The aim is to analysis a mudmat foundation with specific area as a case study under different loading with two different ways, hand calculation and finite element analysing for which PLAXIS 3D Foundations is chosen.

Trondheim, 2018-07-11

Ghazaleh Heravi

Acknowledgment

My appreciation goes all to my main supervisor *Professor Gudmund R. Eiksund* for his time donation and having an door open which made it more easy to ask for advice. Going through the road contained my weakness subjects was not possible with out his help.

I would like to thank my co-supervisor *Seyed Ali Ghoreishian Amiri* for being a great motivator and giving advices even outside office hours.

I want to thank *Professor Steinar Nordal* for his helpful advices and helps through along the way specially his helps with *PLAXIS 3D* and its difficulties.

Last, but not the least, huge gratitude is to my co-students at my office. We shared joy and laugh and gave motivation to each other. Working with this master thesis would not be the same with out them, with their motivational energy and invaluable academic supports.

Gh.H.

Abstract

The ultimate bearing capacity is at its maximum when the foundation is under pure vertical loading. In the field, pure vertical loading is the least likely load combination to happen but, it is mostly combined loading condition applying on a foundation which causes a bearing capacity reduction. The offshore condition is where a structure faces more various load combination of vertical, horizontal and moment loads in different directions.

This report determines the ultimate bearing capacity for different load combinations by using *PLAXIS 3D* which is a finite element(FE) software. Also, several hand calculations based on a method proposed by *DNV* is executed. The main idea of this thesis is to compare the results of analyses from *PLAXIS* or hand calculation.

The foundation is a rectangular mudmat foundation. It has outer skirts embedded for one meter in the soil and no inner skirts are modelled. The soil is assumed as soft clay which has its shear strength increasing with depth. The foundation plates are set elastic and rigid, so it won't fail under loading. Knowing that the plates and soil have interactions, so the interfaces are fully bounded therefore there will be no gap between the plate and soil due to loads on it. The transiently uplifting loads could be resisted by negative pore pressure due to the gap and it might compromise the assumption of untrained condition assumed in this case study.

The vertical bearing capacity of mudmat foundation resulted from *PLAXIS 3D* and hand calculation with the *DNV* method with a good approximation is the same. However, the horizontal bearing capacity differs slightly which seems to be due to the meshing system on *PLAXIS* which would lead to a more accurate answer if the mesh is finer. Also, assumption of roughness ratio as zero on hand calculation could be another reason. Second reason could be that *PLAXIS 3D* is modelling a three-dimensional environment while *DNV* method is based on a review through *Hansen* and *Davis & Booker* methods which are plane strain methods.

Analysing the model on *PLAXIS* is time taking. Having a proper computer with high analysing properties is a must to work in 3D environment. Generally, the results from FE software are more accurate when it is generated by elements which are smaller in length but more in number.

The assumption for hand calculation was not to have any tension loading though *PLAXIS* involves tension in the calculation. It is possible to use tension cut-off option on *PLAXIS* model as well. The model presented in this paper is having this condition to have comparable results. Hence, the failure path for moment loading in hand calculation and FEM results are expected

to match. The results are closer when the moment is acting on the shorter edge than the longer one which is because of some forces on the 3D environment having the influence on the results which are not seen in hand calculation. Further studies over torsional and cyclic loading are recommended.

Contents

Preface	i
Acknowledgment	ii
summary	iii
1 Introduction	4
1.1 Background	4
1.2 Objectives	6
1.3 Limitations	6
1.4 Approach	7
1.5 Structure of the Report	7
2 Literature Review	8
2.1 Offshore Geotechnics	8
2.1.1 Soil Condition	8
2.2 Mudmat Foundations	11
2.2.1 Analysis	11
2.2.2 Installation	12
2.3 Bearing Capacity	13
2.3.1 Method Selection Effect	15
2.3.2 Skirts Effect	18
2.3.3 Interfaces Effect	19
2.3.4 Perforation Effect	19
2.3.5 Load Combination	20
2.4 Finite Element Method Modeling	20

3	Introduction of the Case Study	24
3.1	Geometry	24
3.2	Material Properties	25
3.3	Interfaces	26
4	Hand Calculation	27
4.1	Introduction	27
4.2	Methodology	27
4.3	Load Combination	33
5	FEA Model and Results	35
5.1	Introduction	35
5.2	Meshing System	36
5.3	Model Verification	38
6	Results & Discussion of The Analysis	40
6.1	Vertical and Horizontal Loading	40
6.2	Vertical and Moment Loading	42
6.3	Vertical, Horizontal and Moment Loading	44
7	Summary	47
7.1	Summary and Conclusions	47
7.2	Recommendations for Further Work	48
	Bibliography	50
A	Table of Symbols and Acronyms	54
B	Hand Calculation Results	58
B.1	Introduction	58
B.1.1	Results	58
C	Computer Simulation	66
C.1	Introduction	66
C.1.1	Results	67

C.1.2 Failure Mechanisms	71
C.1.3 Calculations Details	82
C.1.4 Torsion Loading Results	89

MASTER DEGREE THESIS

Spring 2018
for

Student: Ghazaleh Heravi

Bearing Capacity Analysis Over Mudmat Foundations Under Multidimensional Loading

BACKGROUND

Offshore geotechnics is about any construction in the sea including foundations and structures which could be for oil and gas stations, wind farms, submarine pipelines or artificial islands. Offshore structures tend to be tall often more than 100 meters high and are under many various sources of lateral loads such as moment due to the structure load. Structures are also built on a soil with an unusual condition on which investigation is expensive.

Offshore structures design life is expected to be maximum 50 years for which ultimate limit state designing method is mostly used if any failure may cause high financial and environmental consequences. The sedimentary soil, which is mostly considered in the saturated condition, might be under-consolidated due to high sedimentation, normally consolidated because of the sediments deposition has a slow trend, or in less deep water it can be over-consolidated due to previously placed glaciers.

Active faults, landslides, tsunamis or the layered soil nature are some of the many possible geohazards that may happen in an offshore designing and each structure should be monitored for potential geohazards.

On offshore engineering one of the most commonly used foundations are skirted shallow foundations.

Mudmat foundations are a member of shallow foundations category widely used for deep-water offshore structures such as oil and gas stations.

Offshore condition brings diverse types of loading on the structure. A three-dimensional approaching is one of the most recent ways to deal with these conditions especially since 3D FE software are rapidly improving.

Commonly used designing methods are adapted to be applied for horizontal or moment loads, though more concentrated on vertical bearing capacity such as Classification Note for foundations No.30.4 by DNV.

Many methods such as Hansen and Meyerhof methods, introduce some factors regarding shape, the inclination of the load or if there is any eccentricity, to include the affection of the three-dimensional loading.

Many studies have been done for condition with vertical(V), horizontal(H) and moment(M) load combination. This thesis is based on an idea of comparing DNV method and PLAXIS 3D results.

TASK

The first step was to read through literature and learn about the method of hand calculation and start it afterwards. Presenting the results of hand calculation is second step. Afterwards, learning PLAXIS 3D, reading through its references manual, establishing the model, assigning different load combination and presenting the results.

Comparing the results and discuss them was the final part of analysing.

Objective and purpose

The main objectives of this project are

- A general literature review thought different designing methods, criteria and parameters which have affection on the design of a mudmat foundation.
- Introducing a model of mudmat foundation over a soft clay on offshore condition.
- Doing several hand calculations for different load combinations and finding the maximum possible loading and ultimate bearing capacity.
- Establishing a PLAXIS 3D model for the introduced model and running it for different load combinations under which hand calculation is done.
- Discussing the results form hand calculation and PLAXIS 3D modelling.

Professor in charge:

Prof. Gudmund Reidar Eiksund

Department of Civil and Transport Engineering, NTNU

Date: 11.07.2018,



Professor in charge (signature)

Chapter 1

Introduction

1.1 Background

Offshore geotechnics is covering any construction in the sea including foundations and structures. Offshore structures could be built for oil and gas stations, wind farms, submarine pipelines or artificial islands. These structures tend to be tall often more than 100 meters high and are under many various sources of lateral loads such as moment due to the structure load. Structures are also built on a soil with an unusual condition on which investigations are expensive. [Randolph et al. \(2011\)](#)

Offshore structures design life is expected to be maximum 50 years and ultimate limit state designing method is mostly used because any failure may cause high financial and environmental consequences. [Randolph et al. \(2011\)](#)

Offshore soil is mostly assumed to be sedimentary. The soil can be under-consolidated due to high sedimentation, normally consolidated because of the sediments deposition has a slow trend, or in less deep water it can be overconsolidated due to previously placed glaciers [Randolph et al. \(2011\)](#).

Active faults, landslides, tsunamis or the layered soil nature are some of the many possible geohazards that may happen in an offshore environment. Each structure should be monitored for potential geohazards [Randolph et al. \(2011\)](#).

On offshore engineering one of the most commonly used foundations are skirted shallow foundations [Yun and Bransby \(2007\)](#). Mudmat foundations belong to shallow foundations category which are widely used for deep-water offshore structures.

Offshore condition brings many diverse types of loading on the structure. A three-dimensional approaching is one of the most recent ways to deal with these conditions and three-dimensional Finite Element (FE) software are rapidly improving.

Commonly used designing methods such as [DNV \(2010\)](#); [DNV. \(1992\)](#) are adapted to be applied for horizontal or moment loads. Though these methods are more concentrated on vertical bearing capacity. Many methods such as [Hansen \(1970\)](#) and [Meyerhof \(1953\)](#) consider some factors regarding shape, the inclination of the load or if there is any eccentricity, to include the affection of the three-dimensional loading.

Bearing capacity of a foundation is maximum with pure vertical loading. Having different load combinations reduce it and that is the reason for doing this project. Many studies have been done for condition with vertical(V), horizontal(H) and moment(M) load combination such as [Houlsby and Puzrin \(1999\)](#) and [Bransby and Yun \(2009\)](#) yet, there is space for more studies over this subject.

Literature Survey

Through this thesis, many books and papers are presented. The main method is borrowed from [DNV. \(1992\)](#) and the standards are mostly checked using ([DNV, 2010](#)). To understand the different methods [Bowles et al. \(1996\)](#) is a good recourse. The [Hansen \(1970\)](#), [Meyerhof \(1953\)](#) and [Davis et al. \(1985\)](#) were the next papers to check. Reading through these methods helped to a better understanding [DNV. \(1992\)](#) method. Doing hand calculation was mostly based on this method.

PLAXIS 3D is a software based on the finite element analysis (FEA). It provides a three-dimensional space to do modelling. *PLAXIS* has a big family of FEM software. The *PLAXIS 3D Foundation* version 2017 is what is used in this report to Work on bearing capacity on the mudmat foundation . To get to learn 3D modelling on *PLAXIS*, its manual reference by [PLAXIS \(2017\)](#) is reviewed and used.

Offshore environment has many different loads. Loads on a structure could be a combination of vertical and horizontal loads with eccentricity in different directions causing moments. Cyclic loads are a plus. These loads have various resources and their nature differ. Therefore, load combination studies have been done many times such as [Mana et al. \(2012b\)](#); [Dunne \(2015\)](#);

[Gourvenec and Barnett \(2011\)](#); [Watson et al. \(2000\)](#); [Andersen et al. \(1999\)](#); [Dyvik et al. \(1993\)](#) to which it is recommended to refer.

Chapter 2 is presenting a general overview through different papers and presents the basis of different methods.

1.2 Objectives

The main objectives of this project are:

1. A general literature review through different designing methods, criteria and parameters which have affection on the design of a mudmat foundation.
2. Introducing a model of mudmat foundation over soft clay on the offshore condition.
3. Doing hand calculation for different load combinations to find the ultimate bearing capacity.
4. Establishing the PLAXIS 3D model for the introduced model and analysing it for different load combinations under which hand calculation is done.
5. Discussing the results form hand calculation and PLAXIS 3D modelling.

1.3 Limitations

The hand calculation is only done for one method given by [DNV. \(1992\)](#) and other methods are not considered in this thesis though there is a review though some others and are compared generally.

There is only one type of soil model as the *soft clay*. Also the soil is modelled using only Mohr-Coulomb modelling option.

The 3D model is a finite element model applied on PLAXIS 3D 2017.

Practical limitation due to computer power and limited time. A 3D model needs a fine meshing system analysis is time taking. Also to store the information from fine mesh takes much of computer storage. Generally the computer should have sufficient properties to analyse the model accurately.

When a load is applied on a foundation it might causes tension in one side of the foundation. In

a real condition a gap opens between the foundation plate and soil. It is possible to set a model in such a situation but analysing the model takes more time therefore, the separation of soil and structure is not modelled.

Loads are assigned in the static mode and cyclic or seismic loads are not considered in this thesis.

1.4 Approach

Reading through literature and papers to learn about the method of hand calculation is the first step before starting any measurement and analysing.

PLAXIS 3D is new to the author so part of the time is donated to learn it well enough. The best resource is the manual references if it. Modelling a pure vertical loading and checking its result with the results from hand calculation is a good estimation to check if the model is correct.

Hand calculating different load combinations and comparing it a proper computer modelling was done. Comparing the results and discuss them was the final part of analysing.

1.5 Structure of the Report

This master thesis is presented in

- *Chapter 2* A literature review through previous studies and most methods and consideration about mudmat foundations and effect of each parameter.
- *Chapter 3* Introduction of the case study model and assumption for that.
- *Chapter 4* Hand calculation method for the model under different load combinations and any assumption for any factor.
- *Chapter 5* The simulation presentation.
- *Chapter 6* The results and discussion.

Conclusion, appendix, and figures are enclosed afterwards.

Chapter 2

Literature Review

The content of this section is based on published articles about skirted mudmat foundations. Skirted foundations are assumed to be completely penetrated due to the structural self-weight load.

2.1 Offshore Geotechnics

Oil and gas exploration was the beginning of the geotechnical engineering in offshore condition. Increasing demand for energy led to more investment in sustainable energy and in particular offshore wind turbines and farms. The offshore economic condition requires more investigation in deeper water.

In this project, the seabed is considered as a normally consolidated clay. Clay has a low permeability which prevents the shallow water flow to accrue. Yet there are problems with drilling because of the hole closure which is not discussed in this project ([Andersen et al., 2008](#)). Various concerns are presented following.

2.1.1 Soil Condition

Working on deep-water seabeds, geohazards and their consequences, such as fast sedimentation caused by excess pore pressure, shallow water flow, volcanoes should be identified to have a safe design. Also in some areas there might be some seismic activities due to faults.

The seabed in the deep-water areas are mostly under-consolidation soft clay though over-consolidated condition might have existed in areas where there used to be any overburden which is removed

by any means (Andersen et al., 2008).

The offshore geotechnical condition can cause an increase in the size of the foundation. Therefore, in Veritas (1992), it is suggested that soil investigation should be done to have the basis for a proper foundation design including:

- Settlements
- Local stresses
- Skirts retrieval and penetration
- Stability
- Soil response to dynamic loading

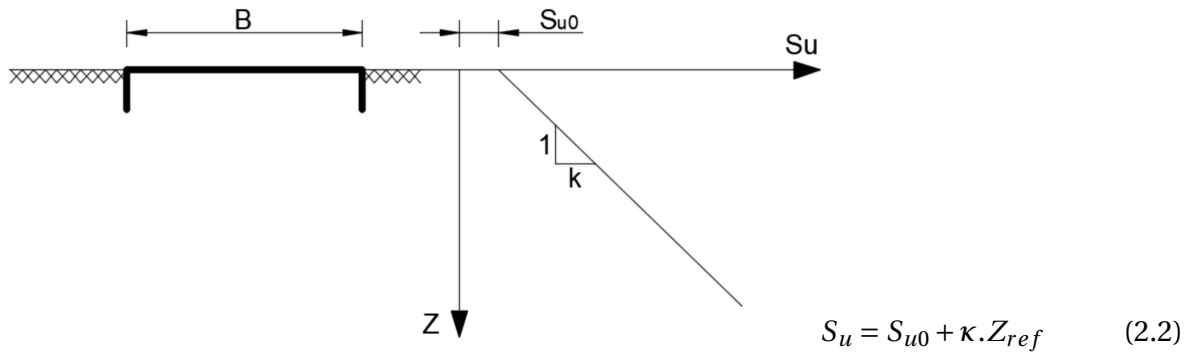
This project is to analyze the bearing capacity of the shallow foundations which is the matter of shear strength. To calculate ultimate bearing capacity, two factors should be taken into consideration, *shear strength* and *shear modulus*, in the next two subsections these two criteria are introduced and presented for this project.

Shear Strength

Subsea surface is covered with mud which is probably with almost no strength though it can not be ignored. *Tresca undrained shear strength* (S_u) analysis on which the model is based with a *linearly elastic-perfectly plastic* material is considered to study *undrained limit state (ULS)* condition.

$$z_r = \frac{B_0}{2(2-r)} \sin\left(\frac{\pi}{4} - \omega\right) \quad (2.1)$$

As the seabed is mostly mud, then the S_u is assumed to increase linearly with ratio of 1 to 1.3kPa per meter with respect to depth (Yun and Bransby, 2007). An estimation for S_u in this condition can be found in Figure 2.2 using depth as the reference depth calculated by equation 2.1 (Emdal, 2011).



According to (Tani and CRAIG, 1995), there is another factor identified as S_{u0} which stands for the undrained shear strength at the foundation or its skirts tip. This factor is used further for calculation. Figure 2.2 illustrate the term S_{u0} .

Shear Modulus

There are many proposed formulas for calculating a soil shear modulus such as Equation 2.3 by Hardin (1978)

$$G_{max} \approx 625 \frac{(OCR)^\mu}{0.3 + 0.7e^2} \sqrt{p_a \bar{\sigma}_0} \quad (2.3)$$

this equation is recommended to be used as a field, laboratory, or primary calculations. For small projects, calculating testing G_{max} could be costly and Hardin's equation could be useful (Gazetas, 1991). The following equation is suggested by Seed (1970) for granular soil types:

$$G_{max} \approx 1000 K_2 \sqrt{\bar{\sigma}_a} \quad (2.4)$$

A ratio of shear strength, S_u , and shear modulus, G_{max} , for saturated clay is:

$$\frac{G_{max}}{S_u} \approx 1000 \quad to \quad 2000 \quad (2.5)$$

The value of $G \approx 100 \cdot S_u$ is offered in most of the soil mechanics lecture notes to have the condition almost on failure (Seed, 1970). In this project, the same assumption is made for G_0 . The term G_0 is the shear modulus at the surface of the seabed. The deeper the layer, the stiffer it becomes in nature. Therefore, it is important to make the model as close as possible to reality. It is possible to have the model shear modulus varying by depth as well. Some increasing patterns can be find in figure 2.1.

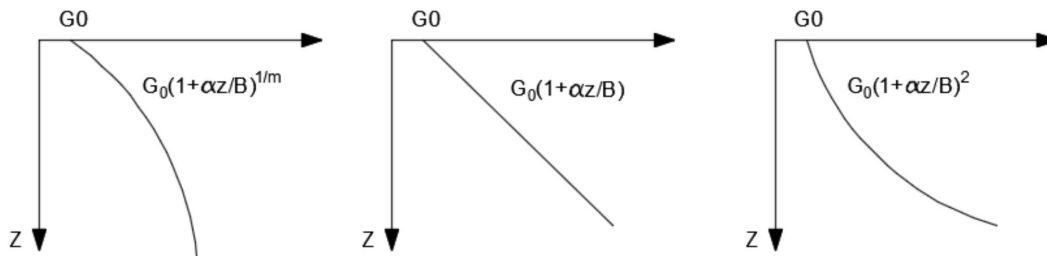


Figure 2.1: Shear modulus varying by depth patterns (Gazetas, 1991)

In this project a failure condition is modelled, therefore it is considered that $G = 100.S_u$. As long as shear strength is assumed to be linearly increasing then the shear modulus is following its pattern.

2.2 Mudmat Foundations

Mudmat foundations are under the shallow foundations' category. The embedment ratio is mostly from 0.1 to 0.5 varying in relation to soil type (Dunne, 2015). The offshore condition is rough and deep in the water therefore, shallow foundations are designed and installed with a skirt along its perimeters. In case of long dimension inner skirts are also considered. These skirts help the foundation to increase the failure line which leads to higher bearing capacity. The skirt increases the tension resistance of the foundation. The tension load could be caused by high overturning moments on the foundation, direct uplift caused by the tripod supporting system for a fixed structure or buoyancy of a floating structure (Acosta-Martinez et al., 2008).

2.2.1 Analysis

To design a mudmat foundation there are five main steps to consider:

- **STABILITY** This part contains failure analysis for bearing capacity, overturning, sliding, as well as any combination of these failings.
- **STATIC DEFORMATION** The structure, its foundation and attached structures damages are included in this analysis part.
- **DYNAMIC CRITERIA** The foundation would face dynamic deformations due to dynamic load which have an influence on structure response and foundation performance.
- **HYDRAULIC INSTABILITY** The wave pressure might damage a structure.

- **INSTALLATION** The effect of pulling out the shear skirts, penetration, the building pressure and the trapped water underneath of the plate upward pressure are parameters that should be considered in a mudmat foundation analysis. (API, 2000)

To design shallow foundation and checking its stability under loads applied to it must include minimum of *Ultimate Limit State(ULS)*, *Accidental Limit State(ALS)*, *Serviceability Limit State(SLS)* as well as the ULS seismic design containing *Extreme Level Earthquake(ELE)* and *Abnormal Level Earthquake(ALE)*. Limit State Analysis along with Finite Element Analysis both 2D and 3D gives a better understanding of the foundation response to various load combinations.

There are many codes available and the most recent ones such as ISO or API are mostly similar to *DNV Classification Notes 30.4-Foundation* (DNV, 1992). The global bearing capacity calculation originated from solutions by Davis&Booker, Terzaghi and Brinch-Hansen, is the basic foundation for all these codes. As studied in this paper, the main goal of codes and studies is to show the relation of different ultimate loads of a foundation in a graph.

Adjusting the suitable load, its factor as well as material factors, bearing capacity analysis is categorized as a Ultimate Limit State (ULS) design (Ulvestad and S. Giese, 2017).

2.2.2 Installation

Rectangular mudmat foundations are the most commonly used shape of these foundations for subsea structures. These foundations face vertical, horizontal, torsional and moment loads simultaneously. Offshore foundations would face many intimidating logistical challenges during installation and maintenance. To start the installation process, the mudmat foundation must be transferred to the exact right place on the seabed which requires special equipment such as ocean vessels (O'Loughlin, 2015).

Due to the variety of the seabed conditions, it is necessary to use the right foundation expertise for each place.

One of the problems is foundation vulnerability to erosion due to salty water as well as marine species which grow or stuck to the steel bodies. These may cause a massive cost to protect or fix the body.

2.3 Bearing Capacity

Bearing capacity identifies the amount of load that the soil can stand with any shear failure. Allowable bearing capacity is calculated by division of the ultimate bearing capacity over the factor of safety (Terzaghi, 1944).

Considering bearing capacity, on a section of soil either on the surface or in depth, three main zones can be distinguished. The main zones illustrated in Figure 2.2 are known as Active Rankine-zone, Prandtl-zone and Passive Rankine-zone. For each one these zones an stress equation can be derived. Combining all these equations of zones ultimate bearing capacity can be calculated.

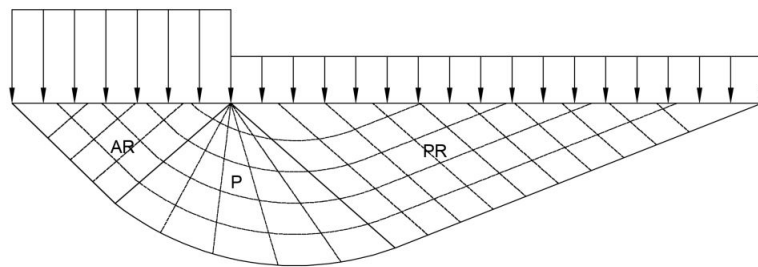


Figure 2.2: Stress Field Different Zones

In designing a mudmat foundation there are two different types of global and local bearing capacity problems which differs and should be taken under consideration separately.

According to (Terzaghi, 1944), there are three types of failures due to bearing capacity known as:

- a General shear failure
- b Local shear failure
- c Punching shear failure

illustrated as follow:

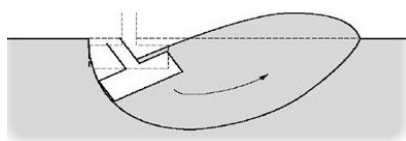


Figure 2.3: General Shear Failure

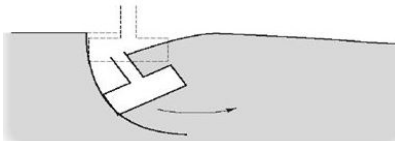


Figure 2.4: Local Shear Failure

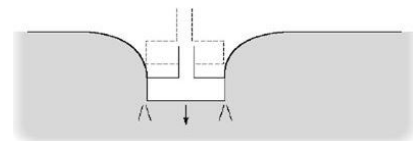


Figure 2.5: Punching Shear Failure

Effective Area Foundations are under both horizontal Q_H and vertical loads Q_V , any axial eccentricity may cause torsional or *moment* loading. To simplify the problem, the load centre can

be shifted by a distance from the centre of foundation as shown in figure 2.6.

There might be axial eccentricity either in one direction or in two. A load with axial eccentricity would cause a *moment/torsion* in the same direction.

As shown in figure 2.6, introducing ΔB and ΔL as the distance of eccentric load then:

$$B_0 = B - 2\Delta B \quad \text{and} \quad L_0 = L - 2\Delta L \quad \Rightarrow \quad A_0 = B_0 * L_0 \quad (2.6)$$

Using the moment equilibrium at the center of the foundation plate given in Figure 2.6 so $\Sigma M_O = 0$ and referring to mechanics of material basics $M = Q_v \Delta B$ is known. The formula for measuring the moment load are:

$$\begin{aligned} \Delta B &= \frac{M_B}{Q_V} \\ \Delta L &= \frac{M_L}{Q_V} \end{aligned} \quad (2.7)$$

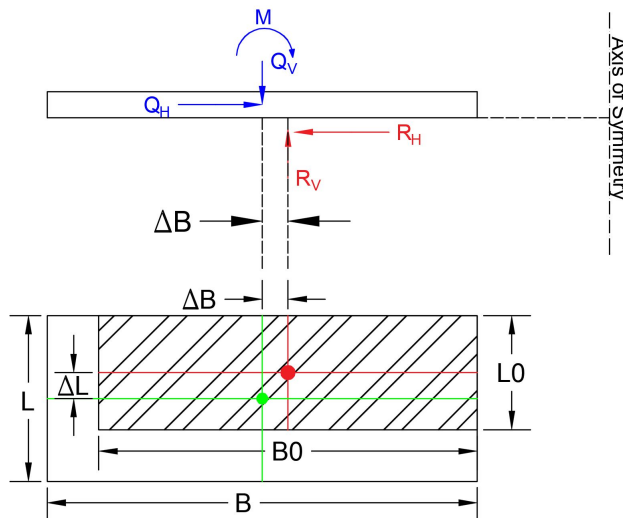


Figure 2.6: Effective dimensions

Effective area geometrical centre and load centre are designed to coincide, and such that it follows as closely as possible the nearest contour of the true area of the foundation base (DNV, 2010).

Bearing capacity generally means to calculate the shear strength under affection of many factors. Though this project is about the affection of various load combination on the bearing capacity of a foundation, other effective parameters are discussed briefly in the following sections.

2.3.1 Method Selection Effect

There are many methods and the general formula widely used are presented in following.

•Terzaghi, 1943

Terzaghi's method is probably the most famous method among civil engineers in many aspects. He was the first to establish the universal evaluation theory for a shallow foundation to calculate ultimate bearing capacity. The term q_{ult} is mathematical symbol set to show it (Das, 2007).

Terzaghi presented the q_{ult} as a function of some bearing capacity and shape factors (N-factors and s-factors respectively) which are discussed in the following.

$$N_q = \frac{a^2}{a \cos^2(45 + \frac{\phi}{2})} \quad , \quad N_c = (N_q - 1) \cot \phi \quad , \quad N_\gamma = \frac{\tan \phi}{2} \left(\frac{K_{P\gamma}}{\cos^2 \phi} - 1 \right) \quad (2.8)$$

He indicated that if the friction angle is zero ($\phi = 0$) then N_c is taken as $1.5\pi + 1$ (Terzaghi, 1944).

In *Terzaghi's* method shape factors are not provided with a formulation therefore, it is not adjustable to foundations with different shapes than what he assumed. They are set as a constant value which are given in Table ?? . One of the uncertainties in *Terzaghi's* method is having constant shape factors.

Table 2.1: Shape Factors for Terzaghi method

Foundation Type	Strip	Round	Square
s_c	1.0	1.3	1.3
s_q	1.0	0.6	0.8

Terzaghi did not provide information about calculating $K_{P\gamma}$ which is one of the parameters to calculate N_γ but the amounts are back calculated by (Bowles et al., 1996). The general formula can be used to calculate the ultimate bearing capacity (q_{ult}) as:

$$q_{ult} = cN_c s_c + \bar{q}N_q + 0.5\gamma N_\gamma s_\gamma \quad (2.9)$$

this theory claims that a foundation with a depth and width ratio equal or less than one ($\frac{d}{B} \leq 1$) should be treated as a shallow foundation. However, investigations suggested that the ratio up to 3 or 4 may be classified as shallow foundations (Das, 2007). Though *Terzaghi's* method is the most popular one, but it is not the method used in this project cause a

3D condition is assumed.

•**Meyerhof, 1963**

This method is very similar to Terzaghi's method and he identified new parameters as factors for shape and depth. Having more factors in an analysis would result to a more accurate answer but also make calculations more complex. Equation 2.10 presents how to involve these factors in calculation of ultimate bearing capacity.

$$\text{Vertical Loading} \rightarrow q_{ult} = cN_c s_c d_c + \bar{q}N_q s_q d_q + 0.5\gamma B_0 N_\gamma s_\gamma d_\gamma \quad (2.10)$$

In the general formula there are many factors. To check details about each factor reviewing [Bowles et al. \(1996\)](#) is recommended.

The ultimate bearing capacity is to set all different loads with their suitable factors. The following two methods are using the same formula for N_q and N_c so they are given in the final section so that it would be easier to look back on them. The N_γ , whose contribution does not make big difference, is what varying and *Meyerhof* is identifying it as a function of friction angle ([Meyerhof, 1953](#)).

$$N_\gamma = (N_q - 1) \tan(1.4\phi) \quad (2.11)$$

As written before, ([Meyerhof, 1953](#)) uses two different formulas to calculate the ultimate bearing capacity (q_{ult}) for pure vertical and inclined loading condition. In this method, N_c is assumed as $\pi + 2$ for the $\phi = 0$ condition.

$$\text{Inclined Loading} \rightarrow q_{ult} = cN_c i_c d_c + \bar{q}N_q i_q d_q + 0.5\gamma B_0 N_\gamma i_\gamma d_\gamma \quad (2.12)$$

Bearing capacity N-factors are ϕ -related. Shape, depth and Inclination factors are given in detail on ([Bowles et al., 1996](#)) paper *Table 4-3, p222* to which one can refer.

$$N_q = e^{\pi \tan \phi} \tan^2\left(45 + \frac{\phi}{2}\right), \quad N_c = (N_q - 1) \cot \phi \quad (2.13)$$

The N_q and N_c are used with the same formula by *Meyerhof, Hansen and Vesic*.

•**Hansen, 1970**

This method is an extension to what *Meyerhof* had introduced before. Its equation is im-

plied to any $D \setminus B$. Therefore, it can be a good method for either shallow or deep foundations. The term $\bar{q}N_q$ makes ultimate bearing capacity increases sharper with depth. *Hansen* also applied some limitation as given following.

$$d_c = \begin{cases} 1 + 0.4 \frac{D}{B}, & \text{if } \frac{D}{B} \leq 1 \\ 1 + 0.4 \tan^{-1} \frac{D}{B}, & \text{if } \frac{D}{B} \geq 1 \end{cases} \quad d_q = \begin{cases} 1 + 2 \tan \phi (1 - \sin \phi)^2 \frac{D}{B}, & \text{if } \frac{D}{B} \leq 1 \\ 1 + 2 \tan \phi (1 - \sin \phi)^2 \tan^{-1} \frac{D}{B}, & \text{if } \frac{D}{B} \geq 1 \end{cases} \quad (2.14)$$

Shape, depth and other factors are presented in (Bowles et al., 1996) to which one can refer. Hansen's general equation contains these factors which are mostly ϕ related.

$$\text{General equation} \quad q_{ult} = c N_c s_c d_c i_c g_c b_c + \bar{q} N_q s_q d_q i_q g_q b_q + 0.5 \gamma B' N_\gamma s_\gamma d_\gamma i_\gamma g_\gamma b_\gamma \quad (2.15)$$

As previously mentioned, N_q and N_c are calculated the same as *Meyerhof* presented. To get the N_γ (Hansen, 1970) introduce his formula as:

$$N_\gamma = 1.5(N_q - 1) \tan \phi \quad (2.16)$$

Knowing $\phi = 0$, then the formula can be written as:

$$q_{ult} = (\pi + 2) s_u (1 + s'_c + d'_c - i'_c - b'_c - g'_c) + \bar{q} \quad (2.17)$$

•Vesic, 1973-1975

This method is basically the same procedure as what *Hansen* presented though identifying a new formula for N_γ as given following.

$$N_\gamma = 2(N_q + 1) \tan \phi \quad (2.18)$$

Vesic's method can be a slightly easier to work with comparing to *Hansen's* cause calculating i factor requires shape factors while *Vesic's* i factors are independent (Bowles et al., 1996).

As a conclusion, methods and their best usage condition is given in the table 2.2

Table 2.2: Methods and their usage (Bowles et al., 1996)

Method	Where to use
Terzaghi	If soil is cohesive <i>Terzaghi's</i> method can be used for a quick calculation as a base for comparing it with other results as long as $D/B \leq 1$ and there is no horizontal or <i>moment</i> forces and the terrain has no inclination
Hansen\Meyerhof\ Vesic	Any situation will fit in these methods the only difference is users familiarity with either of these methods
Hansen\ Vesic	If $D/B > 1$ or the foundation is based on a slope these methods are recommended

Chapter 4, *Hand Calculation*, is presenting calculation based on *Classification Notes-No.30.4's* recommendation which is basically *Hansen's* method combined with David Booker's method.

2.3.2 Skirts Effect

Mudmat foundations have the potential of having internal skirts leading to higher capacity. These skirts ensure that soil plastic displacement is like a rigid body. As shown in figure 2.7, the numbers of skirts can change the failure mechanism compared to solid body foundation under pure vertical or horizontal load for simplification.

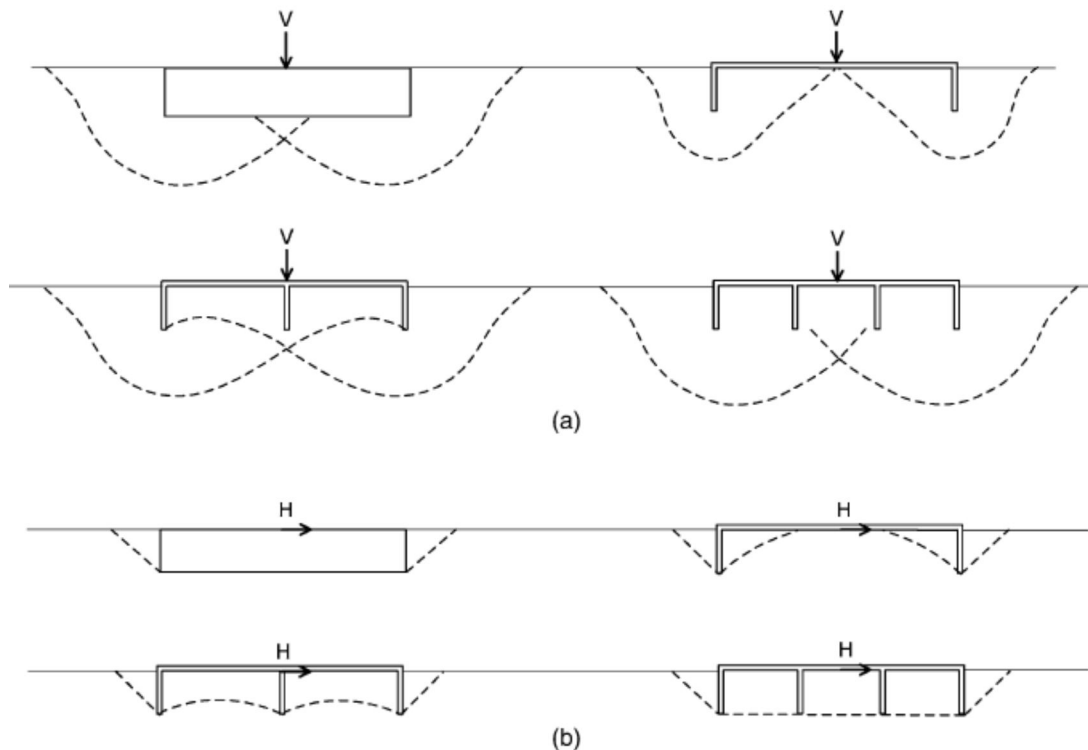


Figure 2.7: Comparing the failure mechanism of skirted shallow and solid foundations under pure vertical and horizontal loading (Mana et al., 2012a)

The previous studies declare that shallow foundation skirts are more likely to have the internal mechanism comparing to deep skirted ones (Mana et al., 2012b; Bransby and Yun, 2009; Yun and Bransby, 2007).

Identifying skirts results in an increase in both horizontal and vertical capacity. Horizontal capacity is more affected by skirts when the foundation is placed on a slope especially when it is pushed into the slope rather than being pulled away from it. On the other hand, increasing capacity under vertical loading happens when skirts are placed in a flat surface condition. (Dunne, 2015)

This project is not discussing the skirts affection on the capacity of mudmat foundations.

2.3.3 Interfaces Effect

Any construction under or on the ground surface where soil and structure are facing then their interface turns as an important issue. In another word, *soil-structure interaction (SSI)* is to define the effect of them on each other due to any movement limitations.

Nonzero-tension interfaces are placed as there is no willing for a gap between the plate and soil. Because that would lead to a local drainage in the vicinity of the skirts. Negative pore pressure would resist the transient uplifting load between soil and base plate. (Mana et al., 2012a,b; Gourvenec and Barnett, 2011; Watson et al., 2000; Andersen et al., 1999; Dyvik et al., 1993).

2.3.4 Perforation Effect

Perforation is useful for foundation installation in an offshore project though excessive perforation may cause performance reduction in many aspect in a foundation. Openings may effect the bearing capacity of a foundation and seeing soft soil, bearing capacity reduction may cause large vertical displacement. To design mudmat foundation considering the amount of soil squeezing through holes and causing small vertical settlement could be a solution.

Perforation is dissipation way for water trapped through the splash zone and also for pore water draining in skirted mudmats. The faster water drain away, the faster penetration of skirt happens in the seabed.

As mentioned before according to Ulvestad and S. Giese (2017), perforation may cause bearing capacity reduction or may leave it untouched and it mostly is depending on the soil heterogeneity. Bearing capacity and footprint reduction could be expected to be equal, for example, having

10% of perforation reduce bearing capacity by 10% which may be conservative in most cases(?). On the other hand, the affection of opening holes on bearing capacity may be too small to be considered and ignoring it is a non-conservative designing (Ulvestad and S. Giese, 2017).

According to Ulvestad and S. Giese (2017), for most of hole diameters, bearing capacity reduction due to perforation is overly conservative. Soil squeezing critical amount should be set considering both structural and geotechnical point of view and if the level is higher than what all models experienced then bearing capacity reduction due to this one could be off of the table as well. As described by Rahardjo et al. (2003), shear strength was set to have small change in depth but for larger increasing with respect to depth perforation influence should be a matter.

2.3.5 Load Combination

Apart from the structure self-load which is vertical, offshore structures faces different loads such as water waves or wind load though these loads have vertical component. (Mana et al., 2012b)

Vertical loads are due to structure and accessories loads, while horizontal loads are due to large pressure and temperature changing, starting and shutting the flow in pipes. These loads all might have some eccentricities which causes moment or torsional loading. A foundation must be designed to stand vertical, horizontal and moment loading application.

Many designing recommendation are based on vertical bearing capacity calculation and modified for lateral and moment loading such as API or ISO. Some semi-empirical shape, load inclination or eccentricity factors are offered by different method as it was presented in Subsection 2.3.1 to be applied for plane strain conditions (Feng et al., 2014).

2.4 Finite Element Method Modeling

The *Finite Element Method (FEM)* also known as *Finite Element Analysis (FEA)*, is a solution with numerical method for engineering, mathematical, and physical problems. Many problems such

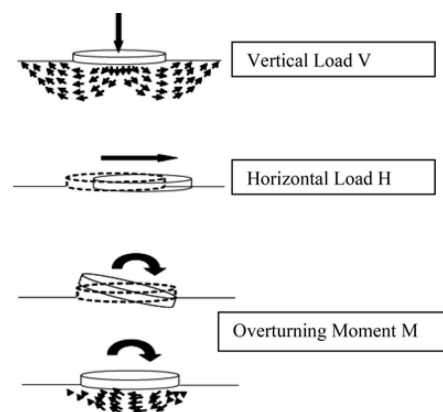


Figure 2.8: Failure mechanism (Kramer, 2014)

as electrical potential, fluid flow analysis or mass transferring can be solved using FEM. Its fame is mostly for structural and mechanical analysis due to resulting to a algebraic equations system which is resulted from boundary condition in partial equations.

Approximate values of unknowns are yielded by this mathematical method in the domain at discrete numbers of points. To solve a large problem, FEA breaks it down into many small ones which are easier to solve and each small problem is called a finite element. Inputting all these small elements and using *variational method*, it ends with a solution with a good approximation for the primary large problem with minimizing errors. To provide a better explanation of this method, one of the special cases of *Galerkin Method* is known as the FEM(Logan, 2011).

Finite Element Analysis (FEA) is widely known as the FEM practical application. In engineering, FEA is referring to an equipment for performing engineering analysis computation. Computing a problem firstly needs to be divided into smaller ones with a use of a mesh generation technique and then applying FEA software which has a FEM algorithm(Reddy, 1993).

FEA elements interconnect through their *nodes* and each of the *nodes*, depending on many factors such as the dimensions of the problem, has its *degrees of freedom* (DOFs). A *degree of freedom* refers to the number of components in a *node* which may change independently.

PLAXIS

One of the most well-known software among *geotechnical engineers* is *PLAXIS*, either two or three-dimensional analysis in which the model is divided into smaller elements using meshing system with different coarseness factors which define the density of the elements on each area. Accuracy and the ability of the computer running the model are the parameters that limit the element type to use. The main elements are mostly known by the number of nodes on the element.

PLAXIS has some basic elements and the figures are presented following.

- Beam elements have 3 nodes compatible with edge of the elements in soil material which are 3-node as well, 2.9.
- Tetrahedral element with 10 nodes are the type of element using for meshing 3D models 2.10.

- Wedge elements are 6 noded used to model geogrids and plates^{2.11}.
- There are 12 noded elements

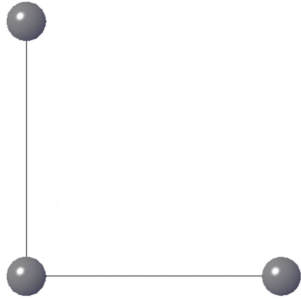


Figure 2.9: Beam Element with 3 nodes

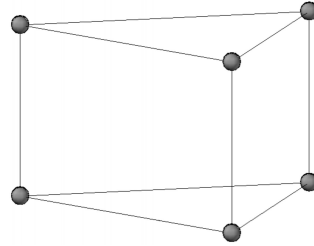


Figure 2.10: Wedge Element with 6 nodes

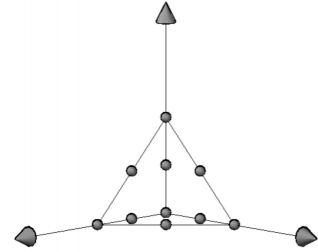


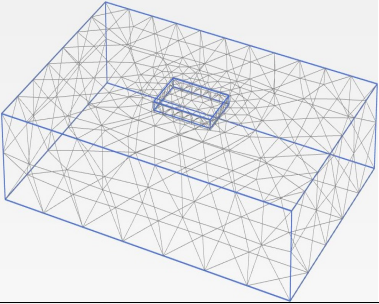
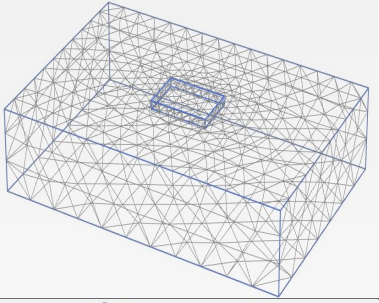
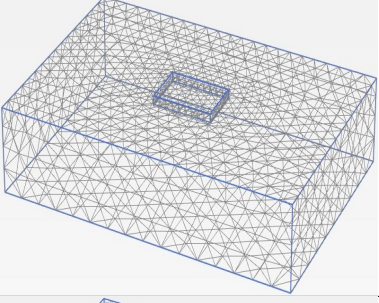
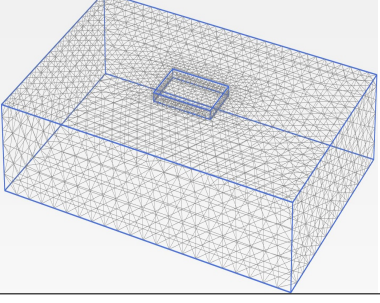
Figure 2.11: Tetrahedrons Element with 10 nodes

Aside from these main elements, *PLAXIS* also uses a 12 noded element to simulate soil-structure interface.

To mesh a model with *PLAXIS*, there are many options either predefined meshing elements or manual ones. very fine to *very coarse* meshing is the domain of meshing and choosing each type is the matter of accuracy, the computer power used which is limited and may become time taking in case of its power. Meshing by *PLAXIS* is not necessarily symmetric under the foundation which may cause some difference.

Some of the possible default meshing styles are done on the model for this project and the number of the elements and nodes are given in Table 2.3. The best way is to combine these different meshing styles using meshing factor and make the model accurate enough while it does not require much of time and storage capacity to run it.

Table 2.3: Different meshing types by default of *PLAXIS 3D* for the model discussed in this thesis

Figure	Meshing Type	Number of Elements & Nodes
	<ul style="list-style-type: none"> • Coarse Meshing Type 	<ul style="list-style-type: none"> • 1381 elements • 2359 nodes
	<ul style="list-style-type: none"> • Medium Meshing Type 	<ul style="list-style-type: none"> • 3702 elements • 5664 nodes
	<ul style="list-style-type: none"> • Fine Meshing Type 	<ul style="list-style-type: none"> • 10367 elements • 15107 nodes
	<ul style="list-style-type: none"> • Very Fine Meshing Type 	<ul style="list-style-type: none"> • 25187 elements • 36166 nodes

Chapter 3

Introduction of the Case Study

This chapter is to present the model studied in this project. This project is about checking the ultimate bearing capacity of the model introduced following in this chapter using *PLAXIS 3D* as well as *hand calculation* which is based on *DNV-GL recommendation* (DNV, 1992). The results are analysed afterwards.

3.1 Geometry

The foundation is L=9m long, B=6m wide and its skirts are 1 meter deep as shown in Figure 3.1.

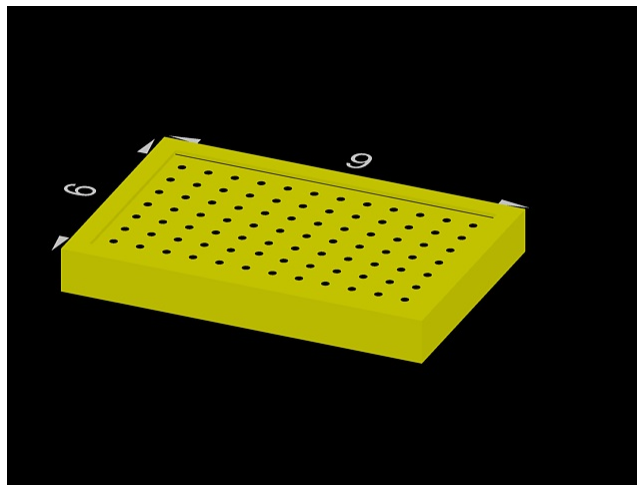


Figure 3.1: A 3D model of the foundation by Autocad 3D

The soil surrounding the foundation is modeled as 5 times bigger than the foundation itself. The model is taken deep enough so that the stress contour lines remain intact at the bottom

of the model so the soil is 10 meter deep. Figure 3.2 presents the model and the ratio of the dimensions is visible on it.

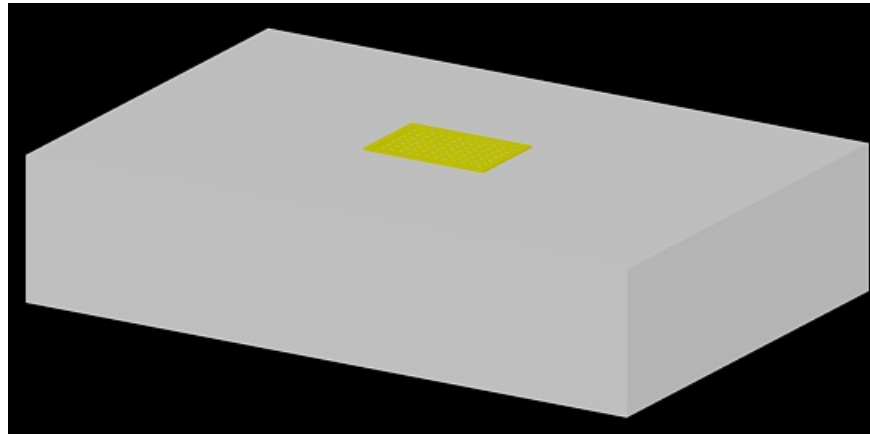


Figure 3.2: A 3D model of the foundation on the soil by Autocad 3D

The model on *PLAXIS 3D* is established using the dimension for soil and foundation given in Table 3.1. The model is made big enough so that the *boundary conditions* do not have a considerable effect on the model. Therefore, *boundary condition* can be avoided.

Table 3.1: Dimension for soil and foundation models

Model	Maximum and Minimum Dimensions					
	X_{min}	X_{max}	Y_{min}	Y_{max}	Z_{min}	Z_{max}
	m	m	m	m	m	m
Soil	0	45	0	30	-10	0
Foundation	18	27	12	18	-1	0

3.2 Material Properties

The plate is assumed to be elastic as presented in Table 3.2, to make sure that it can handle the load assigned to it and it is also adjusted a rigid surface to make sure that the deformation is even over the surface, though the load assigned is through a point load is acting on it.

Table 3.2: Plate assigned to mudmat foundation

Plate type	Steel Plate	Young's Modulus (E)	(kN/m^2)	210.0E6
Material Type	Elastic	Unit Weight (γ)	(kN/m^3)	0
Roughness (R)	0.00	Plate Thickness (d)	(m)	0.1

The analysis over this model is based on *Tresca* method which is mostly focusing over *total stresses* and their relationships while *Mohr-Coulomb* method concentrates on the effective

stresses. Working with total stresses, the *Ultimate* level for each sort of loading can be calculated. The soil is a soft clay model and is modeled on PLAXIS using *Mohr-Coulomb(MC)* modeling option and it is based on *Tresca* analysing method.

As long as the model is a mudmat foundation in deep water condition the soil is considered as a soft clay with characteristics given in Table 3.3. Soil is modeled with shear strength linearly increasing with depth and the range is chosen from 1.0 to 1.3 $kN/m^3/m$ which is suggested by (Yun and Bransby, 2007).

Table 3.3: Soil parameters considered for hand calculation and FE analysis

Soil type	-	Soft Clay	G	(kN/m^3)	100.3
Drainage type	-	<i>Undrained(c)</i> ¹	E_u	(kN/m^2)	300
γ_{unsat}	(kN/m^3)	14.50	$E_{u,inc}$	($kN/m^2/m$)	360
γ_{sat}	(kN/m^3)	14.50	$S_{u,ref}$	(kN/m_2)	1.00
ν_u	-	0.4950	$S_{u,inc}$ ²	($kN/m^2/m$)	1.20
K_0 ³	-	0.65	Z_r	m	0.00
R_{inter}	-	0.9	Ground water level	-	Global

¹ According to PLAXIS manual reference, Undrained type *c* is "Undrained or short-term material behaviour in which stiffness and strength are defined in terms of undrained properties. Excess pore pressures are not explicitly calculated but are included in the effective stresses" (PLAXIS, 2017).

² This is the parameter in PLAXIS and in this thesis it is identified as κ .

³ It is considered that $K_{0,x} = K_{0,y}$.

3.3 Interfaces

The foundation is located on the soil and its skirts are embedded in the soil so the soil and plates affect each other in the reality and to idealize the model, interfaces are placed around each plate to model their interactions.

This project is considering different load combinations and which also causes some tension loads on the foundation. Tension loading is not allowed in the hand calculations and on PLAXIS it is less time consuming if the tension cut off option is selected. Due to the lack of time the tension is not cut off yet the results are compared with a proper discussion and enough figures to show how the tension loads are distributed and how much effect this load has on the results. Interfaces are modelled with the same parameters as the soil model, but they are modelled with higher *roughness*, as the Table 3.3 presents the inputted data for soil modelling the interfaces follow the same just $R_{inter} = 1.0$ is assumed for them on PLAXIS 3D.

Chapter 4

Hand Calculation

4.1 Introduction

Hand calculation is possible through simplified methods which include some limitations as well as uncertainties in bearing capacity calculation for shallow foundation such as:

- Hand calculation for multiple layered soil condition would have many limitation because available methods are mostly for uniform strength or linearly increasing strength in clay. This thesis is also using the linearly increasing strength soil model.
- Foundations with non-standard geometry are facing problems due to methods which are defined for square, rectangular or circular shapes only.
- Structures are not necessarily based on one footing and codes are mostly limited for unusual load distribution or for type of structures with multiple foundations.
- Hand calculation is conservative on effective area measurement.

4.2 Methodology

In this case study *Hansen's* method is used where the general calculation is base on the formula 4.1 given by (DNV, 1992) for ultimate undrained bearing capacity calculation for a soil model with linearly increasing undrained shear strength with respect to depth.

Factors used in the formula are identified shortly as a note under formula yet, each one is explained for this project and if there are any assumptions it is clarified in the following before

presenting any result.

$$q_{ult} = F(N_c \cdot S_{u0} + \frac{\kappa \cdot B_0}{4})(1 + s_{ca} + d_{ca} - i_{ca}) \quad (4.1)$$

where:

N_c = bearing capacity factor

S_{u0} = shear strength at the tip of the skirts

κ = undrained shear strength increasing ratio

B_0 = effective width of the foundation

s_{ca} = shape factor

d_{ca} = depth factor

i_{ca} = factor for load inclination

Knowing that *friction angel* is zero ($\phi = 0$), working on the *undrained* condition and using *Hansen's* method results having $N_c = \pi + 2 = 5.14$ (Hansen, 1970).

In an undrained shear strength analysis for a soft clay with shear strength linearly increasing with depth assuming a ratio of $\kappa \setminus m$ so $S_u = S_{u-Base} + \kappa \cdot z$. For this case study soil type is soft clay and the surface shear strength, S_{u-Base} , is assumed as $100 \frac{kN}{m^2}$ according to table 4.1 and the increasing factor is assumed as 1.2 per meter depth cause the range is suggested to be from 1.0 to 1.3 (Yun and Bransby, 2007).

Table 4.1: Presumptive bearing capacity values as per IS1904-1978

Type of soil/rock	safe/allowable bearing capacity(kN/m^2)
Rock	3240
Soft rock	440
Coarse sand	440
Medium sand	245
Fine sand	440
Soft shell/Stiff clay	100
Soft clay	100
Very soft clay	50

Figure 4.1 illustrate the different S_u used in the general formula (refer to Formula 4.1), or other shear strength used in though the *Hansen's* method.

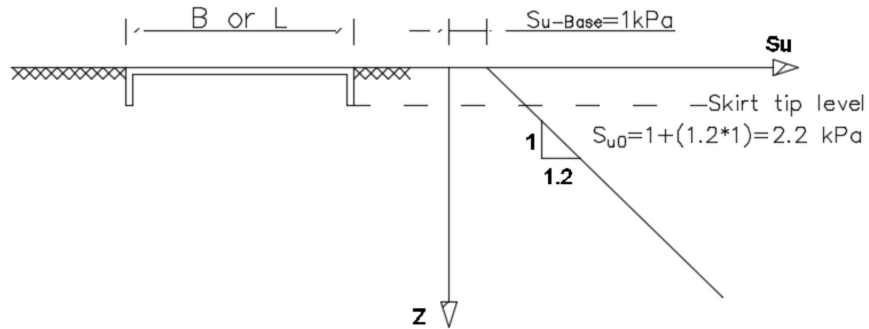


Figure 4.1: Different shear strength

Calculation of the effective width is given in previous chapter under Figure 2.6. In this thesis effective dimensions are calculated through following formula.

$$\Delta B = \frac{M_y}{F_z} \quad \Delta L = \frac{M_x}{F_z} \tag{4.2}$$

$$B_0 = B - 2\Delta B \quad L_0 = L - 2\Delta L \quad A_0 = B_0 \cdot L_0 \tag{4.3}$$

The correction factor (F) is driven by the graph presented in the Figure 4.2 as a function of $\frac{\kappa B_0}{S_{u0}}$ which differs smooth and rough footings (Davis et al., 1985).

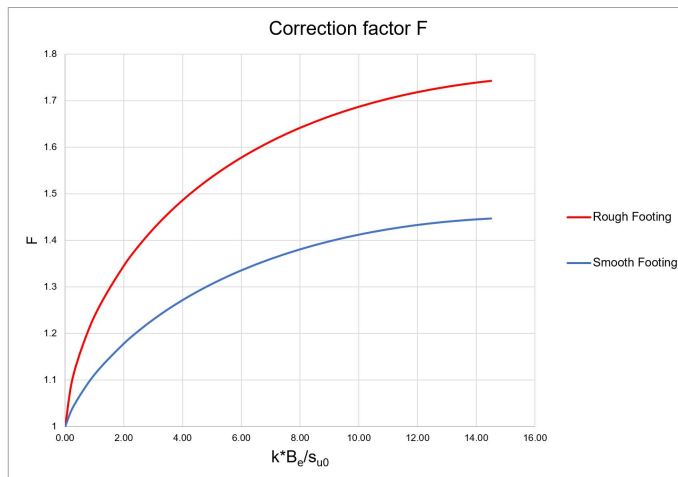


Figure 4.2: Correction factor F given for rough smooth footing (Davis et al., 1985)

Knowing s_{cv} is shaping factor for circular foundations is also a function of $\frac{\kappa B_0}{S_{u0}}$ for pure vertical loading condition and this factor is presented by (Salençon and Matar, 1982) given in the Table 4.2 which is showed as a line graph by author. Yet, this project is done with a rectangular shaped mudmat foundation. To calculate shape factor (s_{ca}) DNV GL identify the Formula 4.4

$\kappa B_0/S_{u0}$	s_{cv}
0	0.20
2	0.00
4	-0.05
6	-0.07
8	-0.09
10	-0.10

Table 4.2: Shape factor for pure vertical loading & circular foundations

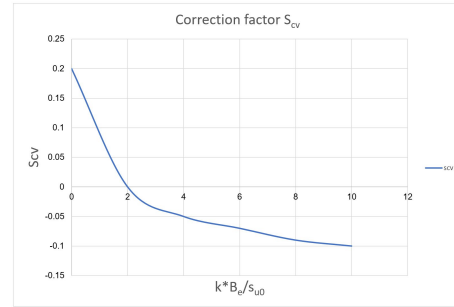


Figure 4.3: Shape factor given in Table 4.2 shown in a graph

with whom the shape factor for circular shaped to a factor satiable for rectangular one (DNV, 1992).

$$s_{ca} = s_{cv}(1 - 2i_{ca})\frac{B_0}{L} \tag{4.4}$$

The shape factor for *Hansen's* method is given in Equation 2.14 but (DNV, 1992) introduce another formula which is not far from what *Hansen* identified. It is based on the ratio of average shear strength above the base level (S_{u1}) and equivalent shear strength below it (S_{u2}).

$$d_{ca} = 0. \frac{S_{u1}}{S_{u2}} \arctan \frac{D_s}{B_0} \tag{4.5}$$

Identifying D_s as the skirt depth, then S_{u1} & S_{u2} can be calculated as:

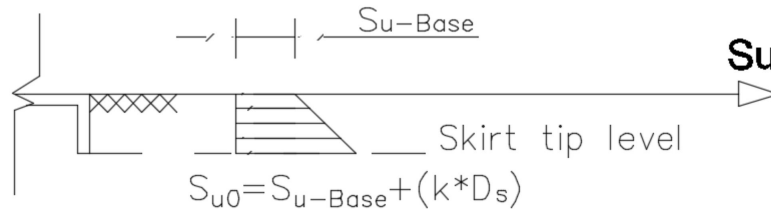


Figure 4.4: Parameters involved in S_{u1} calculation

$$S_{u1} = \int_{S_{u-Base}}^{S_{u0}} S_u = \frac{(S_{u-Base} + S_{u0}) * D}{2} \tag{4.6}$$

And:

$$S_{u2} = F(N_c \cdot S_{u0} + \kappa B_0 / N_c) \quad \& \text{ knowing } N_c = 5.14 \quad \Rightarrow \quad S_{u2} = F(5.14 \cdot S_{u0} + \kappa B_0 / 5.14) \tag{4.7}$$

Loads are not always necessarily pure vertical specially when it comes to offshore condition where there are many loads from environment such as waves or pipeline loads so load inclination is also included in the general formula as a load inclination factor (*ica*). Load inclination factor formula is:

$$i_{ca} = 0.5 - 0.5 \sqrt{1 - \frac{F_{H1}}{A_0 S_u}} \quad (4.8)$$

In Formula 4.8, F_{H1} represent the horizontal forces in ant direction including the total horizontal load applied on the foundation as well as the resistances of the horizontal soil pressure on the embedded, $R_{H,EP}$, base friction, $R_{H,B}$, and side friction, $R_{H,S}$. This can be calculated by formula 4.9.

$$F_{H1} = F_H - R_{H0} - R_{HP} \quad (4.9)$$

To calculate the resistances, introduced above, their eccentricities should be measured. According to (Hansen, 1970) and identifying ΔB_{hor} and ΔL_{hor} as the symbols for eccentricities as a function of forces in different directions named F_x & F_y and the earth pressure(P), evaluation is through the formula given following:

$$\Delta B_{hor} = \frac{F_x}{2P + 2\tau_x \cdot L} \quad \text{if} \quad |\Delta B_{hor}| < \frac{B}{2} \quad (4.10)$$

$$\Delta L_{hor} = \frac{F_y}{2P + 2\tau_y \cdot L} \quad \text{if} \quad |\Delta L_{hor}| < \frac{B}{2} \quad (4.11)$$

And the contribution of the resistances is taken under consideration through the equation 4.12 to 4.15.

$$\text{For earth pressure} \rightarrow R_{H,EP,x} = P \left(\frac{B^2}{4} - \Delta B_{hor}^2 \right) \quad \& \quad R_{H,EP,y} = P \left(\frac{L^2}{4} - \Delta L_{hor}^2 \right) \quad (4.12)$$

$$\text{For base friction} \rightarrow R_{H,B,x} = \tau_x \cdot L \left(\frac{B^2}{4} - \Delta B_{hor}^2 \right) \quad \& \quad R_{H,B,y} = \tau_y \cdot B \left(\frac{L^2}{4} - \Delta L_{hor}^2 \right) \quad (4.13)$$

Knowing that side friction is while the foundation is sliding and the soil is remoulded so side friction resistance is a function of the remoulded shear strength ($S_{u,rem}$) along the skirt and for this project it is taken as 1kPa for this thesis analysis.

$$\text{For side friction along the skirt} \rightarrow R_{H,S,x} = S_{u,rem} (2 \cdot B \cdot L > D) \quad (4.14)$$

$$\text{For side friction for only passive earth pressure} \rightarrow R_{H,S,x} = S_{u,rem}(B.L > D) \quad (4.15)$$

Through the resistance calculations there are two parameters named P as earth pressure on the side of the skirt and τ_x and τ_y which are shear stresses on the base of the foundation. The calculation of these parameters are presented following.

$$\begin{aligned} P &= P_p - P_a \\ &= \left[\frac{1}{2} \gamma^2 D^2 + D \cdot (S_{u-Base} + \kappa \cdot \frac{D}{2}) \cdot k_p / \gamma_m \right] - \left[\frac{1}{2} \gamma^2 D^2 + D \cdot (S_{u-Base} + \kappa \cdot \frac{D}{2}) \cdot k_a / \gamma_m \right] \\ &= (k_p - k_a) \cdot D \cdot (S_{u-Base} + \frac{\kappa \cdot D}{2}) / \gamma_m \end{aligned} \quad (4.16)$$

where:

P_A = Active earth pressure

P_p = Passive earth pressure

D = Depth of the skirt

κ = undrained shear strength increasing ratio

k_p = Passive earth pressure coefficient

k_a = Active earth pressure coefficient

If the analysis is for long term loading then in the active side of the foundation a gap may open and tension loading is not permitted and in this condition $k_a = 0$ and for short term loading tension is permitted therefore $k_a = 2$. In this thesis the assumption is that $k_p = k_a = 2$ so the passive earth pressure exists and on *PLAXIS 3D* the interfaces accept the tension.

Let's identify $\beta = \frac{\tau_y}{\tau_x}$ as the ratio of shear stresses in the x and y directions. For small torsional loading this ratio is also calculable using the ratio of loads in different direction and for considerable torsional loading the ratio should be set up to achieving the maximum bearing capacity. Knowing the ratio β the shearing stress in the base of foundation is calculated through the Equation 4.17.

$$\tau_x^2 + \tau_y^2 = (r \cdot S_{u-Base} / \gamma_m)^2 \quad (4.17)$$

inputting the ratio β then

$$\tau_x = r \cdot (S_{u-Base} / \gamma_m) / (1 + \beta^2)^{0.5} \quad \& \quad \tau_y = r \cdot (S_{u-Base} / \gamma_m) / (\frac{1}{\beta^2} + 1)^{0.5} \quad (4.18)$$

4.3 Load Combination

As long as this thesis is based on comparing the results from hand calculation with *PLAXIS 3D* results and knowing that the FEM software will load the model until it fails, then γ_m is equal to one. All loads which are applied to the foundation is shown in the Figure 4.5 for which calculation method and formula are given above.

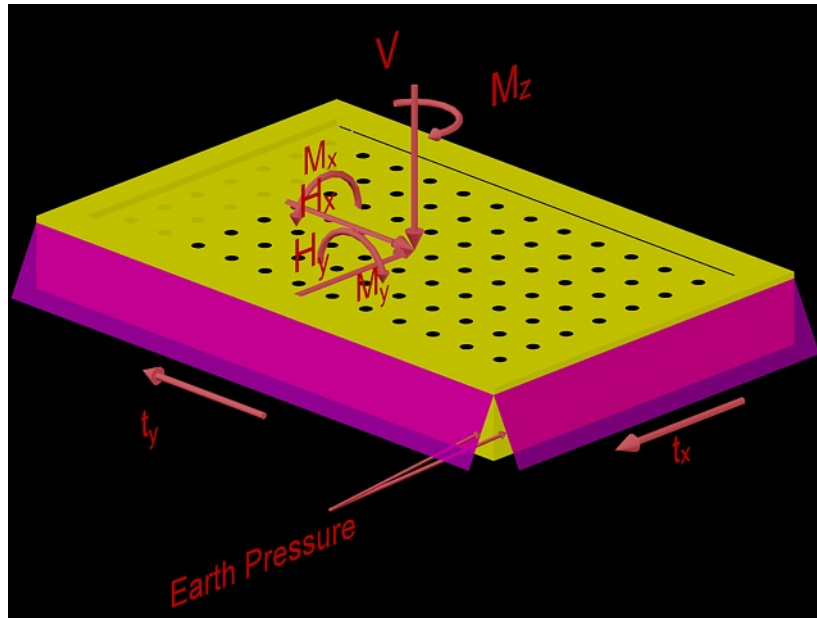


Figure 4.5: Loads applied to the foundation in a 3D environment modeled by AutoCAD 3D

This chapter is to present hand calculation for different load combinations given table 4.3.

Table 4.3: Different load combination considered in this thesis

Load Combinations	Vertical	Horizontal x-Direction (H_x)	Horizontal y-Direction (H_y)	Moment x-Direction (M_x)	Moment y-Direction (M_y)
Comb-1	Max^*	0	0	0	0
Comb-2	0	Max	0	0	0
Comb-3	0	0	Max	0	0
Comb-4	0	0	0	Max	0
Comb-5	0	0	0	0	Max
Comb-6	0	0	0	0	0
Comb-7	$\frac{1}{2}Max^{**}$	Max	0	0	0
Comb-8	$\frac{1}{2}Max$	0	Max	0	0
Comb-9	$\frac{1}{2}Max$	0	0	Max	0
Comb-10	$\frac{1}{2}Max$	0	0	0	Max
Comb-11	$\frac{1}{2}Max$	0	0	0	0
Comb-12	$\frac{1}{2}Max$	$\frac{1}{2}Max$	0	Max	0
Comb-13	$\frac{1}{2}Max$	$\frac{1}{2}Max$	0	0	Max
Comb-14	$\frac{1}{2}Max$	$\frac{1}{2}Max$	0	0	0
Comb-15	$\frac{1}{2}Max$	0	$\frac{1}{2}Max$	Max	0
Comb-16	$\frac{1}{2}Max$	0	$\frac{1}{2}Max$	0	Max
Comb-17	$\frac{1}{2}Max$	0	$\frac{1}{2}Max$	0	0

* The term Max is the shorter version of the word Maximum and it indicates that the maximum of the load is calculated for a specific condition.

** This term is to show that half of the possible maximum load is set to find the maximum of another load.

Chapter 5

FEA Model and Results

5.1 Introduction

The FE software used in this thesis is *PLAXIS* which has a large family of software presented in both 2D and 3D versions and this thesis used the *PLAXIS 3D Foundations* package which is for analysis of foundation structures in a three-dimensional environment.

The model is started on 0, 0, 0 location so all the model is in the x and y positive direction of the axes and the in the z direction model is embedded in the soil with a negative location. Figure 5.1 is to illustrate the location of the model.

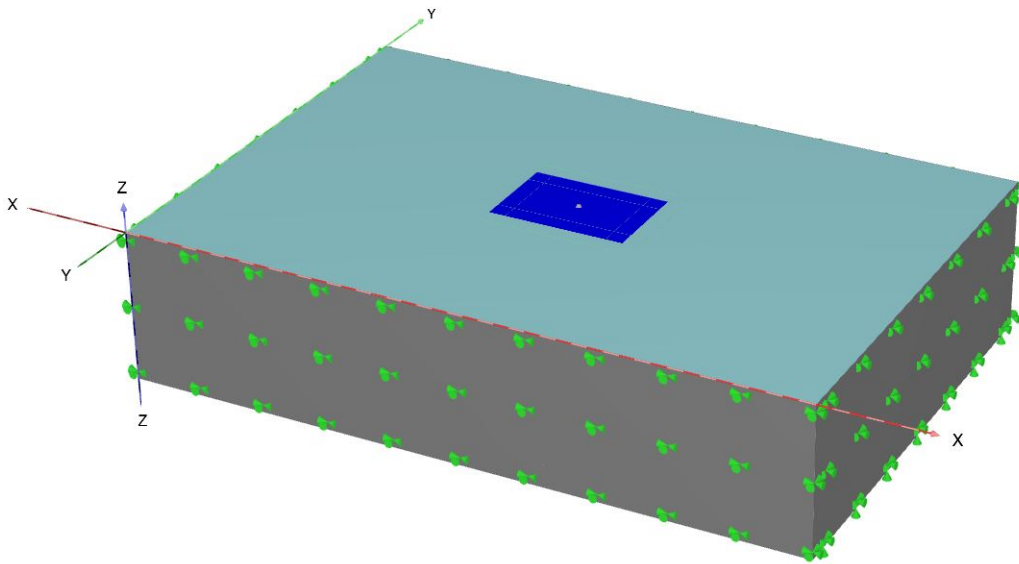


Figure 5.1: The location of the model

5.2 Meshing System

Meshing on *PLAXIS* indicates the accuracy of the results and at the same more time consuming. Therefore, meshing all the model with a very fine meshing system was not possible. According to [Martin et al. \(2015\)](#), a coarse mesh at the interfaces is more accurate when it comes to failure, therefore, having very fine meshing does not necessarily results to more accurate answer. For this thesis, the model is meshed using different meshing factors to have more dense meshing system on the plate and its environment where the yielding surface is happening and a lower meshing factor is set for the exterior environment.

Different meshing style possible by default of *PLAXIS* is given in [Table 2.3](#). The model is generally meshed by fine meshing default system of *PLAXIS* and the foundation area has meshed with a high coarseness meshing factor set as 0.15 for meshing. (see [Figure 5.2](#)). The number of elements and nodes on the model is given in [Table 5.1](#).

Table 5.1: Number of elements and nodes after meshing with different coarseness

Elements	132405
Nodes	193955

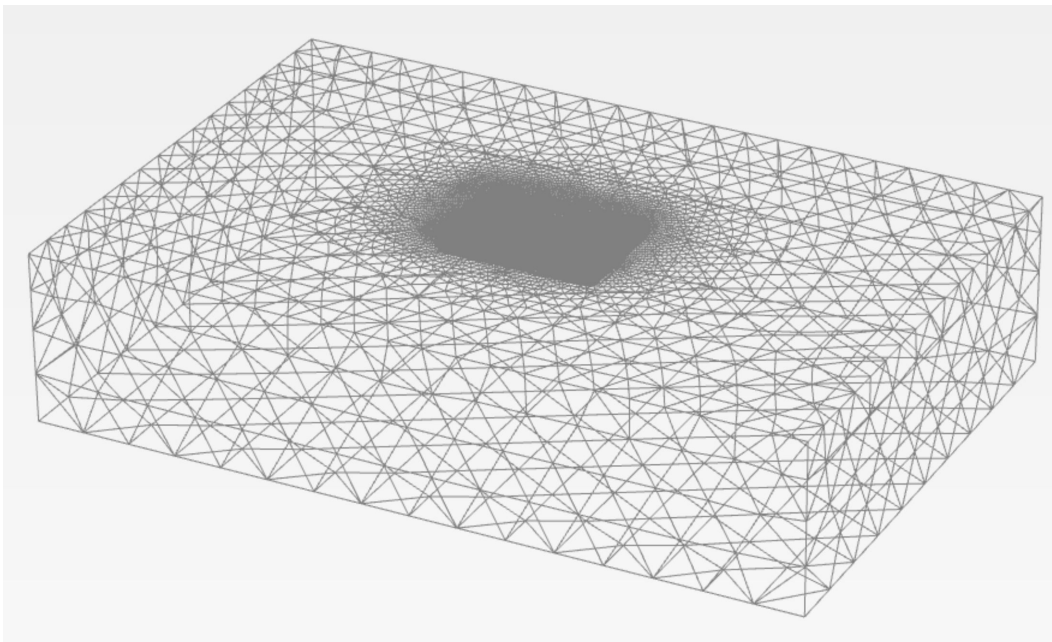


Figure 5.2: Mesh density on the model

Also to make sure that the results are accurate, the model is set to have enough elements in

depth as well. Figure 5.3 illustrates the meshing elements on skirts of the foundation and the soil trapped inside of the foundation so the result is accurate enough comparing the results for few loading condition from PLAXIS and hand calculation.

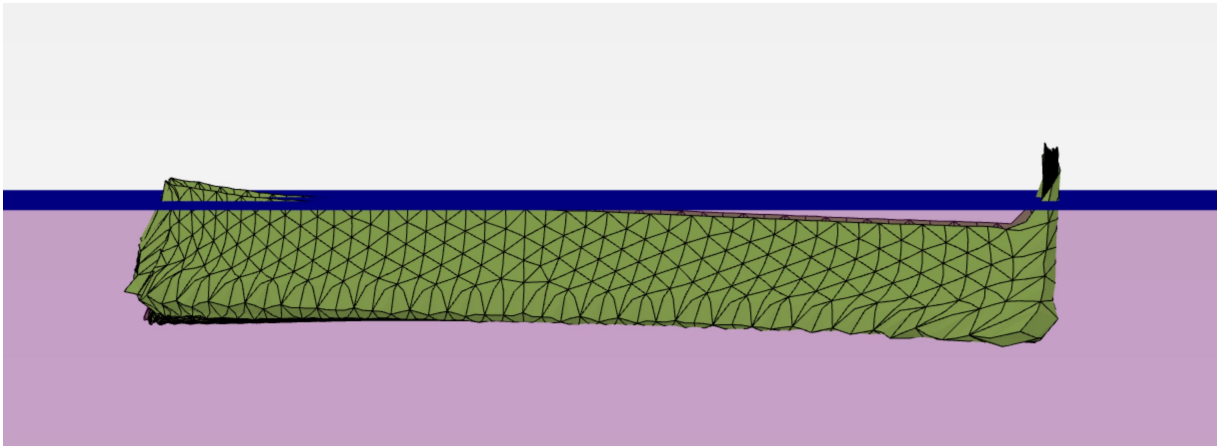


Figure 5.3: Mesh elements on illustrated on one of the skirts

Meshing is not symmetric on *PLAXIS* therefore, there might be some differences. As an example, Figure 5.4 and 5.5 illustrate the failure mechanism on the length of the foundation and its width respectively. The model is under pure vertical loading, the plate is set as a rigid body and the failure path is expected to be symmetric for skirts in the same direction. Yet in both figures, there is a very small difference in the path and the reason for that is unsymmetrical meshing under the skirts tip.

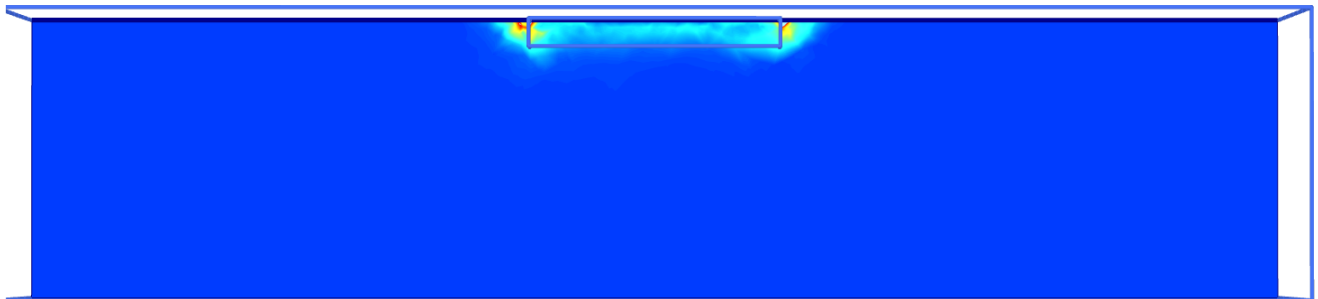


Figure 5.4: Failure mechanism for pure vertical loading in the longer edge

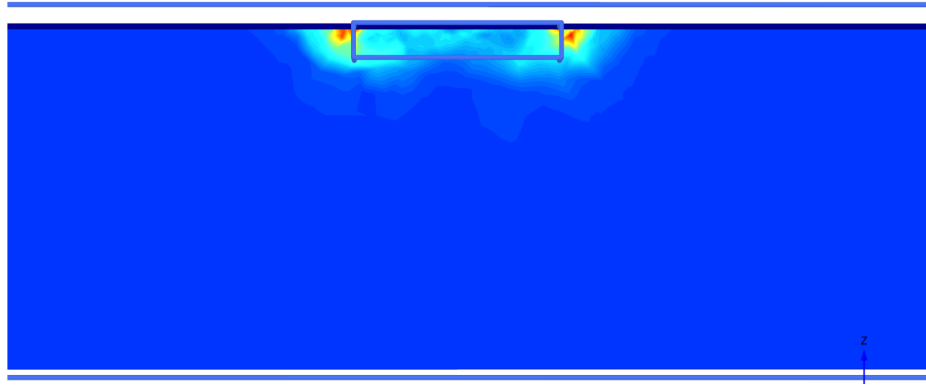


Figure 5.5: Failure mechanism for pure vertical loading in the smaller edge

As long as the figures above are exported from a three-dimensional software the lines around are to show the model environment and the box is showing the plate area of the front skirt and is set just to show the skirt depth.

5.3 Model Verification

Knowing that the failure mechanism under pure vertical loading should be as illustrated in Figure 5.6 then the two failing mechanism on the model done for this project is correct, but if the mesh was adoptive then the failing line would be more visible. To find failure mode for other loading condition see Appendix C.1.2.

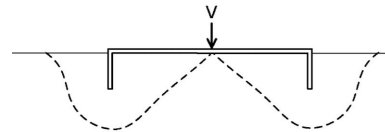


Figure 5.6: Failure mechanism (Mana et al., 2012a)

To calculate the ultimate of each type of loading combination, the model is loaded up to failing point and the point is calculated as follow.

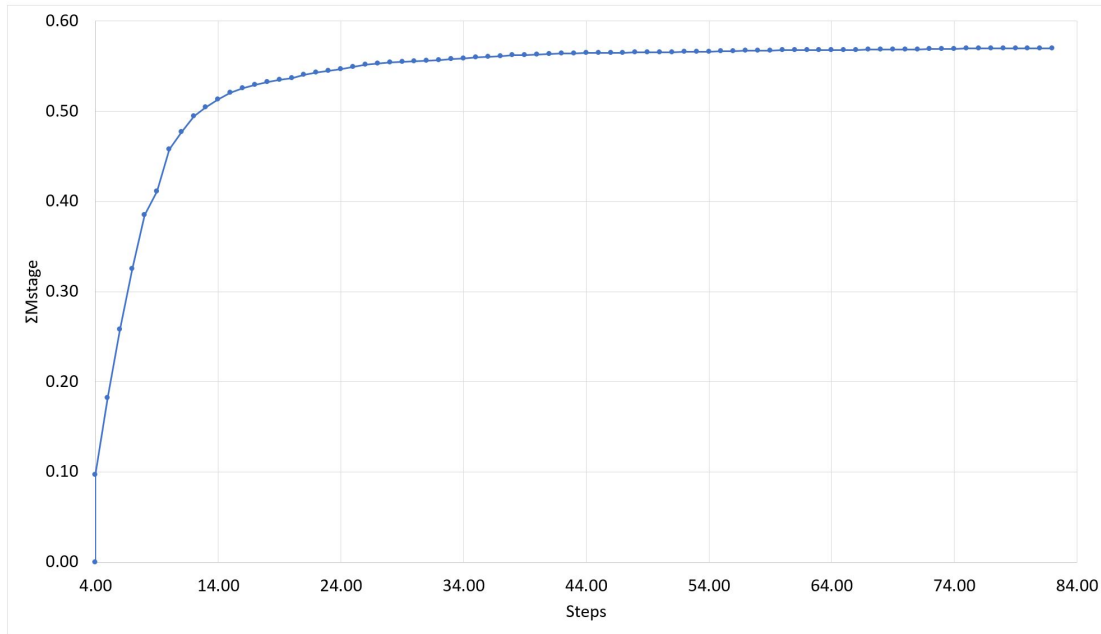


Figure 5.7: Loading steps in pure vertical loading condition up to failure point

As showed in figure 5.7 exported from the *PLAXIS 3D* tables, the ΣM_{stage} which the percentage of the assigned basic load applied on the foundation is 0.5701 which declare that 57.01% of the primary point load, 1100 kN, is applied on the foundation and it reached its failure.

$$\text{Ultimate Vertical Load } V_{max} = \Sigma M_{stage} * V_{primary} \quad (5.1)$$

Therefore,

$$V_{max} = 0.5701 * 1100 = 627.11kN \quad \& \quad \text{from hand calculation } V_{max} = 610.63kN \quad (5.2)$$

This method is held for calculating all maximum loads possible for different load combinations. All the graph outputs from *PLAXIS* is provided in Appendix C.

Chapter 6

Results & Discussion of The Analysis

This section presents results from hand calculation and *PLAXIS 3D* analysis. For more graph in details and tables of specific results in hand calculation please refer to Appendixes [B](#) and result from computer simulation can be found in [C](#).

All the results are normalised to have dimensionless values to compare. To perform normalisation, a constant factor is set for all results by hand calculation or *PLAXIS 3D*. The factor is given in the following table:

Table 6.1: Loads and used factors for normalising

Loading type	Factor	Value
Vertical Load	$S_{u0.A}$	118.8
Horizontal Load	$S_{u0.A}$	118.8
Moment (If horizontal load is in x-direction)	$S_{u0.A.B}$	712.8
Moment (If horizontal load is in y-direction)	$S_{u0.A.L}$	1069.2

6.1 Vertical and Horizontal Loading

Analysing the model by hand or with *PLAXIS*, the vertical bearing capacity is almost meeting and results are 97.4% the same. Vertical loading a foundation and checking the results from different methods is to approve that the simulating model is accurate enough.

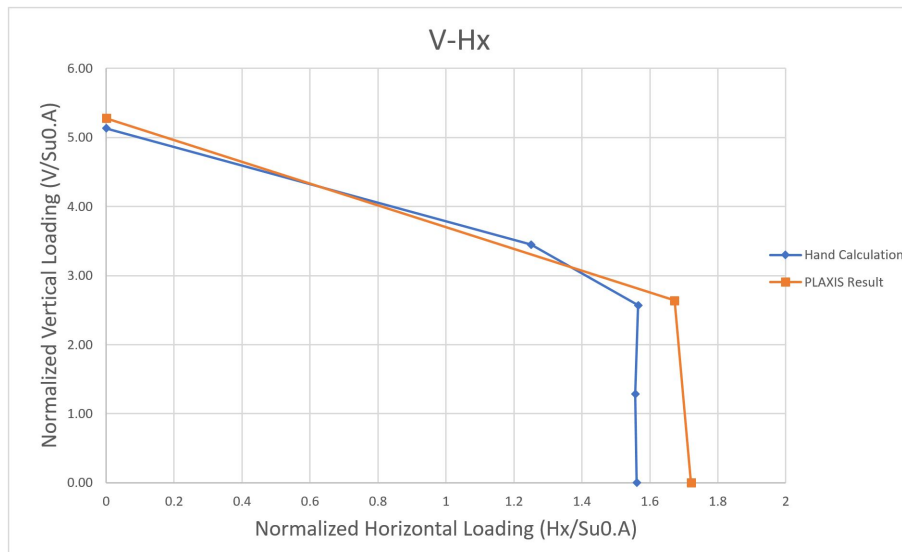


Figure 6.1: Comparison of PLAXIS 3D and hand calculation in $V-H_x$ normalised load space

As illustrated in Graph 6.1, both calculation are following the same pattern. Ultimate horizontal bearing capacity in the x direction slightly differ from results of hand calculation and PLAXIS result is 10% higher. And for the point with half of maximum vertical loading, sliding capacity only differs by 6%.

The y direction of the foundation is 6 meter and the sliding capacity is estimated 12% more on PLAXIS than hand calculation. Also PLAXIS results seems to be linear but having more results would show the curve. The author knows that more results are required yet, due to the lack of time it is not possible to provide more results.

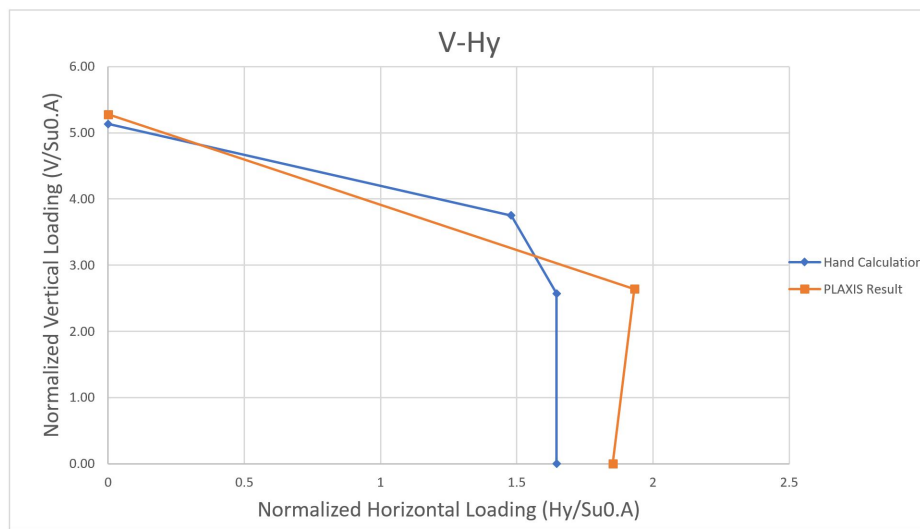


Figure 6.2: Comparison of PLAXIS 3D and hand calculation in $V-H_y$ normalised load space

For hand calculation the roughness ratio is considered to be zero as given in the Figure 6.3 and the horizontal load on the foundation and the earth pressure on the skirts are assumed to be in the same level. Though in a 3D environment roughness ratio can be up to 1 as illustrated in Figure 6.4. The earth pressure and horizontal load have eccentricities which causes a moment and deformation would change.

In the first case the $k_p = k_a = 2$ and $k_p + k_a = 4$ while in the second case the sum of the two



Figure 6.3: Deformation pattern and load assumption in hand calculation

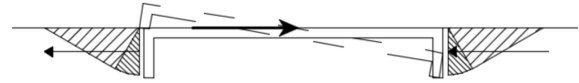


Figure 6.4: Deformation pattern and load assumption in a 3D environment

active and passive earth pressure coefficient may get higher approximately $k_p + k_a = 5.14$. Doing hand calculation for this condition showed that the answer is with a good approximation the same as the result from PLAXIS. This over-shooting could also be due to some 3D affection that is considered in PLAXIS 3D environment which is not seen in the hand calculation formula. Meshing system may make difference as well. Several models with different meshing system was done to find an accurate answer. The results showed that having meshing system more fine then the failure line is more clear and the result is more accurate. The final model was consisting of approximately 139000 elements. Having a a system with enough fine meshing requires better computer facilities.

6.2 Vertical and Moment Loading

Loading the model with pure moment load on PLAXIS 3D is possible while in the hand calculation the moment is a factor of the vertical load.

Three PLAXIS model is set each graph and the results are given yet, there should be more models to have enough information each graph. Therefore, there was a sharp line between two points as it was not clear if the PLAXIS results are always higher. More simulations could be performed, but due to the lack of time only four models are presented. With a glance at the vertical and moment loading curves from hand calculation and PLAXIS 3D, it declares that PLAXIS results are slightly higher. Having a smoother graph is possible with more PLAXIS modelling.

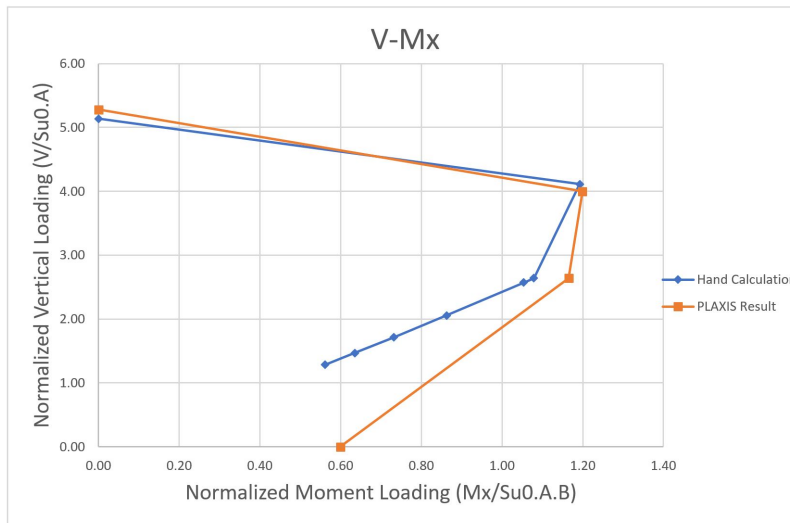


Figure 6.5: Comparison of PLAXIS 3D and hand calculation in $V-M_x$ normalised load space

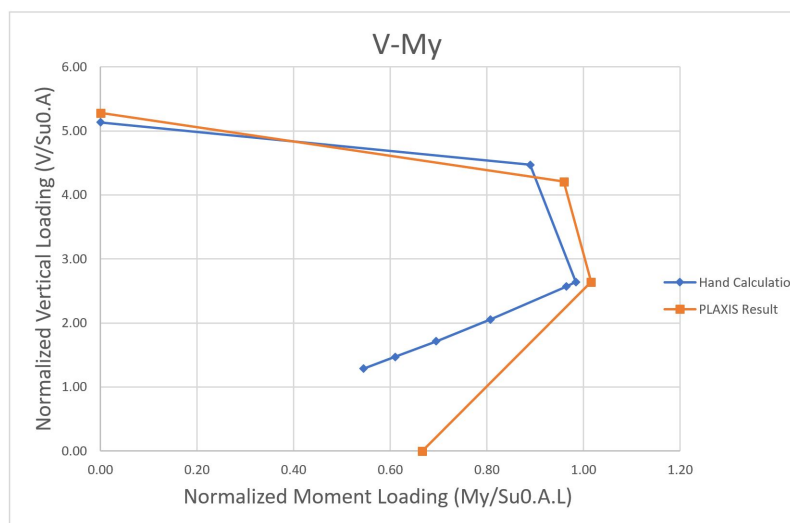


Figure 6.6: Comparison of PLAXIS 3D and hand calculation in $V-M_y$ normalised load space

In the hand calculation, the moment load is expected to increase with vertical load up to a specific level. After its maximum is achieved, the moment load will decrease and end to zero point on the graph where vertical load is at its maximum. As the Graphs 6.5 and 6.6 show the expected pattern is almost followed in hand calculation results.

When the soil is separating from skirt plates a tension load appears which is not taken into consideration in hand calculation process. Therefore, in the PLAXIS model the "tension cut-off" option is activated as well.

Even though in PLAXIS 3D the tension cut-off is selected, there is some attachment forces among

soil elements and the plates elements. This attachment forces may be the reason for having a moment bearing capacity in the absence of vertical loading. The foundation is embedded in the soil, so 3D model with consider some environmental parameters as well. These forces also could be a reason for the over estimation on PLAXIS 3D. Yet 3D environment may have some affection, especially when it comes to estimate pure moment loading and there is some capacity on PLAXIS for this condition.

The explanation about roughness ratio and moment due to earth pressure loads given in Part 6.1 is also a plus to the discussion above.

The load combination of vertical and moment loads, hand calculation results do not differ much from PLAXIS and it is not possible to say if the PLAXIS is over-shooting or the hand calculation is Conservative.

6.3 Vertical, Horizontal and Moment Loading

Using hand calculation to combine three different loads on one model is a challenging task and many factors are involved which cause some differences in the results.

Due to time limitation, only three PLAXIS model results are depicted in the following graphs. In figure 6.7, it is indicated that the results are following almost the same pattern yet some differences in values.

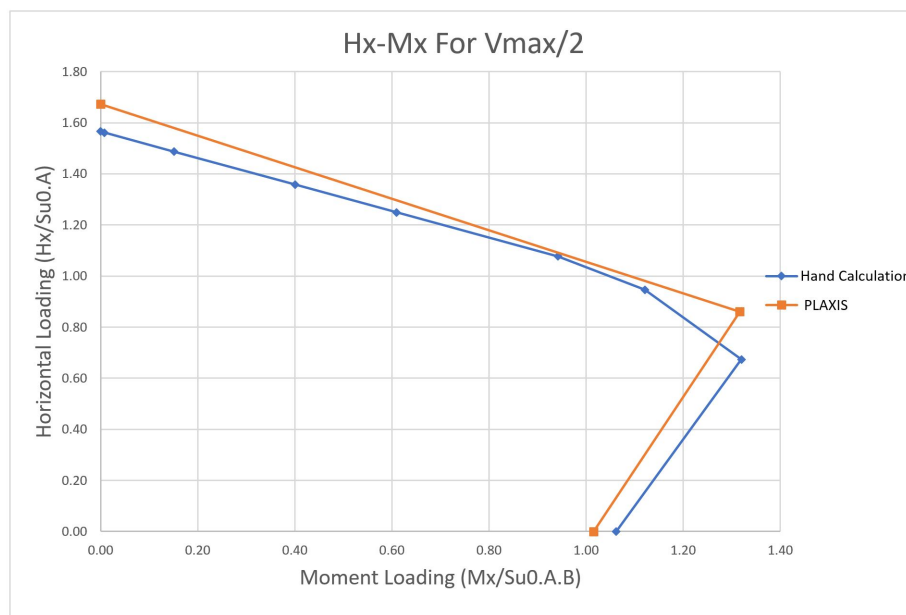


Figure 6.7: Comparison of PLAXIS 3D and hand calculation in $H_x - M_x$ normalised load space having $V_{max}/2$ constantly applied

Having more points before reaching the pure moment loading on Graph 6.7 could show if the PLAXIS has overshooting results or its the same as the hand calculation.

For moment in x direction (M_x) is the only condition where hand calculation gives higher amount than PLAXIS.

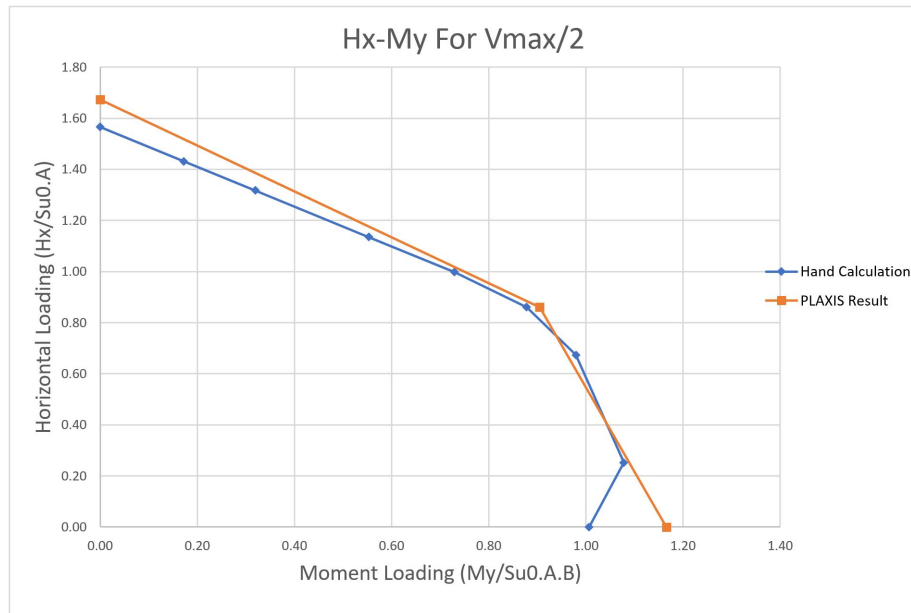


Figure 6.8: Comparison of PLAXIS 3D and hand calculation in $H_x - M_y$ normalised load space having $V_{max}/2$ constantly applied

Moment in y direction is acting on the longer side of the foundation, therefore there is longer skirts. There is some soil and structure attachment forces though the tension cut-off option is used. The forces along the longer skirts have higher value and that is why the results from PLAXIS is almost 16% more than the hand calculation ones.

As depicted in figure 6.2, hand calculation sliding result in the y direction differs from PLAXIS results by 12% which is the reason to have such difference in the results in figure 6.9. Having more models can indicate that how much these two differ for different combinations.

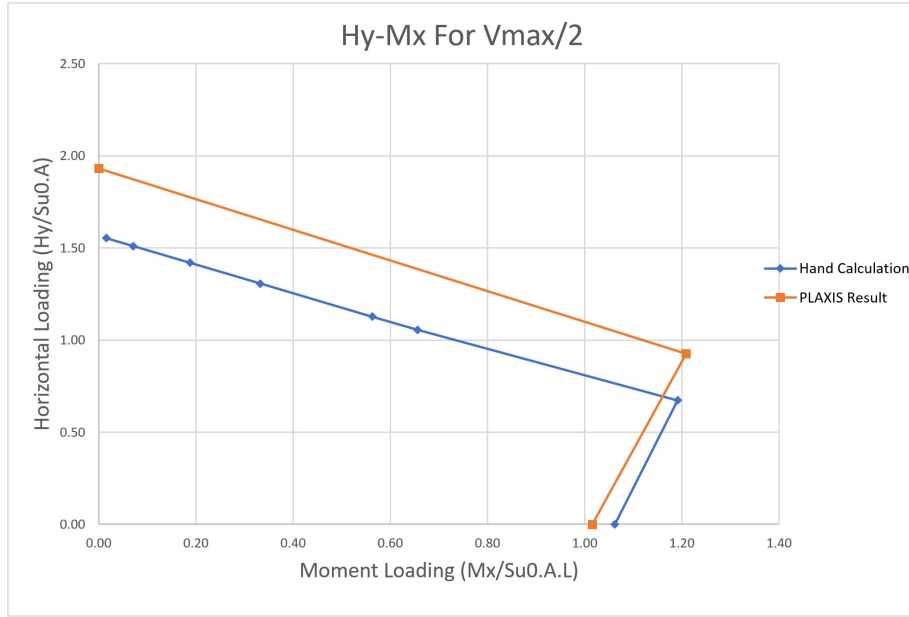


Figure 6.9: Comparison of PLAXIS 3D and hand calculation in $H_y - M_x$ normalised load space having $V_{max}/2$ constantly applied

Having the gap in both horizontal load in y direction explains the two points. These points are the second point of the PLAXIS modeling and its peer point on hand calculation line where H_y and M_y are combined. These points have almost the same moment load though the horizontal load varies due to many reasons given previously.

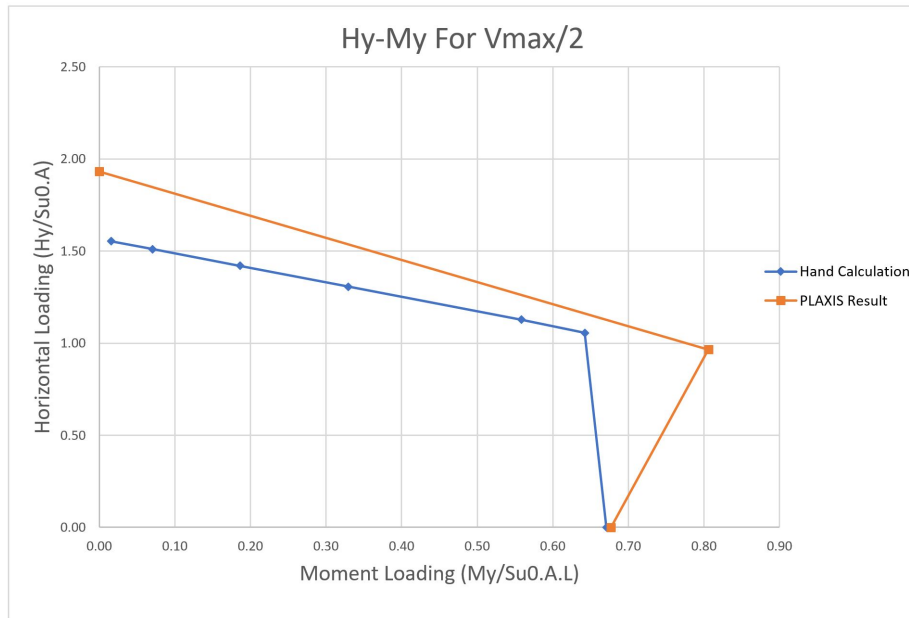


Figure 6.10: Comparison of PLAXIS 3D and hand calculation in $H_y - M_y$ normalised load space having $V_{max}/2$ constantly applied

Chapter 7

Summary and Recommendations for Further Work

7.1 Summary and Conclusions

The purpose of this thesis is to determine the bearing capacity of a rectangular mudmat foundation. The foundation is under different load combination including vertical, horizontal and moment in different direction. The ultimate bearing capacity is measured using hand calculation and a finite element(FE) software. The FE software is *PLAXIS 3D* and hand calculations are based on [DNV. \(1992\)](#) Classification Note. The final results are set on graphs and a respective comparison is made to point out the differences.

The vertical bearing capacity evaluated by PLAXIS is 2% more than hand calculation which is a accurate approximation to approve the model's accuracy.

Horizontal bearing capacity differs by 12% which shows that either PLAXIS 3D is overshooting in results or there are some parameters which are not considered by hand calculation.

For pure moment loading hand calculation analysis is expected to raise with respect of the vertical load increasing up to an specific point and then to be reduced. Having no vertical load force, the moment is expected to be zero as well as in hand calculation. The reason is that no tension load is included in hand calculation formula.

To model the pure moment load on PLAXIS 3D, the option for tension cut-off is selected to set the model in the same position as it is in hand calculation. Although the tension cut-off is activated on all soil-structure interfaces yet, some capacity for moment loading is resulted in the

absence of vertical loading. The reason is that there are some forces along the surface of the plate and soil elements which go along the skirt plates and resist the model from failing.

Graph 7.1 presents the maximum of each load reached either using PLAXIS 3D or hand calculation.

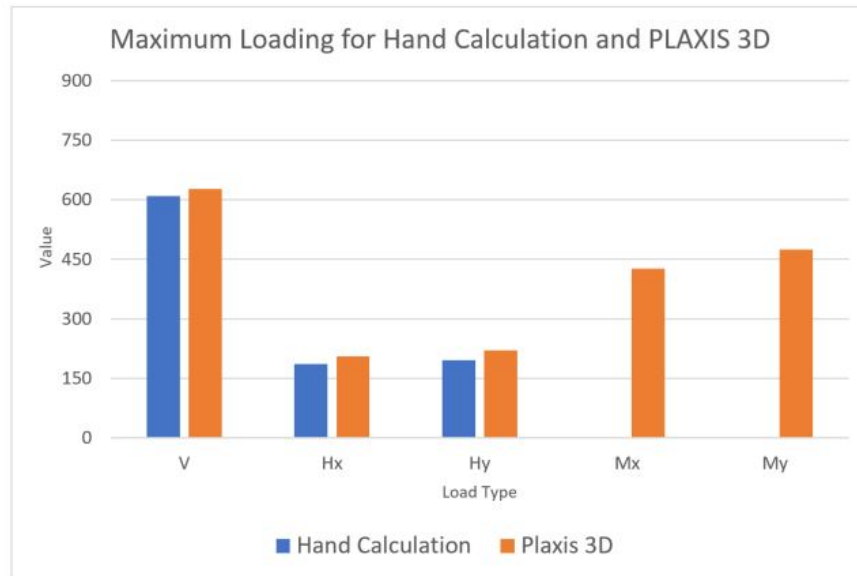


Figure 7.1: Comparing results from hand calculation and PLAXIS 3D

Generally pure loading does not happen in the real condition. On offshore condition there are many different loading happening to a structure simultaneously. Different load combination is possible to happen and that is the main aim for this thesis. Different combination of the loads are modelled and the results are presented through this thesis.

Chapter 6 provides the graph for each loading condition. According the graphs in this chapter hand calculation is more conservative than *PLAXIS 3D*. The *PLAXIS 3D* modelling results are mostly higher than evaluation with hand calculation.

7.2 Recommendations for Further Work

Recommended feature works are as follows:

- This thesis does not consider dynamic and cyclic load and as a future study subject it is recommended to analyse the bearing capacity of a mudmat foundation under these type of loads.

- Torsional loading is modelled on PLAXIS by the author just to check the results and deformation. The results are provided in Appendix C.1.4. Another possible subject is to analyse the effect of the torsional loading on the foundation as a combination with other loads.
- This thesis provided an overview on different methods which is based on Classification Notes by DNV. (1992). It is recommended to compare PLAXIS results with the results from different methods.
- Having vertical, horizontal and moment loads varying in different direction is a possibility which needs a six-dimensional graph. It is not possible to draw such a graph, yet it is possible to do the analysis which is a recommendation for future studies.

Bibliography

- Acosta-Martinez, H. E., Gourvenec, S. M., and Randolph, M. F. (2008). An experimental investigation of a shallow skirted foundation under compression and tension. *Soils and Foundations*, 48(2):247–254.
- Andersen, K. H., Jostad, H. P., et al. (1999). Foundation design of skirted foundations and anchors in clay. In *Offshore technology conference*. Offshore Technology Conference.
- Andersen, K. H., Lunne, T., Kvalstad, T. J., and Forsberg, C. F. (2008). Deep water geotechnical engineering. In *Proceedings of the 24th National Conference of the Mexican Society of Soil Mechanics, Aguascalientes, Mexico City, Mexico*, pages 26–29.
- API, R. (2000). 2a-wsd. *Recommended practice for planning, designing and constructing fixed offshore platforms-working stress design*, 21.
- Bowles, L. et al. (1996). *Foundation analysis and design*. McGraw-hill.
- Bransby, M. and Yun, G.-J. (2009). The undrained capacity of skirted strip foundations under combined loading. *Géotechnique*, 59(2):115–125.
- Das, B. (2007). *Principles of Foundation Engineering (6th ed.)*. Stamford, CT: Cengage Publisher.
- Davis, E., Booker, J., et al. (1985). The effect of increasing strength with depth on the bearing capacity of clays. *Golden Jubilee of the International Society for Soil Mechanics and Foundation Engineering: Commemorative Volume*, page 185.
- DNV. (1992). *Foundation. Classification notes No.30.4*. Høvik, Norway: DNV.
- DNV, A. G. (2010). *Offshore Standard DNV-OS-J101*. Oslo: DNV.

- Dunne, H., M. C. M. L. B. N. . W. R. (2015). Undrained bearing capacity of skirted mudmats on inclined seabeds. *Frontiers in Offshore Geotechnics III - 3rd International Symposium on Frontiers in Offshore Geotechnics, ISFOG*, 2:783–788.
- Dyvik, R., Andersen, K. H., Hansen, S. B., and Christophersen, H. P. (1993). Field tests of anchors in clay. i: Description. *Journal of Geotechnical Engineering*, 119(10):1515–1531.
- Emdal, A. G. (2011). *Theoretical Soil Mechanics in TBA4105*. NTNU; Trondheim.
- Feng, X., Randolph, M., Gourvenec, S., and Wallerand, R. (2014). Design approach for rectangular mudmats under fully three-dimensional loading. *Géotechnique*, 64(1):51–63.
- Gazetas, G. (1991). Foundation vibrations. In *Foundation engineering handbook*, pages 553–593. Springer.
- Gourvenec, S. and Barnett, S. (2011). Undrained failure envelope for skirted foundations under general loading. *Géotechnique*, 61(3):263–270.
- Hansen, J. B. (1970). A revised and extended formula for bearing capacity.
- Hardin, B. O. (1978). The nature of stress-strain behavior for soils. In *From Volume I of Earthquake Engineering and Soil Dynamics—Proceedings of the ASCE Geotechnical Engineering Division Specialty Conference, June 19-21, 1978, Pasadena, California. Sponsored by Geotechnical Engineering Division of ASCE in cooperation with;* number Proceeding.
- Houlsby, G. and Puzrin, A. (1999). The bearing capacity of a strip footing on clay under combined loading. In *Proceedings of the Royal Society of London A: Mathematical, Physical and Engineering Sciences*, volume 455, pages 893–916. The Royal Society.
- Kramer, S. L. (2014). *Geotechnical Earthquake Engineering*. Pearson Education Limited. Pearson New International Edition.
- Logan, D. L. (2011). *A first course in the finite element method*. Cengage Learning.
- Mana, D. S., Gourvenec, S., and Martin, C. M. (2012a). Critical skirt spacing for shallow foundations under general loading. *Journal of geotechnical and geoenvironmental engineering*, 139(9):1554–1566.

- Mana, D. S., Gourvenec, S. M., Randolph, M. F., and Hossain, M. S. (2012b). Failure mechanisms of skirted foundations in uplift and compression. *International Journal of Physical Modelling in Geotechnics*, 12(2):47–62.
- Martin, C., Dunne, H., Wallerand, R., and Brown, N. (2015). Three-dimensional limit analysis of rectangular mudmat foundations. In *Proceedings of the 3rd international symposium on frontiers in offshore geotechnics (ISFOG 2015)*, pages 789–794. CRC Press London, UK.
- Meyerhof, G. t. (1953). The bearing capacity of foundations under eccentric and inclined loads. In *Proc. of the 3rd Int. Conf. on SMFE*, volume 1, pages 440–445.
- O’Loughlin, C. D. (2015). Session report: offshore geotechnics at icpmg 2014. *International Journal of Physical Modelling in Geotechnics*, 15(2):98–115.
- PLAXIS (2017). *PLAXIS 3D Reference Manual*. Delft, The Netherlands.
- Rahardjo, H., Hritzuk, K., Leong, E. C., and Rezaur, R. (2003). Effectiveness of horizontal drains for slope stability. *Engineering Geology*, 69(3-4):295–308.
- Randolph, M., Gourvenec, S., White, D., and Cassidy, M. (2011). *Offshore geotechnical engineering*, volume 2. Spon Press New York.
- Reddy, J. N. (1993). *An introduction to the finite element method*, volume 2. McGraw-Hill New York.
- Salençon, J. and Matar, M. (1982). Bearing capacity of circular shallow foundations. *Foundation engineering*, pages 159–168.
- Seed, H. B. (1970). Soil moduli and damping factors for dynamic response analysis. *EERC*.
- Tani, K. and CRAIG, W. (1995). Bearing capacity of circular foundations on soft clay of strength increasing with depth. *Soils and Foundations*, 35(4):21–35.
- Terzaghi, K. (1944). *Theoretical soil mechanics*. Chapman And Hali, Limited John Wiler And Sons, Inc; New York.
- Ulvestad, A. and S. Giese, A. S. (2017). mudmat perforation- geotechnical serviceability assessment of foundation performance on soft soil. *ISFOG*.
- Veritas, D. N. (1992). Classification notes no. 30.4 foundations. *Oslo, Norway, February*.

- Watson, P., Randolph, M., Bransby, M., et al. (2000). Combined lateral and vertical loading of caisson foundations. In *Offshore technology conference*. Offshore Technology Conference.
- Yun, G. and Bransby, M. (2007). The undrained vertical bearing capacity of skirted foundations. *Soils and foundations*, 47(3):493–505.

Appendix A

Table of Symbols and Acronyms

A Foundation area.

A_0 Foundation effective area.

AR Active Rankine-zone.

B Foundation width.

B_0 Foundation effective width.

c The undrained shear strength.

D Skirt depth.

d_c Depth factor for shear strength.

d_q Depth factor for load over the foundation.

E_u Young's modulus at the surface.

E_{inc} Young's modulus increasing inclination factor.

F_{H1} Total horizontal forces

G Soil shear modulus.

G_0 The surface shear modulus.

G_{max} Maximum soil shear modulus.

H_x Horizontal loading in the x direction.

H_y Horizontal loading in the y direction.

i_c Inclination factor for shear strength.

i_q Inclination factor for load over the foundation.

s_γ Inclination factor for soil unit weight.

K_0 Coefficient of lateral earth pressure.

k_a Active earth pressure coefficient.

k_p Passive earth pressure coefficient.

L Foundation length.

L_0 Foundation effective length.

M_B Moment along the width of the foundation.

M_L Moment along the length of the foundation.

N_c bearing capacity factor for shear strength.

N_γ bearing capacity factor for soil unit weight.

N_q bearing capacity factor for load over the foundation.

P Earth pressure.

P_a Active earth pressure.

Pl Prandtl-zone.

PR Passive Rankine-zone.

P_p Passive earth pressure.

Q_V Vertical load.

q_{ult} The ultimate bearing capacity.

\bar{q} Average load on foundation.

r Roughness ratio.

- R_{inter} Roughness ratio on PLAXIS.
- $R_{H,EP}$ Resistances of the embedded horizontal soil pressure.
- $R_{H,B}$ Resistances of base friction.
- $R_{H,s}$ Resistances of side friction.
- s_c Shape factor for shear strength.
- s_q Shape factor for load over the foundation.
- s_γ Shape factor for soil unit weight.
- S_u The undrained shear strength.
- S_{u0} The undrained shear strength at the foundation or its skirts tip.
- S_{u1} average strength above the base level.
- S_{u2} equivalent shear strength below base level.
- S_{u-Base} The undrained shear strength at the surface.
- S_{inc} The undrained shear strength increasing inclination factor.
- $S_{u,rem}$ Remoulded shear strength.
- V Vertical Loading.
- Z_r Reference depth.
- Z Depth.
- 3D** Three-Dimensional.
- ALE** Abnormal Level Earthquake.
- ALS** Accidental Limit State.
- API** American Petroleum Institute.
- DOF** Degrees Of Freedom
- ELE** Extreme Level Earthquake.

FEM Finite Element Method.

FEA Finite Element Analysis.

ISO International Organization for Standardization.

SLS Serviceability Limit State.

SSI Soil-Structure Interaction

ULS Ultimate Limit State.

α Fitting in the experimental results parameter.

β τ_y/τ_x

γ_m Material factor.

γ_{sat} Soil unit weight for saturated condition.

γ_{unsat} Soil unit weight for unsaturated condition.

ΔB Eccentricity along the width of the foundation.

ΔL Eccentricity along the length of the foundation.

κ Undrained shear strength increasing ratio.

ν Poisson ratio.

τ_x Shear stress in the x direction.

τ_y Shear stress in the y direction.

ϕ Friction angle.

Appendix B

Hand Calculation Results

This chapter is to present all the result from hand calculation. The method to do calculation is given in Chapter 4. Graphs are made using *Excel 2016*.

B.1 Introduction

The hand calculation is based on (DNV, 1992) and all assumption are given. There are more hand calculation results comparing to PLAXIS because it is faster to do and it does not need to have a computer.

B.1.1 Results

Hand calculation method is presented through the chapter 4. Following table and graphs are showing different load combinations. Loads in different directions are normalised with a constant amount of $S_{u0}.A$. For moment loading to make a dimensionless comparable results, $S_{u0}.A.B$ and $S_{u0}.A.L$ are used to do normalisation in the x and y direction respectively.

Table B.1: Vertical and horizontal loading in x direction ratio

V	H_x	$V/S_{u0}.A$	$H_x/S_{u0}.A$
kN	kN	-	-
610.632	0	5.14	0
409.86	148.5	3.45	1.25
305.32	186.0	2.57	1.57
152.66	185.0	1.29	1.56
0	185.5	0	1.56

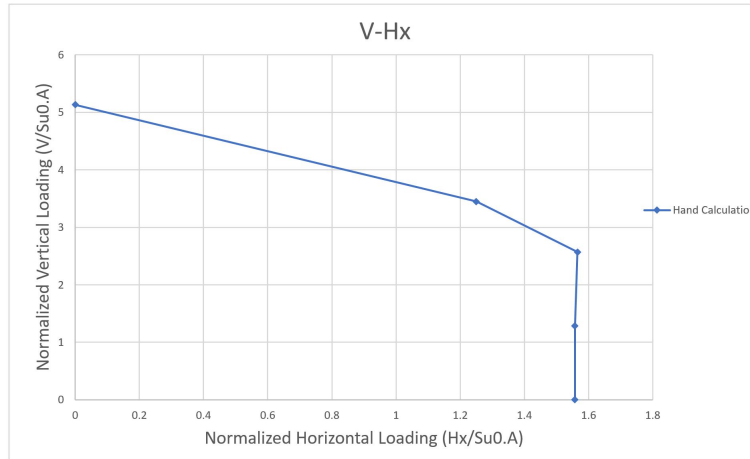


Figure B.1: The normalized vertical versus horizontal loading in x direction graph for hand calculation

Table B.2: Vertical and horizontal loading in y direction ratio

V	H_y	$V/S_{u0}.A$	$H_y/S_{u0}.A$
kN	kN	-	-
610.632	0	5.14	0
445.50	175.824	3.75	1.48
305.316	195.6.0	2.57	1.65
0	195.6	0	1.65

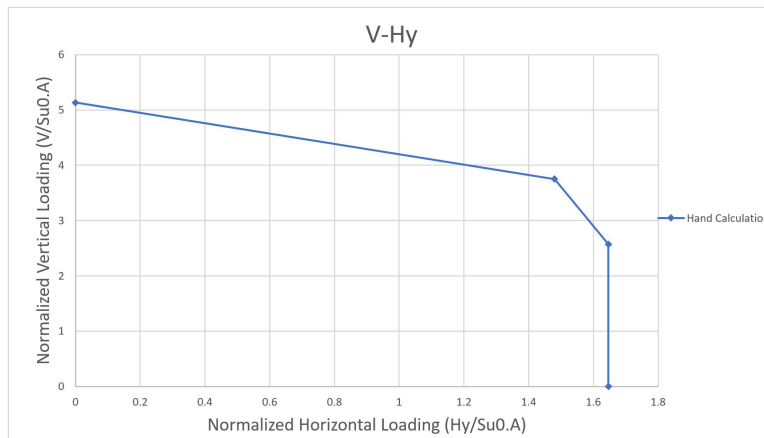


Figure B.2: The normalized vertical versus horizontal loading in y direction graph for hand calculation

Table B.3: Vertical and moment loading in x direction ratio

V	M_x	$V/S_{u0}.A$	$M_x/S_{u0}.A.L$
kN	kN.m	-	-
610.00	0	5.13	0.00
488.51	850.00	4.11	1.192
313.56	769.00	2.64	1.079
305.32	751.00	2.57	1.054
244.25	615.00	2.06	0.863
203.54	521.30	1.71	0.731
174.47	452.50	1.47	0.635
152.66	400.00	1.29	0.561

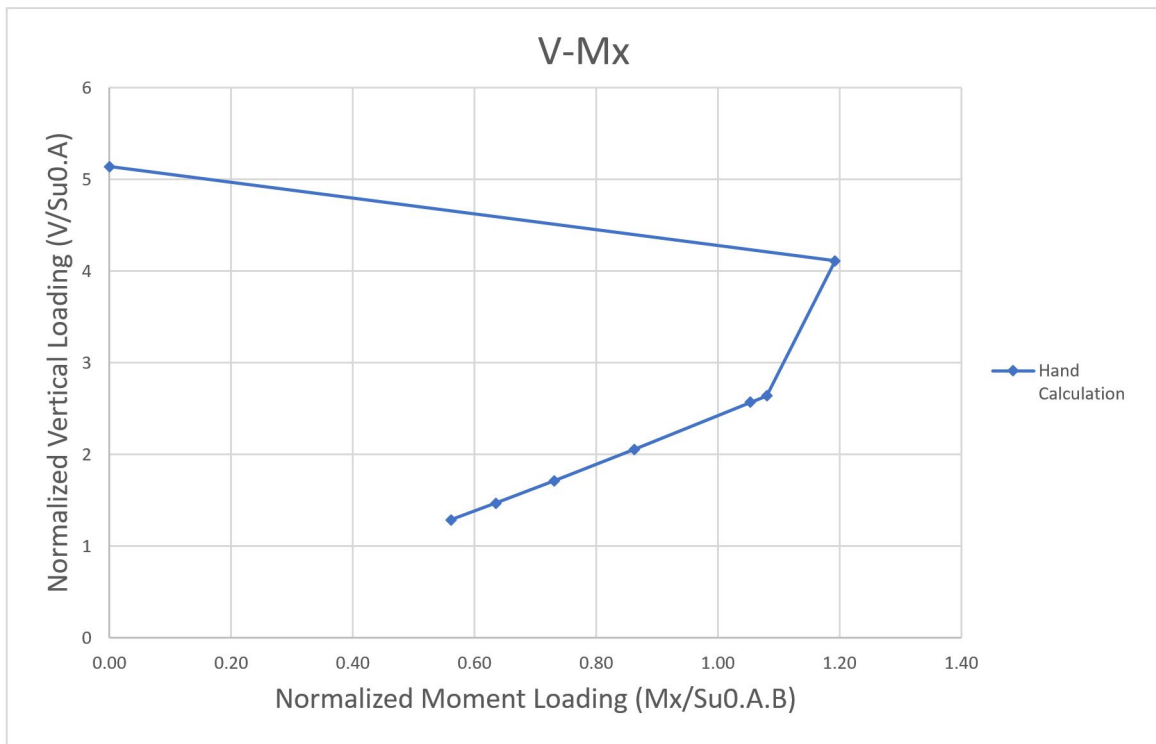


Figure B.3: The normalized vertical versus moment loading in x direction graph for hand calculation

Table B.4: Vertical and moment loading in y direction ratio

V	M_y	$V/S_{u0.A}$	$M_y/S_{u0.A.B}$
kN	kN.m	-	-
610.00	0	5.13	0.00
530.98	634.20	4.47	0.890
313.56	701.50	2.64	0.984
305.32	687.10	2.57	0.964
244.25	575.50	2.06	0.807
203.54	495.30	1.71	0.695
174.47	434.90	1.47	0.610
152.66	387.80	1.29	0.544

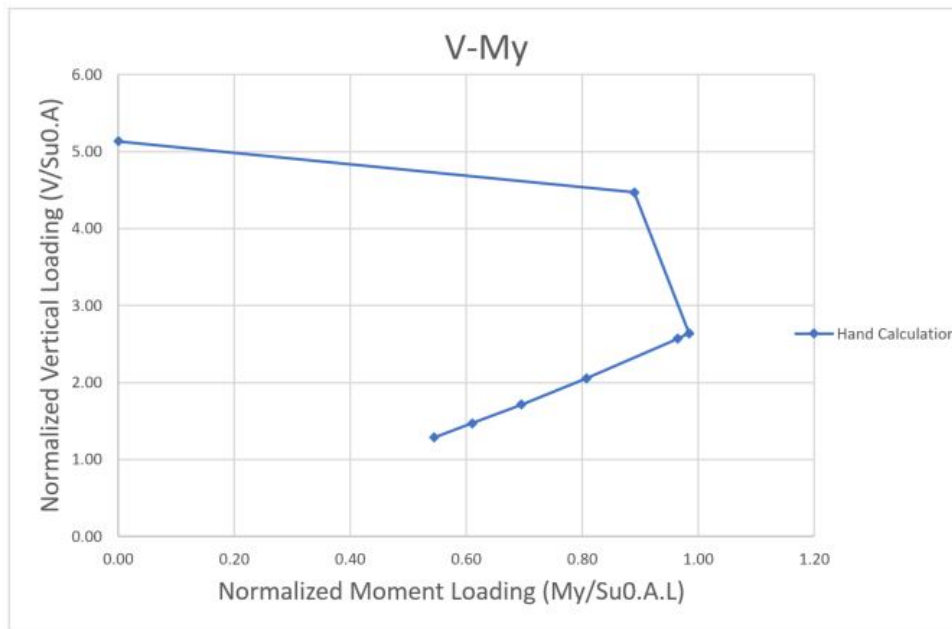


Figure B.4: The normalized vertical versus moment loading in y direction graph for hand calculation

Table B.5: Horizontal and moment loading in x direction ratio while the vertical loading is kept constant as half of its maximum

V	H_x	M_x	$V/S_{u0}.A$	$H_x/S_{u0}.A$	$M_x/S_{u0}.A.L$
kN	kN	kN.m	-	-	-
305.32	0	756.9	2.57	0.00	1.06
305.32	80.00	940.80	2.57	0.67	1.32
305.32	112.42	799.00	2.57	0.95	1.12
305.32	127.93	671.55	2.57	1.08	0.94
305.32	148.40	434.80	2.57	1.25	0.61
305.32	161.30	285.60	2.57	1.36	0.40
305.32	176.67	107.92	2.57	1.49	0.15
305.32	185.50	5.60	2.57	1.56	0.01
305.32	186.00	0.00	2.57	1.57	0.00

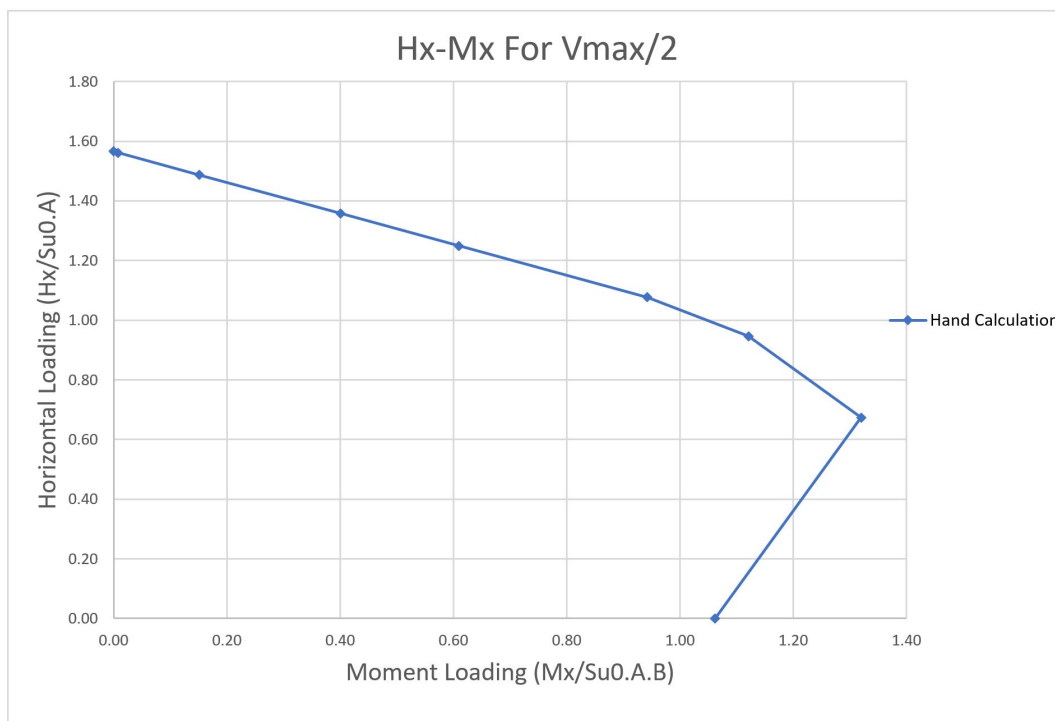


Figure B.5: The normalized horizontal versus moment loading in x direction graph for hand calculation

Table B.6: Horizontal load in the x direction and moment loading in y direction ratio while the vertical loading is kept constant as half of its maximum

V	H_x	M_y	$V/S_{u0.A}$	$H_x/S_{u0.A}$	$M_y/S_{u0.A.B}$
kN	kN	kN.m	-	-	-
305.316	0	717.51	2.57	0.00	1.01
305.32	30.00	768.25	2.57	0.25	1.08
305.32	80.00	698.25	2.57	0.67	0.98
305.32	102.25	625.71	2.57	0.86	0.88
305.32	118.55	520.00	2.57	1.00	0.73
305.32	134.90	394.00	2.57	1.14	0.55
305.32	156.48	227.59	2.57	1.32	0.32
305.32	170.09	122.60	2.57	1.43	0.17
305.32	186	0	2.57	1.57	0

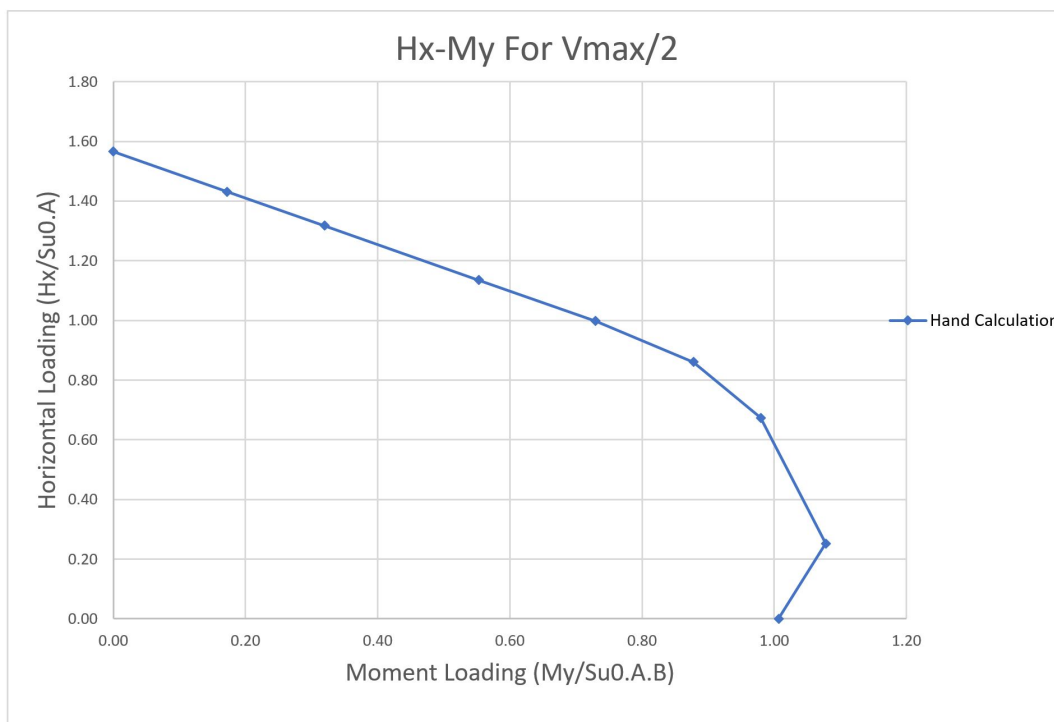


Figure B.6: The normalized x directed horizontal load versus moment loading in y direction graph for hand calculation

Table B.7: Horizontal load in the y direction and moment loading in x direction ratio while the vertical loading is kept constant as half of its maximum

V	H_y	M_x	$V/S_{u0}.A$	$H_y/S_{u0}.A$	$M_x/S_{u0}.A.L$
kN	kN	kN.m	-	-	-
305.32	0.00	756.90	2.57	0.00	1.06
305.32	80.00	849.21	2.57	0.67	1.19
305.32	125.38	467.34	2.57	1.06	0.66
305.32	133.97	401.10	2.57	1.13	0.56
305.32	155.24	237.10	2.57	1.31	0.33
305.32	168.62	133.99	2.57	1.42	0.19
305.32	179.45	50.50	2.57	1.51	0.07
305.32	184.53	11.30	2.57	1.55	0.02
305.32	0.00	0.00	2.57	0.00	0.00

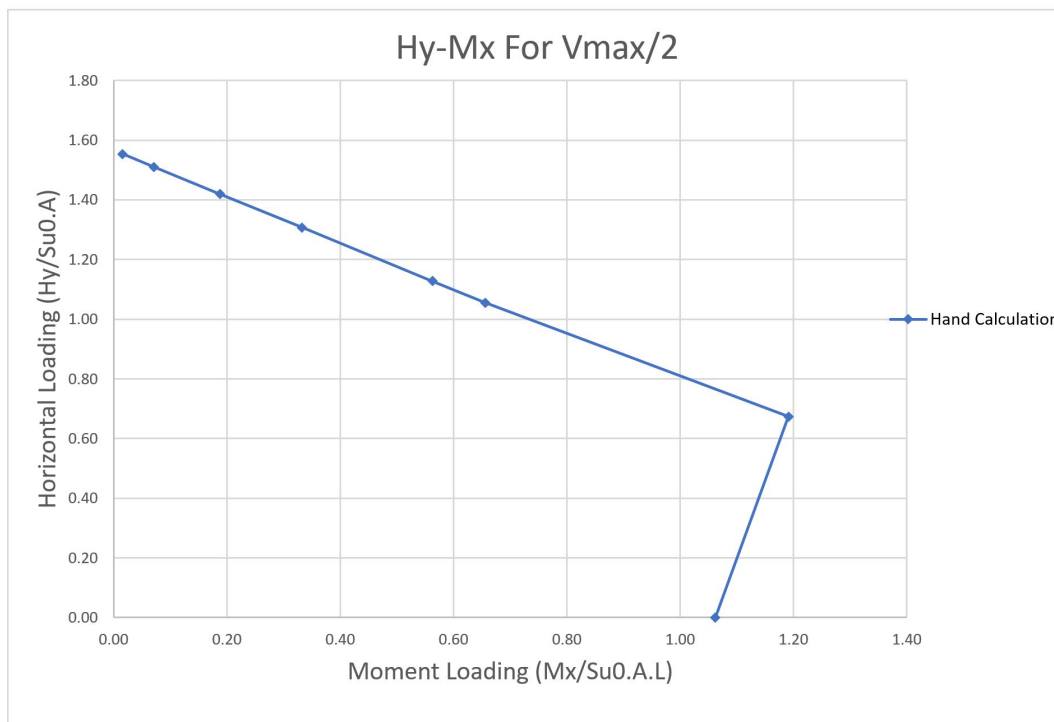


Figure B.7: The normalized y directed horizontal load versus moment loading in x direction graph for hand calculation

Table B.8: Horizontal and moment loading in y direction ratio while the vertical loading is kept constant as half of its maximum

V	H_y	M_y	$V/S_{u0}.A$	$H_y/S_{u0}.A$	$M_y/S_{u0}.A.B$
kN	kN	kN.m	-	-	-
305.32	0.00	717.51	2.57	0.00	1.01
305.32	125.38	686.96	2.57	1.06	0.96
305.32	133.97	597.36	2.57	1.13	0.84
305.32	155.24	352.29	2.57	1.31	0.49
305.32	168.62	199.12	2.57	1.42	0.28
305.32	179.45	75.74	2.57	1.51	0.11
305.32	184.53	16.96	2.57	1.55	0.02

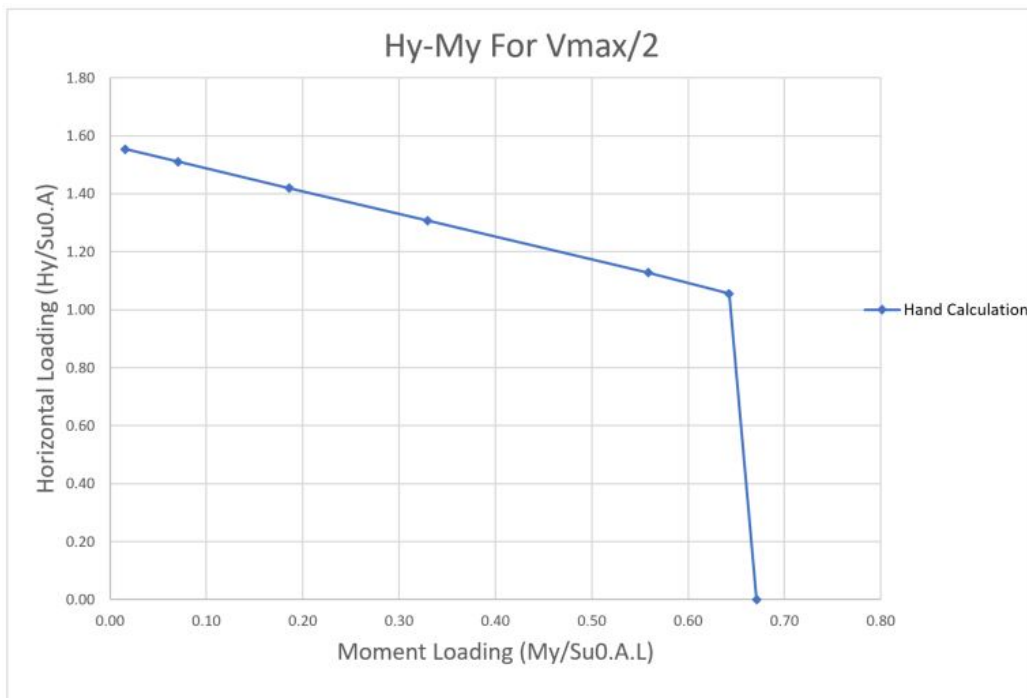


Figure B.8: The normalized horizontal versus moment loading in y direction graph for hand calculation

Appendix C

Computer Simulation

In this chapter results from PLAXIS 3D- 2017 are presented. Graphs are mostly made in *Excel 2016* yet, some are exported from *PLAXIS 3D*.

C.1 Introduction

Working with PLAXIS 3D needs high-quality computers and much of time in hand so meshing is fine enough to have a better understanding of the results and having more accurate graphs. This thesis was held with normal computers with limited storage capacity. The author knows that saving all the steps of calculation in PLAXIS is the best condition for the results yet, due to limitation previously mentioned not as many steps could be saved. To get following results, the model characteristics are kept constant. Chapter [3](#) presents the model properties.

C.1.1 Results

Table C.1: Vertical and horizontal loading in *x* direction ratio

V	H_x	$V/S_{u0}.A$	$H_x/S_{u0}.A$
kN	kN	-	-
627.11	0	5.28	0
313.56	198.67	2.64	1.67
0	204.50	0	1.72

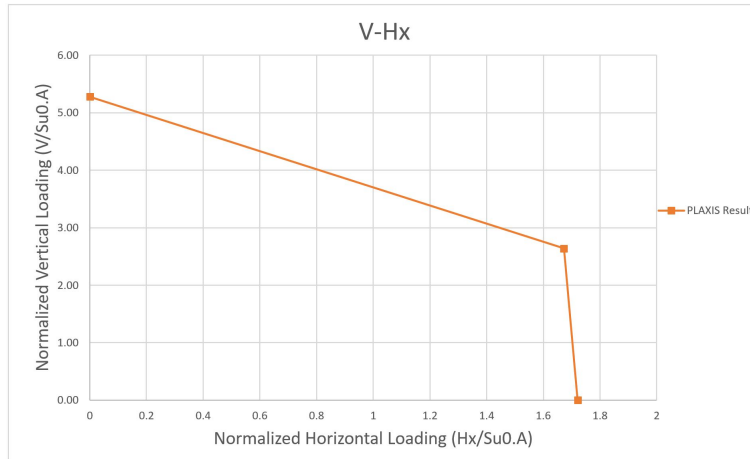


Figure C.1: The normalized vertical versus horizontal loading in *x* direction graph resulted by PLAXIS 3D

Table C.2: Vertical and horizontal loading in *y* direction ratio

V	H_y	$V/S_{u0}.A$	$H_y/S_{u0}.A$
kN	kN	-	-
627.11	0	5.28	0
313.55	229.50	2.64	1.93
0	220.10	0	1.85

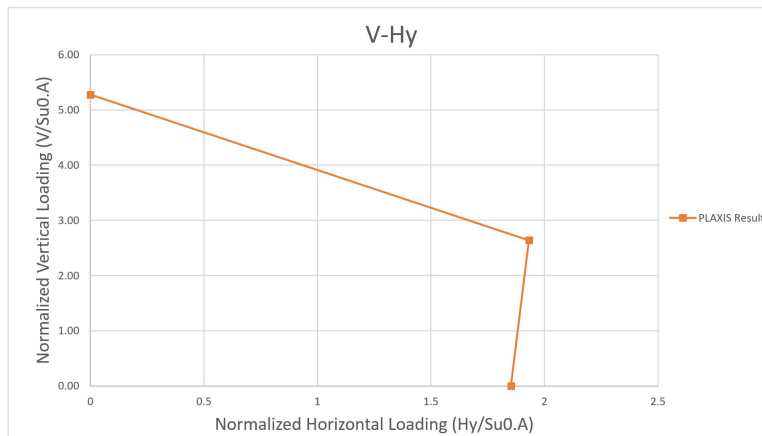


Figure C.2: The normalized vertical versus horizontal loading in *y* direction graph resulted by PLAXIS 3D

Table C.3: Vertical and moment loading in *x* direction ratio

V	M_x	$V/S_{u0} \cdot A$	$M_x/S_{u0} \cdot A \cdot L$
kN	kN.m	-	-
627.11	0	5.28	0
475	854.89	4.00	1.20
313.56	830.60	2.64	1.17
0	427.10	0	0.60

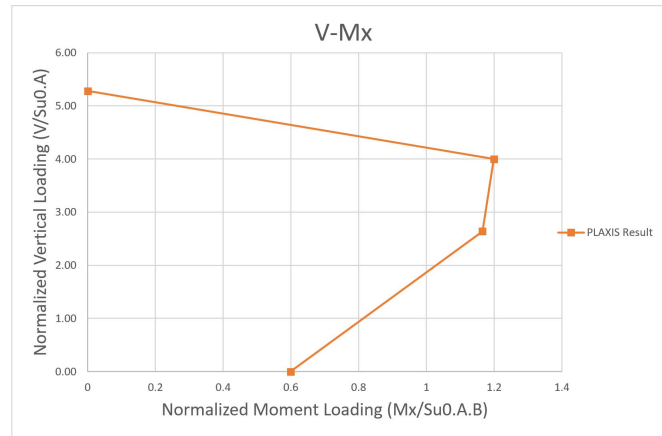


Figure C.3: The normalized vertical versus moment loading in *x* direction graph resulted by PLAXIS 3D

Table C.4: Vertical and moment loading in *y* direction ratio

V	M_y	$V/S_{u0} \cdot A$	$M_y/S_{u0} \cdot A \cdot B$
kN	kN.m	-	-
627.11	0	5.28	0
500.00	638.78	4.2	0.96
313.56	723.75	2.64	1.02
0	475.00	0	0.67

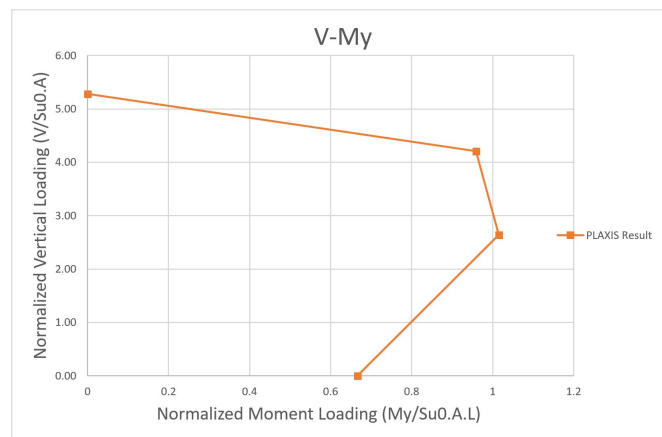


Figure C.4: The normalized vertical versus moment loading in *y* direction graph resulted by PLAXIS 3D

Table C.5: Horizontal and moment loading in x direction ratio while the vertical loading is kept constant as half of its maximum

V	H_x	M_x	$V/S_{u0} \cdot A$	$H_x/S_{u0} \cdot A$	$M_x/S_{u0} \cdot A \cdot L$
kN	kN	kN.m	-	-	-
313.56	0	723.75	2.64	0	1.02
313.56	102.25	938.40	2.64	0.86	1.32
313.56	198.69	0	2.64	1.67	0

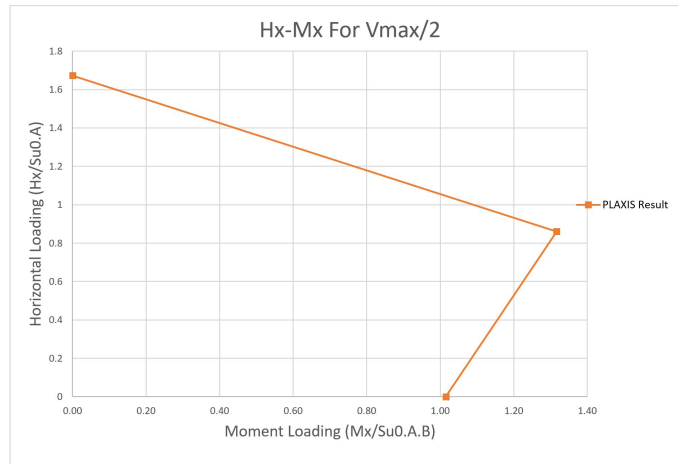


Figure C.5: The normalized horizontal versus moment loading in x direction graph for hand calculation

Table C.6: Horizontal and moment loading in y direction ratio while the vertical loading is kept constant as half of its maximum

V	H_x	M_y	$V/S_{u0} \cdot A$	$H_x/S_{u0} \cdot A$	$M_y/S_{u0} \cdot A \cdot B$
kN	kN	kN.m	-	-	-
313.555	0	830.60	2.64	0	1.17
313.555	102.25	644.90	2.64	0.86	0.90
313.555	198.69	0	2.64	1.67	0

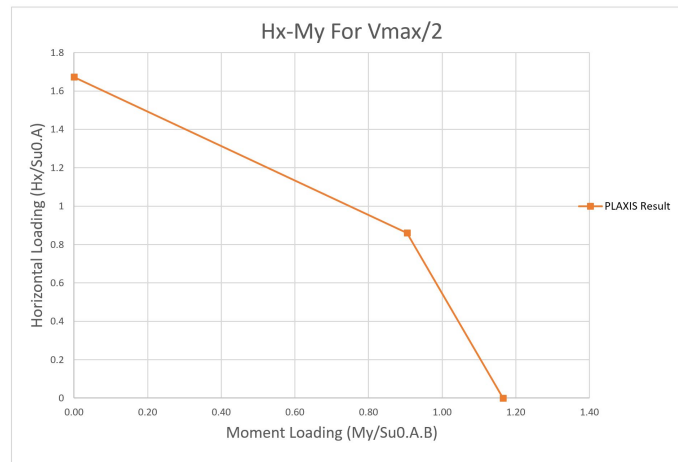


Figure C.6: The normalized horizontal versus moment loading in y direction graph for hand calculation

Table C.7: Horizontal and moment loading in x direction ratio while the vertical loading is kept constant as half of its maximum

V	H_y	M_x	$V/S_{u0}\cdot A$	$H_y/S_{u0}\cdot A$	$M_x/S_{u0}\cdot A\cdot B$
kN	kN	kN.m	-	-	-
313.555	0	723.75	2.64	0	1.02
313.555	110.05	861.50	2.64	0.93	1.21
313.555	229.50	0	2.64	1.93	0

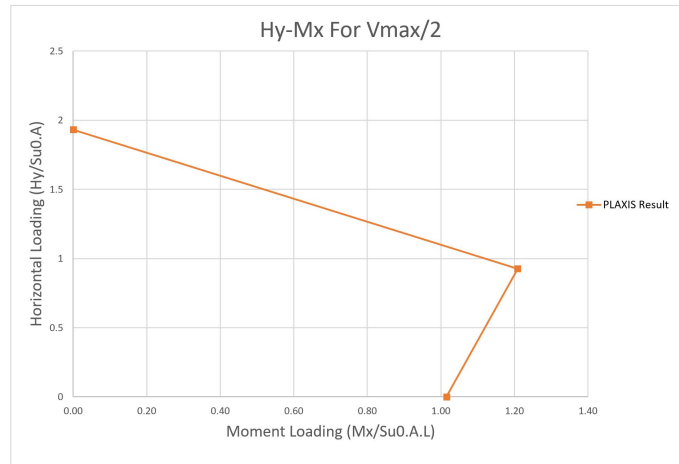


Figure C.7: The normalized horizontal versus moment loading in x direction graph for hand calculation

Table C.8: Horizontal and moment loading in y direction ratio while the vertical loading is kept constant as half of its maximum

V	H_y	M_y	$V/S_{u0}\cdot A$	$H_y/S_{u0}\cdot A$	$M_y/S_{u0}\cdot A\cdot B$
kN	kN	kN.m	-	-	-
313.555	0	830.60	2.64	0	1.17
313.555	114.75	816.75	2.64	0.97	1.15
313.555	229.50	0	2.64	1.93	0

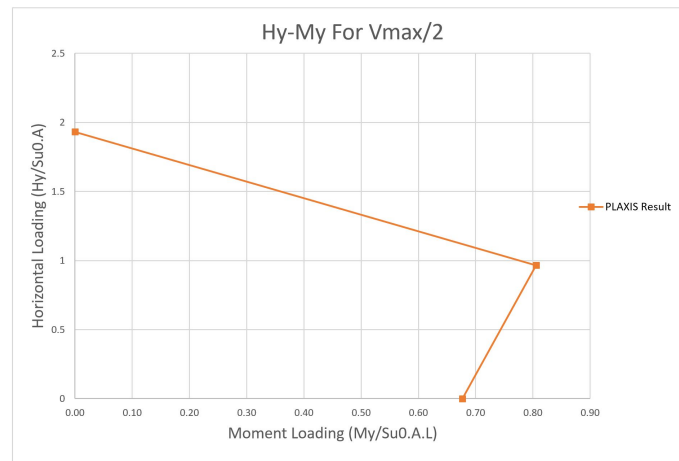


Figure C.8: The normalized horizontal versus moment loading in y direction graph for hand calculation

C.1.2 Failure Mechanisms

To see the failure mechanism and compare among different condition. To show the failure line the legend is adopted for each graph and they are presented in three categories.

One Dimensional Loading

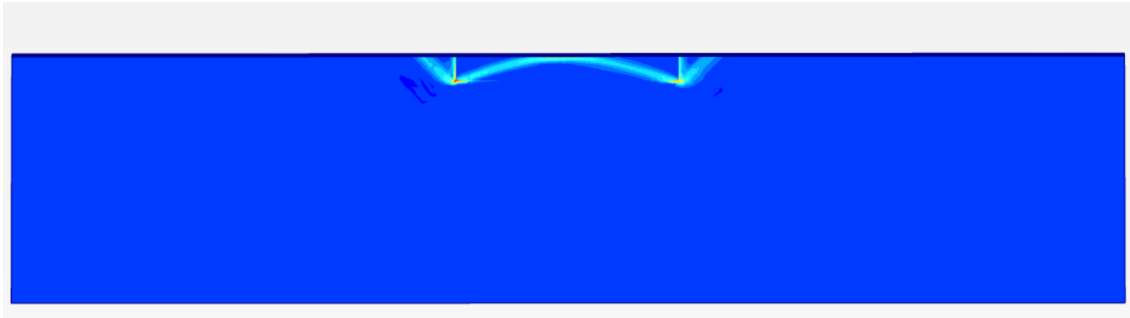


Figure C.9: Failure mechanism for pure horizontal loading in the x direction on the longer edge

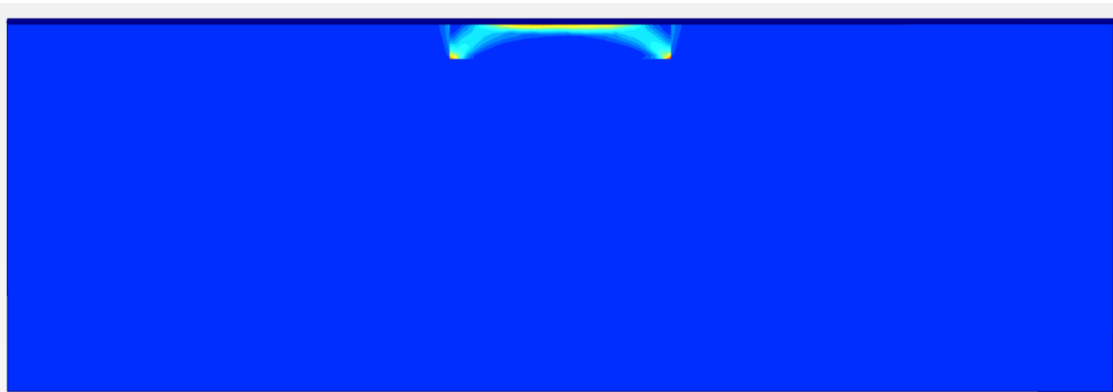


Figure C.10: Failure mechanism for pure horizontal loading in the x direction on the smaller edge

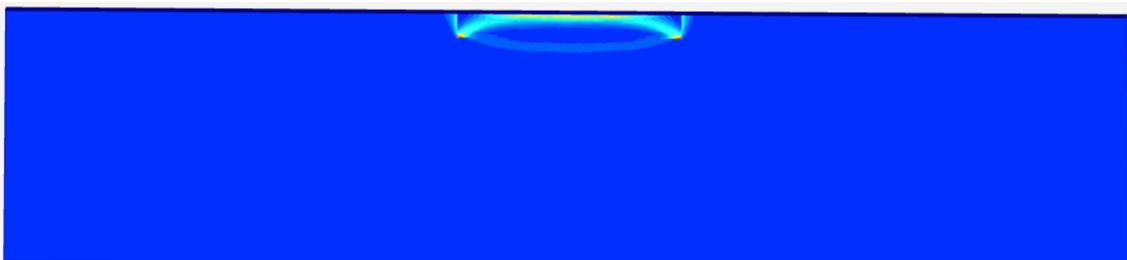


Figure C.11: Failure mechanism for pure horizontal loading in the y direction on the longer edge

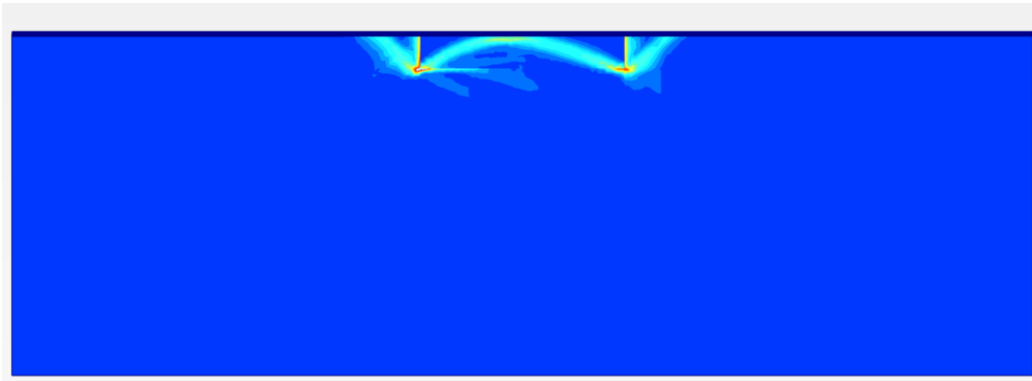


Figure C.12: Failure mechanism for pure horizontal loading in the y direction on the smaller edge



Figure C.13: Failure mechanism for pure moment loading in the x direction on the longer edge

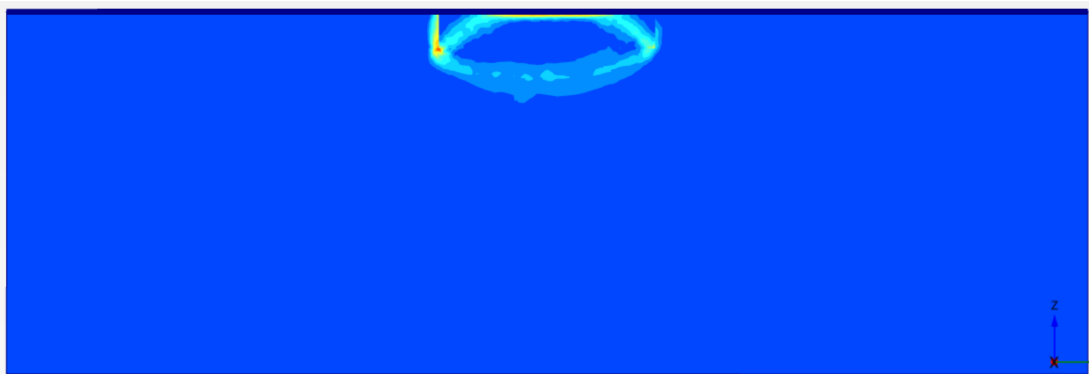


Figure C.14: Failure mechanism for pure moment loading in the x direction on the smaller edge

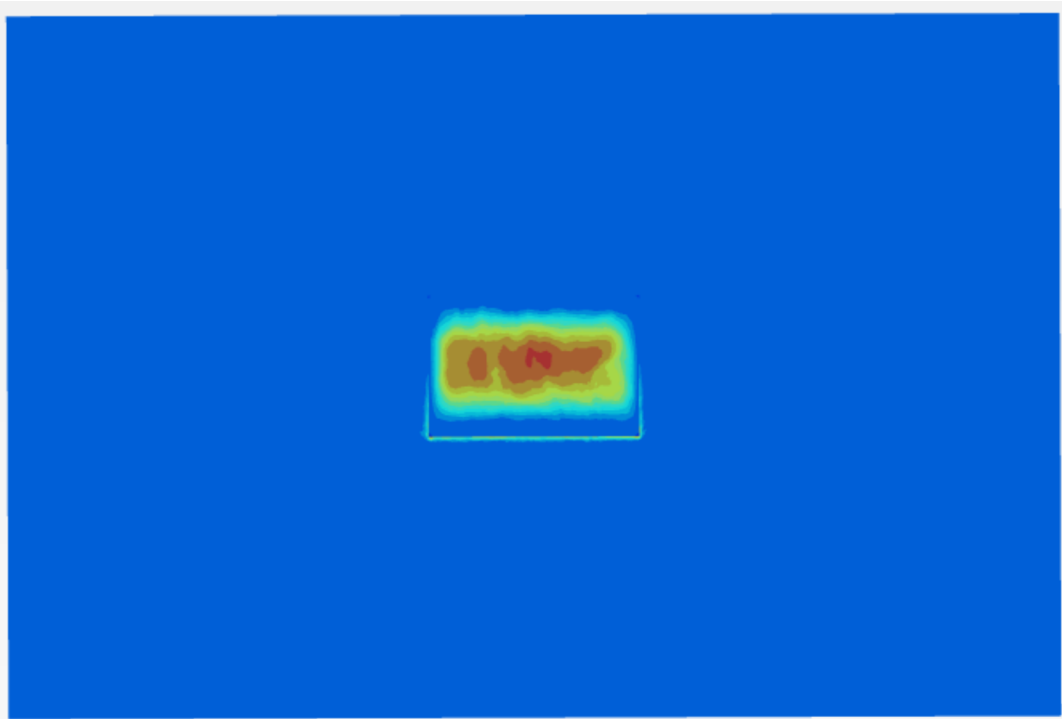


Figure C.15: Failure mechanism for pure moment loading in the x direction on the surface

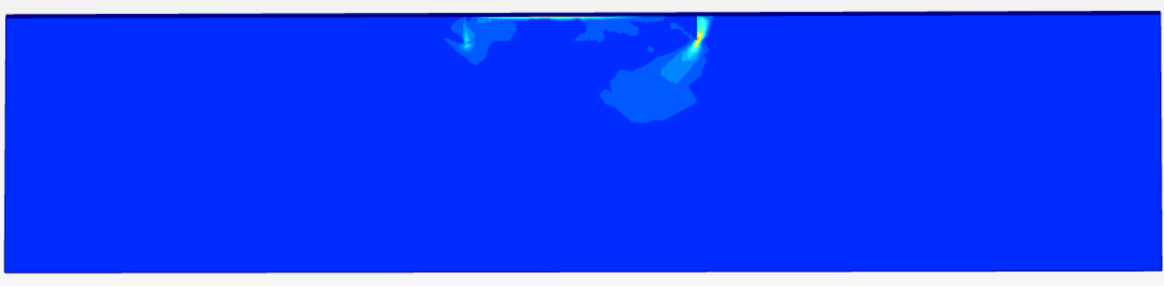


Figure C.16: Failure mechanism for pure moment loading in the y direction on the longer edge



Figure C.17: Failure mechanism for pure moment loading in the y direction on the smaller edge

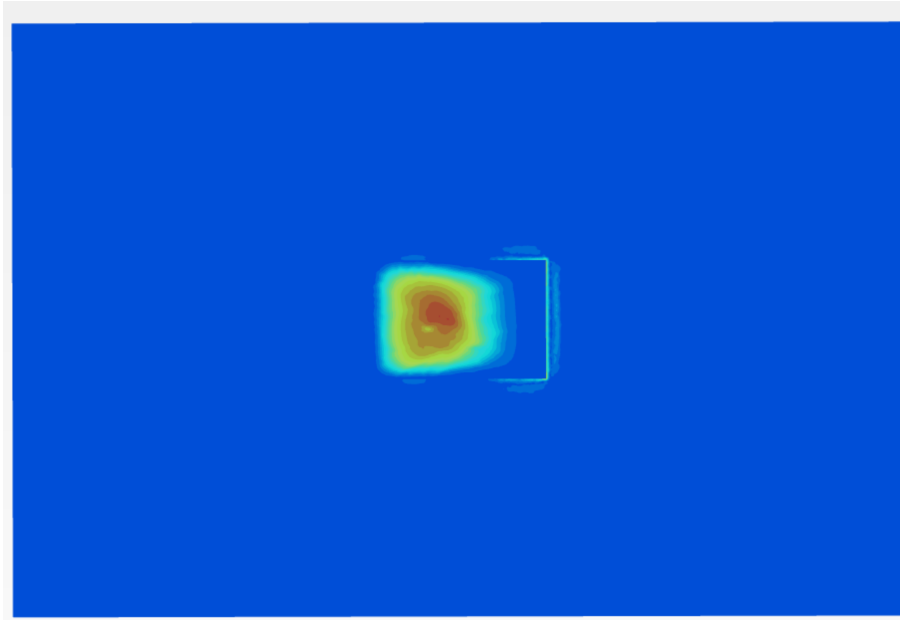


Figure C.18: Failure mechanism for pure moment loading in the y direction on the surface

Two Dimensional Loading

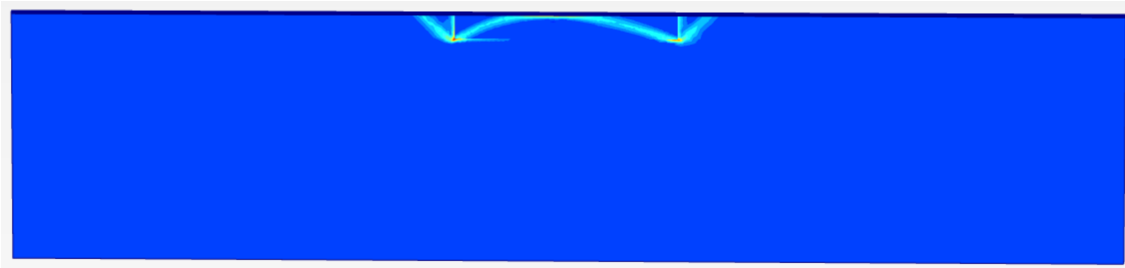


Figure C.19: Failure mechanism for ultimate horizontal loading in the x direction on the longer edge while having $\frac{V_{max}}{2}$ applied

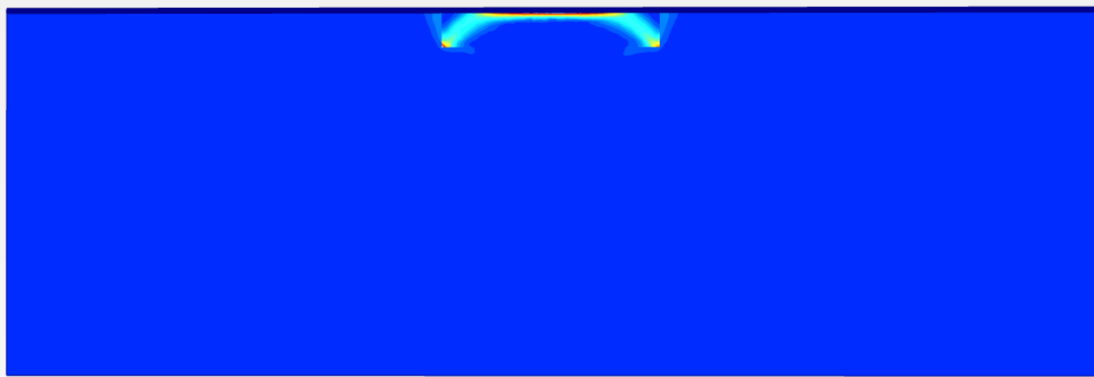


Figure C.20: Failure mechanism for ultimate horizontal loading in the x direction on the smaller edge while having $\frac{V_{max}}{2}$ applied



Figure C.21: Failure mechanism for ultimate horizontal loading in the y direction on the longer edge while having $\frac{V_{max}}{2}$ applied

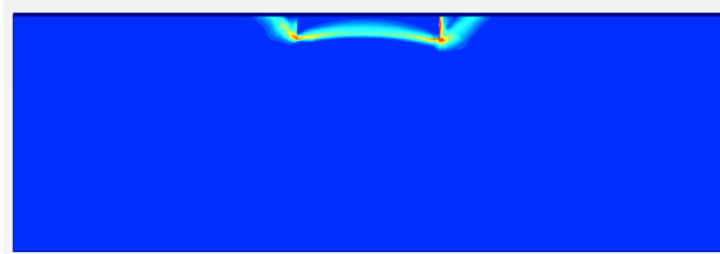


Figure C.22: Failure mechanism for ultimate horizontal loading in the y direction on the smaller edge while having $\frac{V_{max}}{2}$ applied



Figure C.23: Failure mechanism for ultimate moment loading in the x direction on the longer edge while having $\frac{V_{max}}{2}$ applied

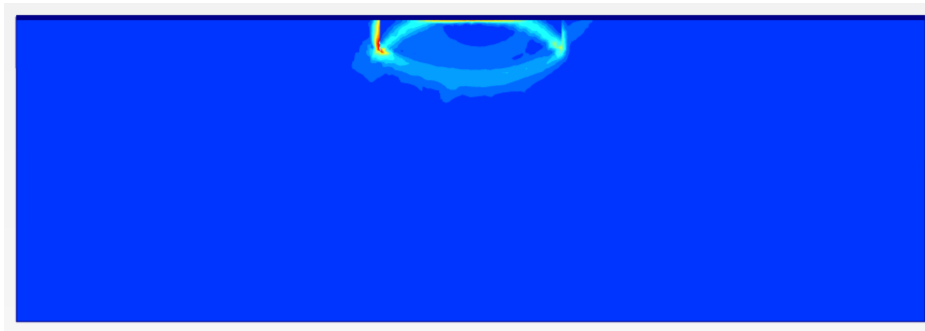


Figure C.24: Failure mechanism for ultimate moment loading in the x direction on the smaller edge while having $\frac{V_{max}}{2}$ applied

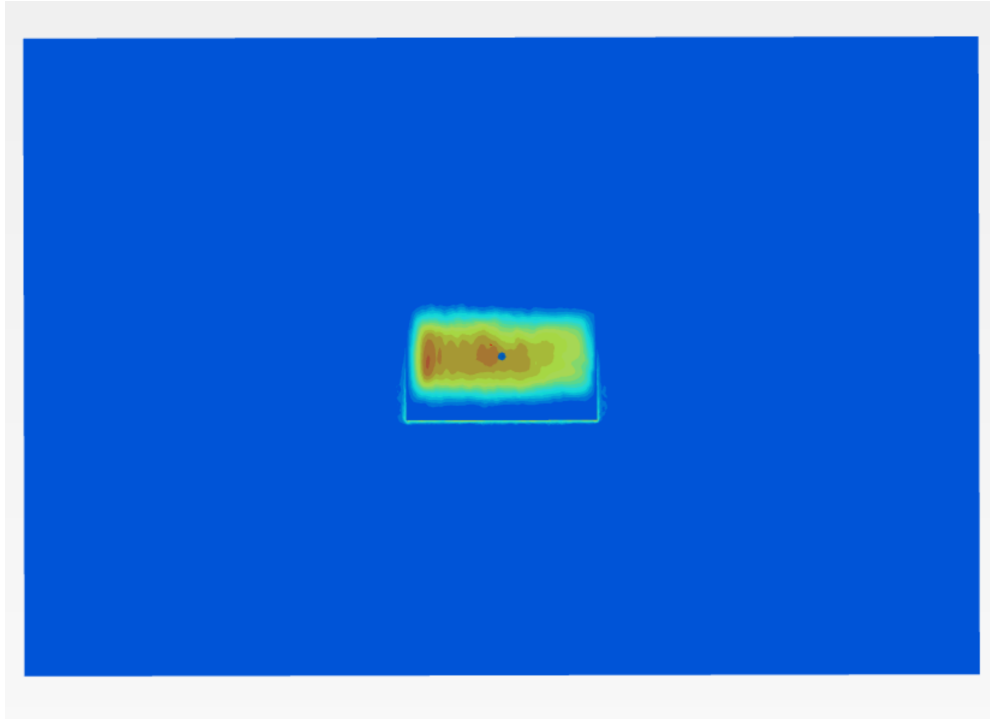


Figure C.25: Failure mechanism for ultimate moment loading in the x direction on the surface while having $\frac{V_{max}}{2}$ applied

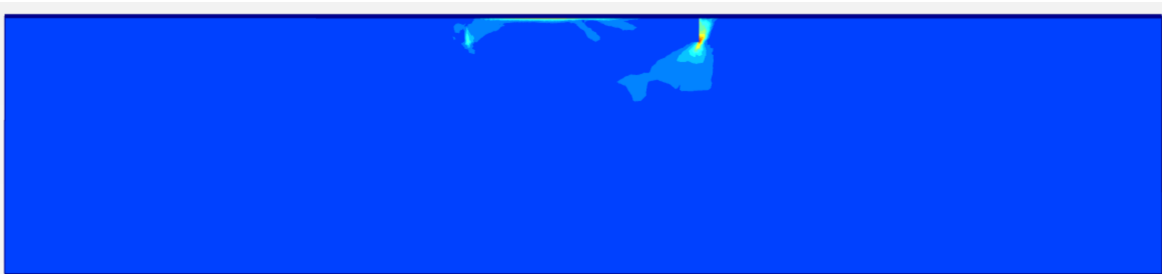


Figure C.26: Failure mechanism for ultimate moment loading in the y direction on the longer edge while having $\frac{V_{max}}{2}$ applied



Figure C.27: Failure mechanism for ultimate moment loading in the y direction on the smaller edge while having $\frac{V_{max}}{2}$ applied

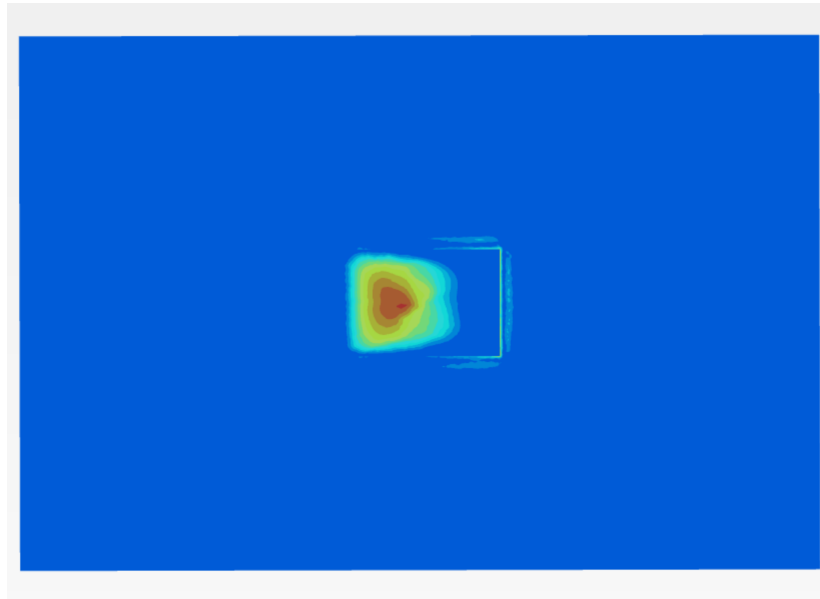


Figure C.28: Failure mechanism for ultimate moment loading in the y direction on the surface while having $\frac{V_{max}}{2}$ applied

Three Dimensional Loading

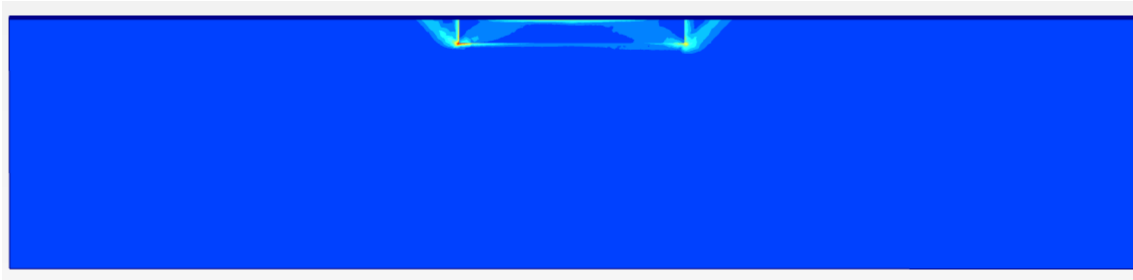


Figure C.29: Failure mechanism for ultimate moment loading in the x direction on the longer edge while having $\frac{V_{max}}{2}$ and $\frac{H_{x,max}}{2}$ applied

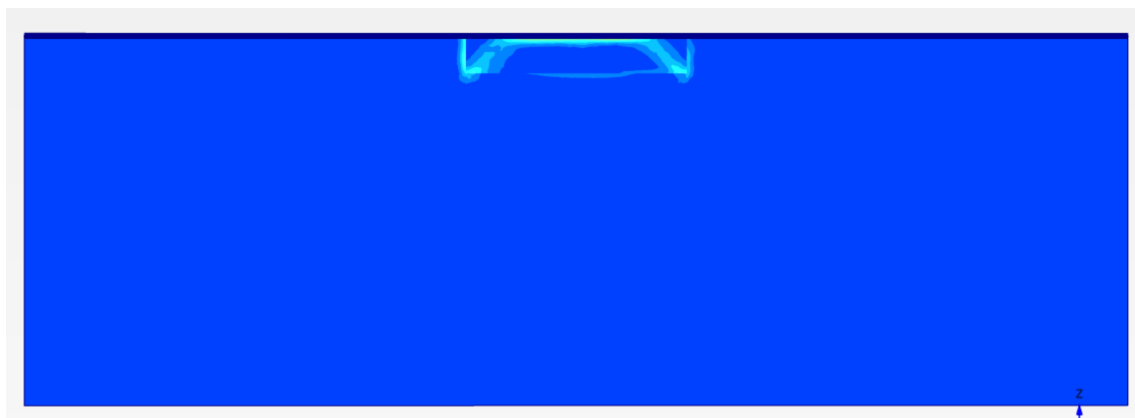


Figure C.30: Failure mechanism for ultimate moment loading in the x direction on the smaller edge while having $\frac{V_{max}}{2}$ and $\frac{H_{x,max}}{2}$ applied

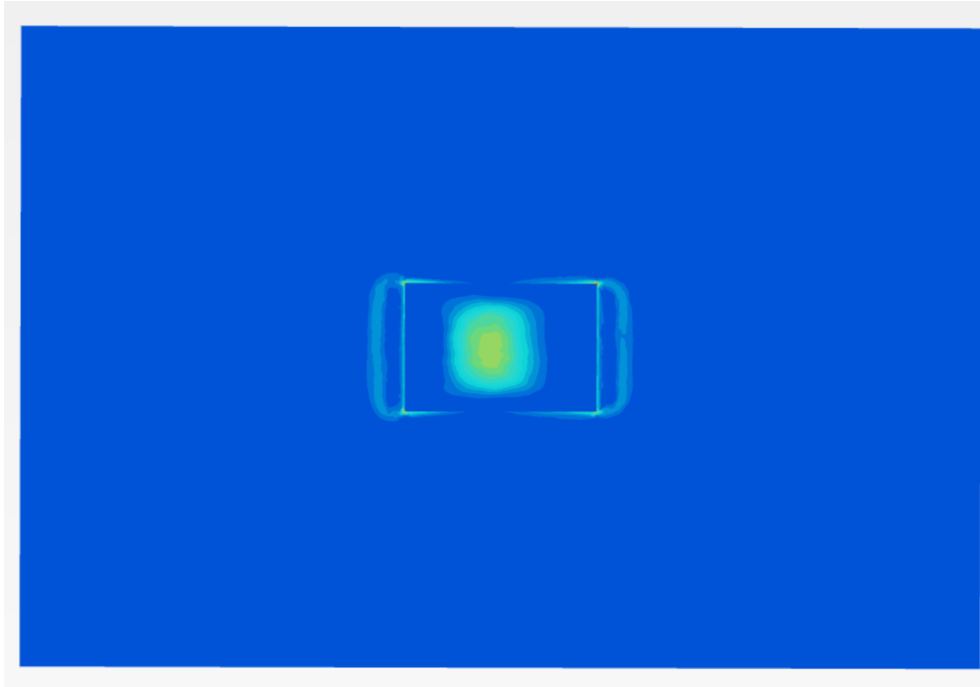


Figure C.31: Failure mechanism for ultimate moment loading in the x direction on the surface while having $\frac{V_{max}}{2}$ and $\frac{H_{x,max}}{2}$ applied

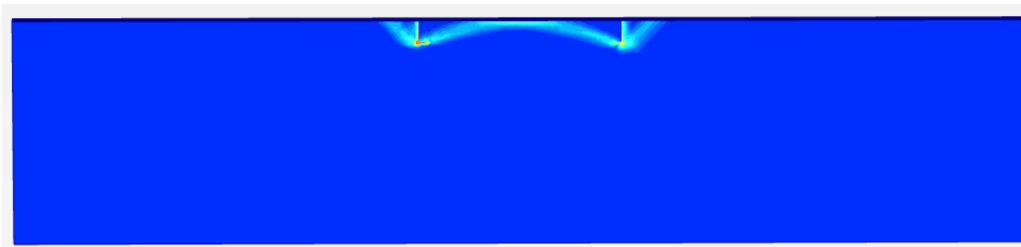


Figure C.32: Failure mechanism for ultimate moment loading in the y direction on the longer edge while having $\frac{V_{max}}{2}$ and $\frac{H_{x,max}}{2}$ applied

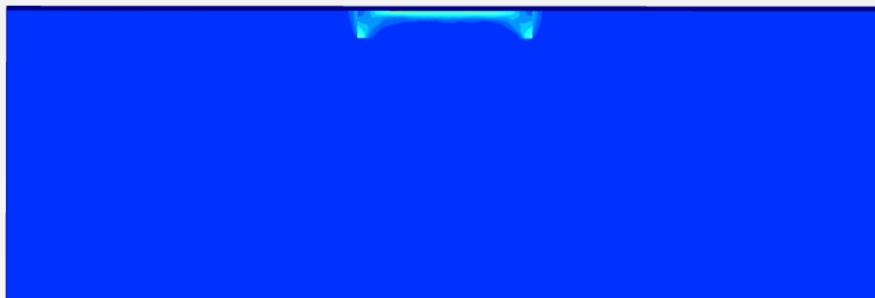


Figure C.33: Failure mechanism for ultimate moment loading in the y direction on the smaller edge while having $\frac{V_{max}}{2}$ and $\frac{H_{x,max}}{2}$ applied

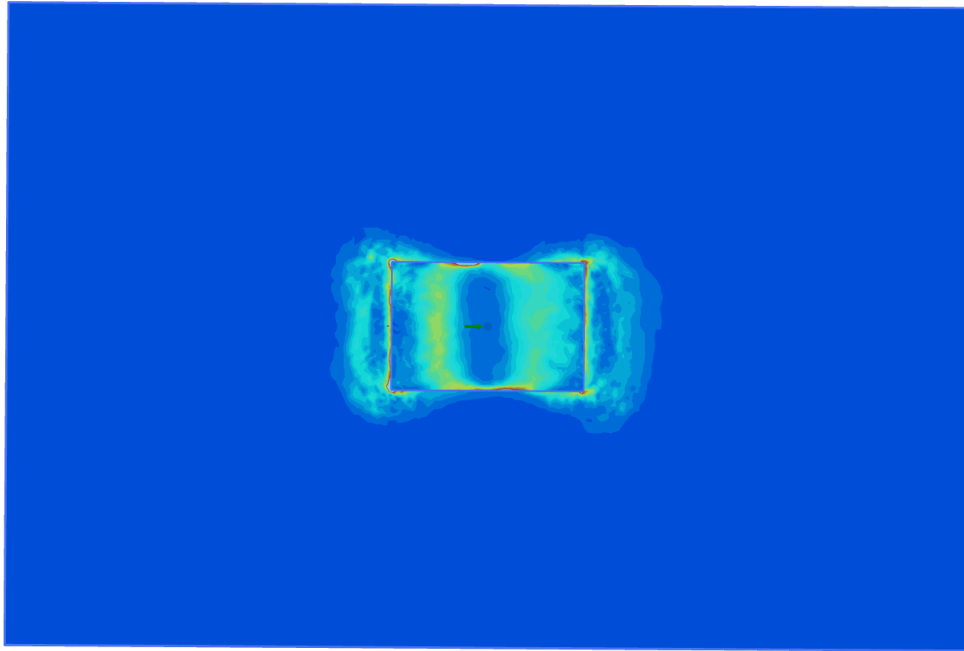


Figure C.34: Failure mechanism for ultimate moment loading in the y direction on the surface while having $\frac{V_{max}}{2}$ and $\frac{H_{x,max}}{2}$ applied

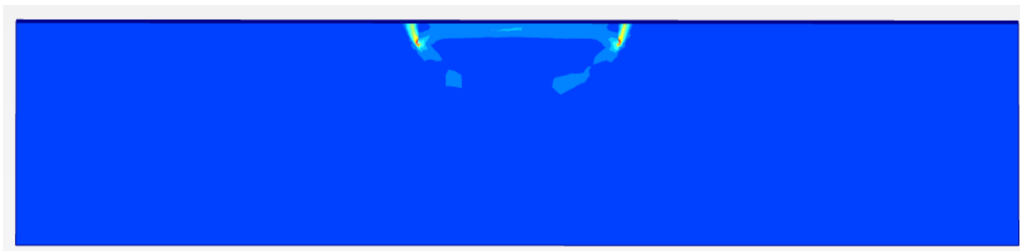


Figure C.35: Failure mechanism for ultimate moment loading in the x direction on the longer edge while having $\frac{V_{max}}{2}$ and $\frac{H_{y,max}}{2}$ applied

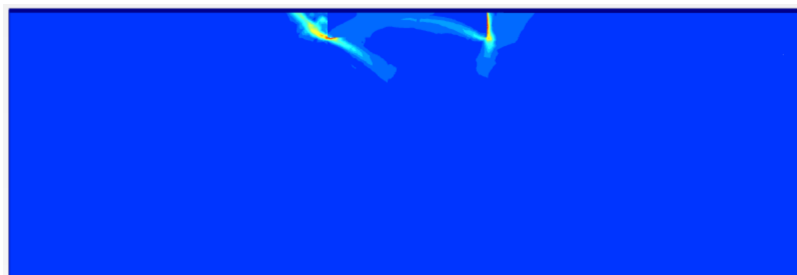


Figure C.36: Failure mechanism for ultimate moment loading in the x direction on the smaller edge while having $\frac{V_{max}}{2}$ and $\frac{H_{y,max}}{2}$ applied



Figure C.37: Failure mechanism for ultimate moment loading in the x direction on the surface while having $\frac{V_{max}}{2}$ and $\frac{H_{y,max}}{2}$ applied

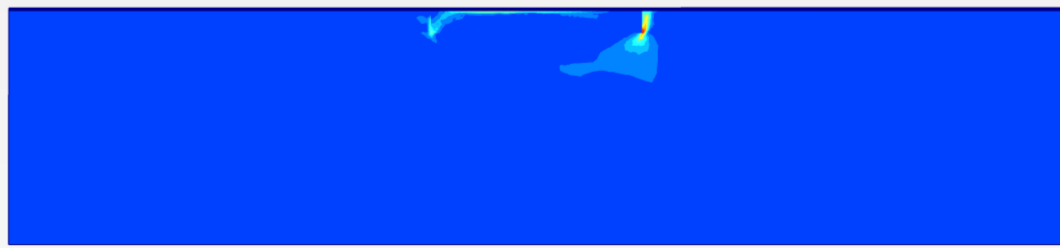


Figure C.38: Failure mechanism for ultimate moment loading in the y direction on the longer edge while having $\frac{V_{max}}{2}$ and $\frac{H_{y,max}}{2}$ applied



Figure C.39: Failure mechanism for ultimate moment loading in the y direction on the smaller edge while having $\frac{V_{max}}{2}$ and $\frac{H_{y,max}}{2}$ applied

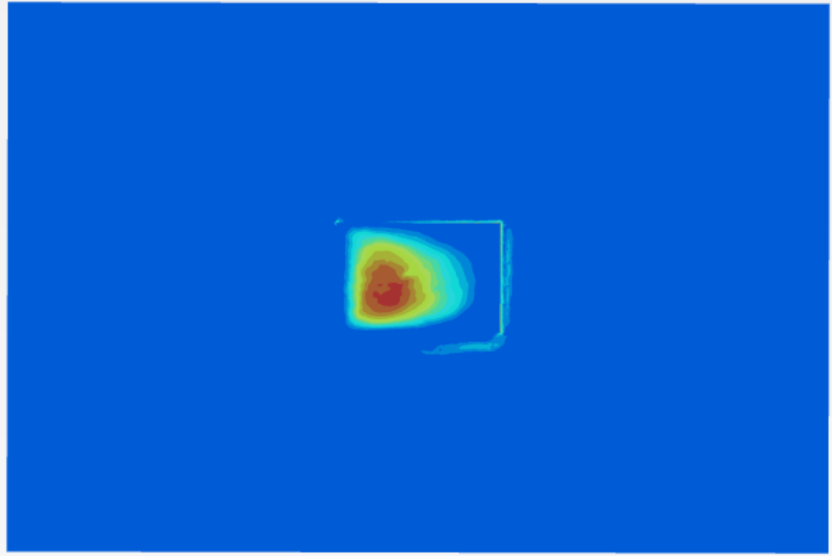


Figure C.40: Failure mechanism for ultimate moment loading in the y direction on the surface while having $\frac{V_{max}}{2}$ and $\frac{H_{y,max}}{2}$ applied

C.1.3 Calculations Details

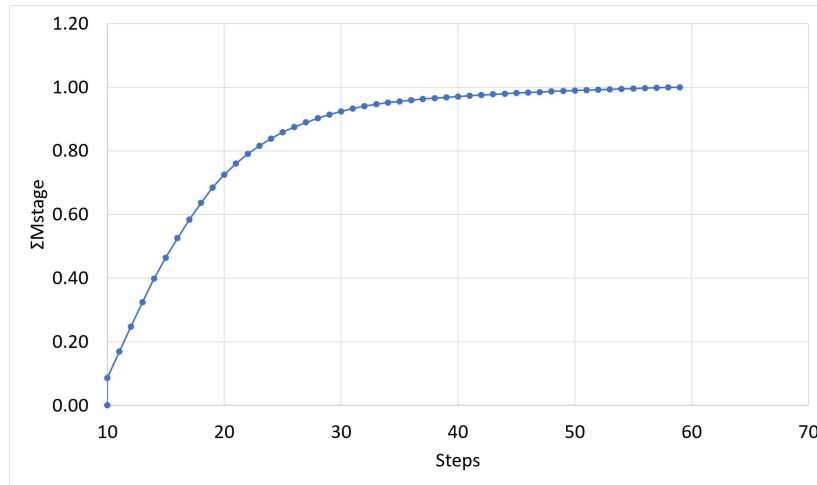


Figure C.41: Ultimate horizontal loading in x direction

The ΣM_{stage} is 0.8180 and the primarily horizontal load applied is 250 kN. Therefore:

$$\text{Pure horizontal load} \rightarrow H_{x,max} = 0.8180 * 250 = 204.5 \text{ kN} \quad (\text{C.1})$$

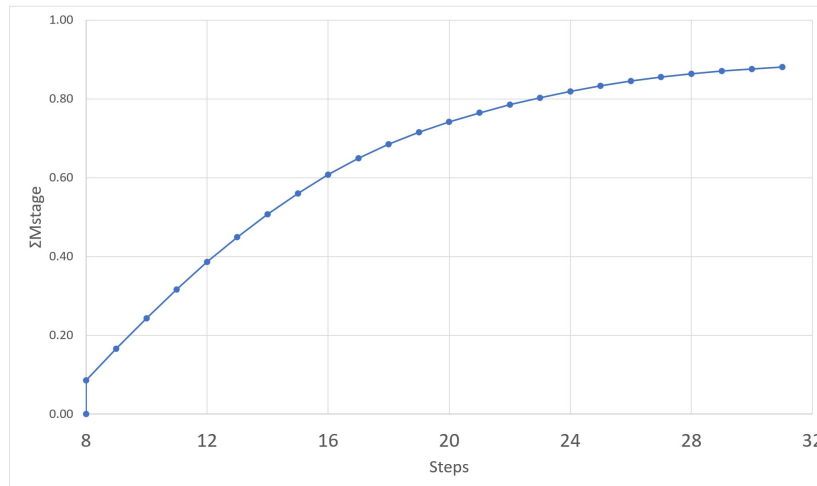


Figure C.42: Ultimate horizontal loading in y direction

The ΣM_{stage} is 0.8804 and the primarily horizontal load applied is 250 kN. Therefore:

$$\text{Pure horizontal load} \rightarrow H_{y,max} = 0.8804 * 250 = 220.1 \text{ kN} \quad (\text{C.2})$$

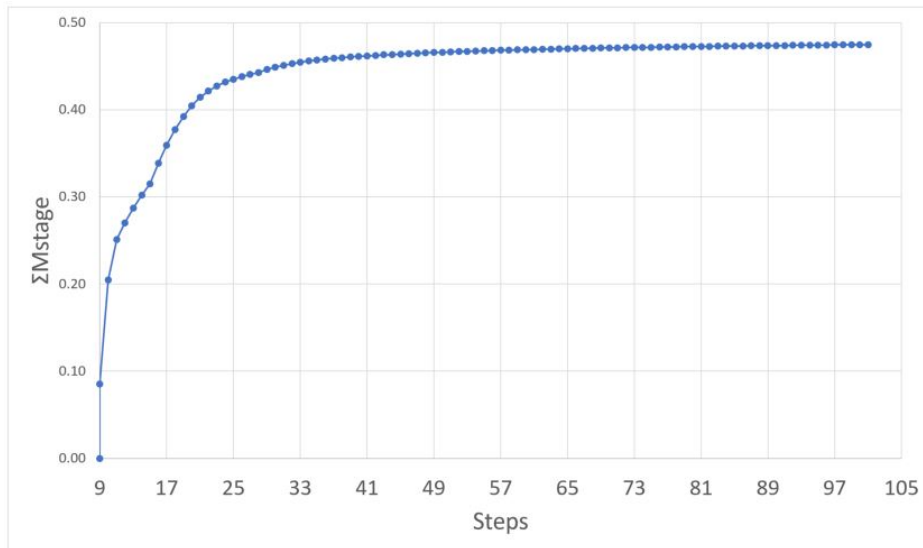


Figure C.43: Ultimate moment loading in x direction

The ΣM_{stage} is 0.4750 and the primarily moment load applied is 1000 kN.m. Therefore:

$$\text{Pure moment load} \rightarrow M_{x,max} = 0.4750 * 1000 = 475.0 \text{ kN.m} \quad (\text{C.3})$$

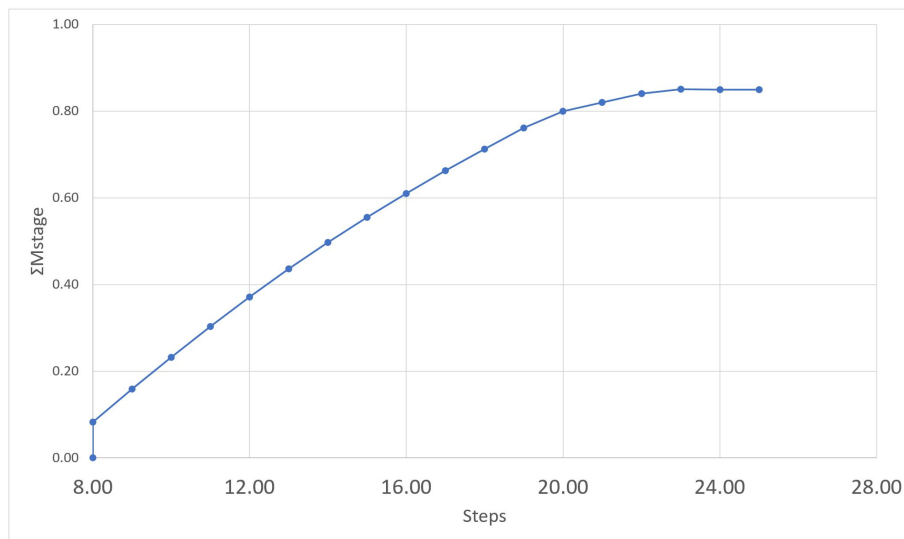


Figure C.44: Ultimate moment loading in y direction

The ΣM_{stage} is 0.8542 and the primarily moment load applied is 500 kN.m. Therefore:

$$\text{Pure moment load} \rightarrow M_{y,max} = 0.8542 * 500 = 427.10 \text{ kN.m} \quad (\text{C.4})$$

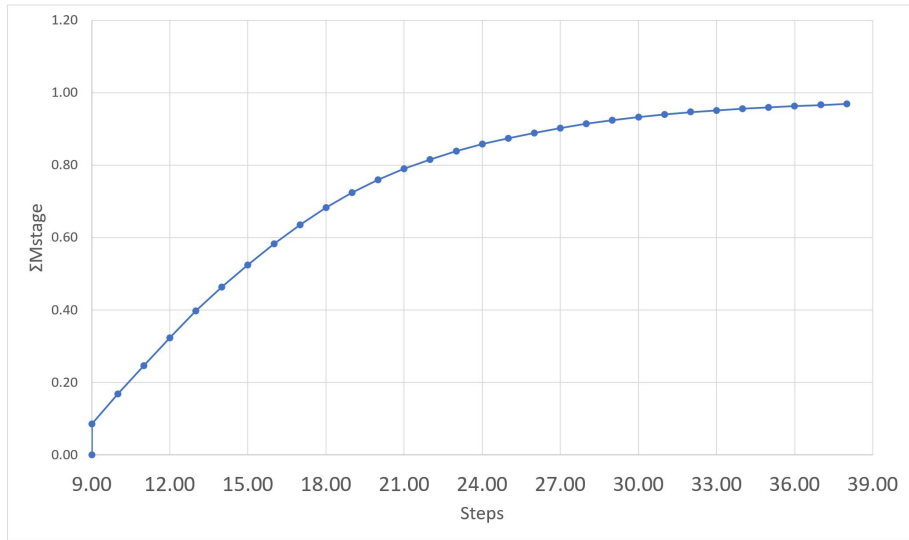


Figure C.45: Ultimate horizontal loading in x direction having $V_{max}/2$ applied

The ΣM_{stage} is 0.9692 and the primarily horizontal load applied is 205 kN for the condition that half of the maximum possible vertical load is also assigned to the structure. Therefore:

$$\text{For } \frac{V_{max}}{2} + H_x \rightarrow H_{x,max} = 0.9692 * 205 = 198.69kN \quad (C.5)$$

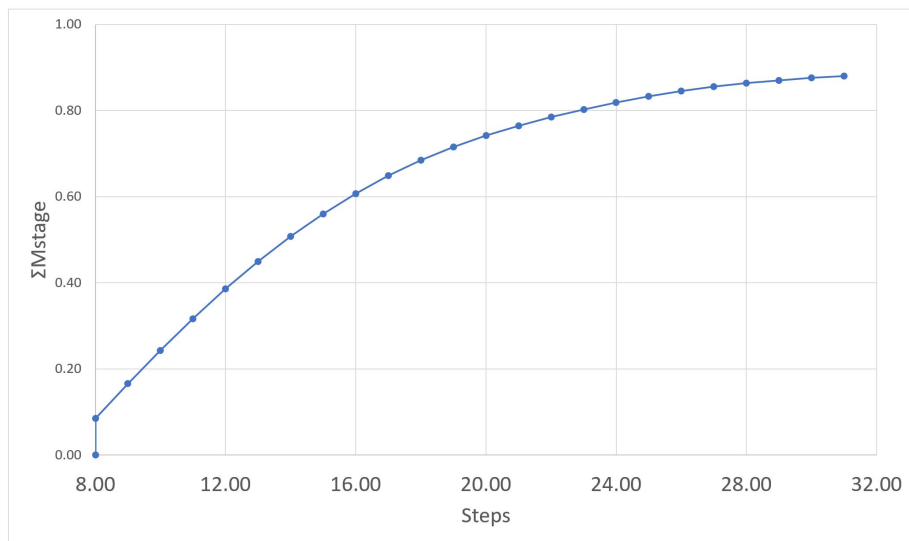


Figure C.46: Ultimate horizontal loading in y direction having $V_{max}/2$ applied

The ΣM_{stage} is 0.765 and the primarily horizontal load applied is 300 kN for the condition

that half of the maximum possible vertical load is also assigned to the structure. Therefore:

$$\text{For } \frac{V_{max}}{2} + H_y \rightarrow H_{y,max} = 0.765 * 300 = 229.5 kN \quad (C.6)$$

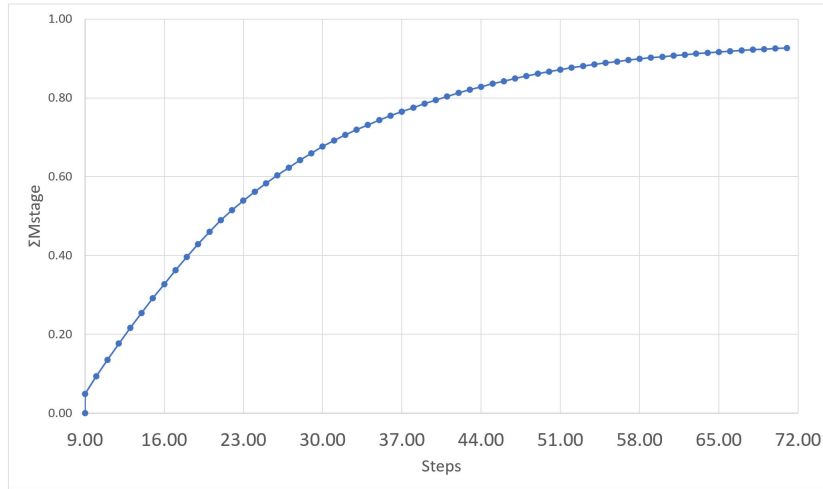


Figure C.47: Ultimate moment loading in x direction having $V_{max}/2$ applied

The ΣM_{stage} is 0.2895 and the primarily moment load applied is 2500 kN.m for the condition that half of the maximum possible vertical load is also assigned to the structure. Therefore:

$$\text{For } \frac{V_{max}}{2} + M_x \rightarrow M_{x,max} = 0.2895 * 2500 = 723.75 kN.m \quad (C.7)$$

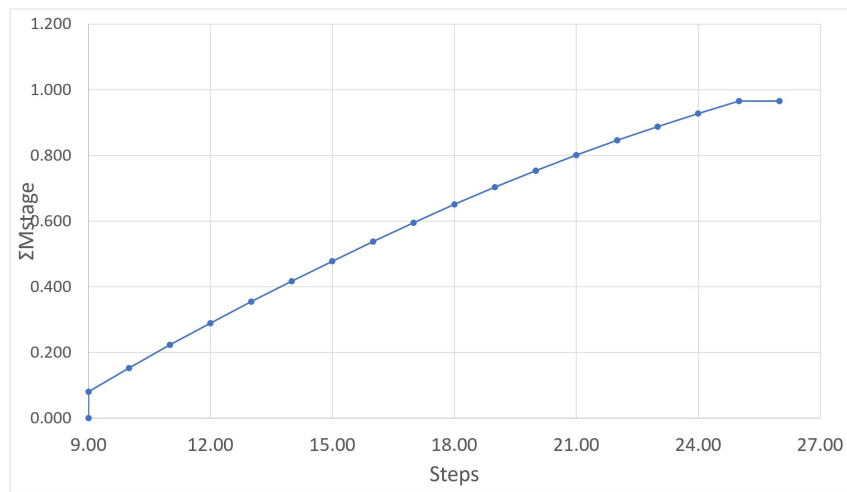


Figure C.48: Ultimate moment loading in y direction having $V_{max}/2$ applied

The ΣM_{stage} is 0.4153 and the primarily moment load applied is 2000 kN.m for the condition

that half of the maximum possible vertical load is also assigned to the structure. Therefore:

$$\text{For } \frac{V_{max}}{2} + M_y \rightarrow M_{y,max} = 0.4153 * 2000 = 830.60 kN.m \quad (C.8)$$

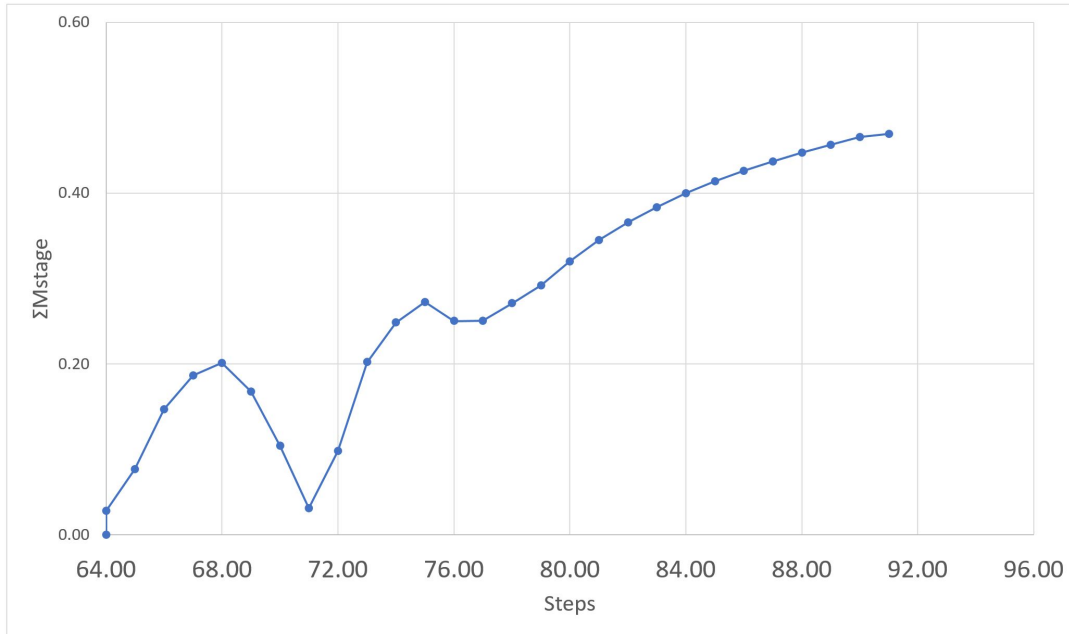


Figure C.49: Ultimate moment loading in x direction having $V_{max}/2$ & $H_{x,max}/2$ applied

The graph shows illustrates fluctuating because *PLAXIS* is trying different paths. The ΣM_{stage} is 0.4692 and the primarily moment load applied is 2000 kN.m for the condition that half of the maximum possible vertical and horizontal load in x direction is also assigned to the structure. Therefore:

$$\text{For } \frac{V_{max}}{2} + \frac{H_{x,max}}{2} + M_x \rightarrow M_{x,max} = 0.4692 * 2000 = 938.40 kN.m \quad (C.9)$$

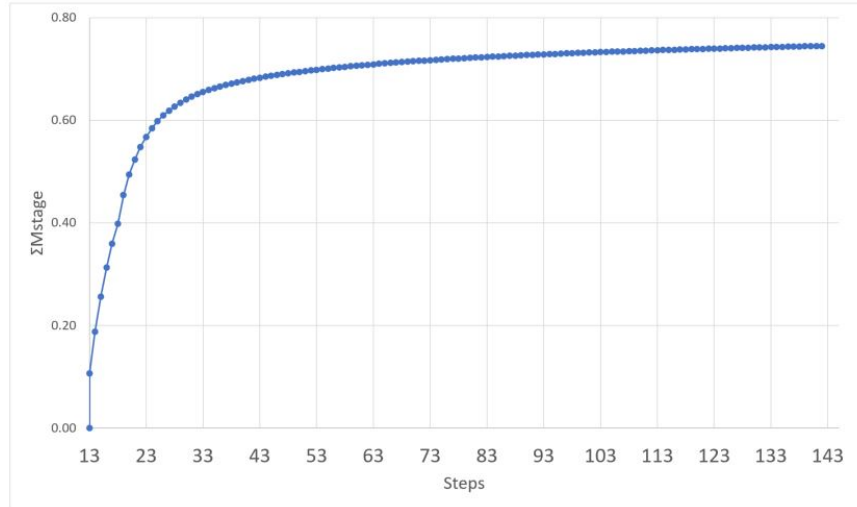


Figure C.50: Ultimate moment loading in y direction having $V_{max}/2$ & $H_{x,max}/2$ applied

The ΣM_{stage} is 0.6449 and the primarily moment load applied is 1000 kN.m for the condition that half of the maximum possible vertical and horizontal load in x direction is also assigned to the structure. Therefore:

$$\text{For } \frac{V_{max}}{2} + \frac{H_{x,max}}{2} + M_y \rightarrow M_{y,max} = 0.6449 * 1000 = 644.90kN.m \quad (C.10)$$

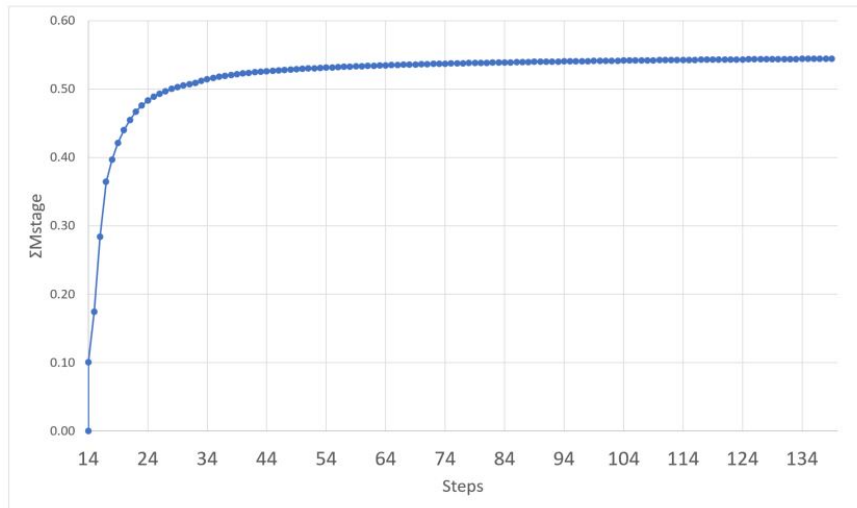


Figure C.51: Ultimate moment loading in x direction having $V_{max}/2$ & $H_{y,max}/2$ applied

The ΣM_{stage} is 0.8615 and the primarily moment load applied is 1000 kN.m for the condition that half of the maximum possible vertical and horizontal load in y direction is also assigned to

the structure. Therefore:

$$\text{For } \frac{V_{max}}{2} + \frac{H_{y,max}}{2} + M_x \rightarrow M_{x,max} = 0.8615 * 1000 = 861.50 kN.m \quad (C.11)$$

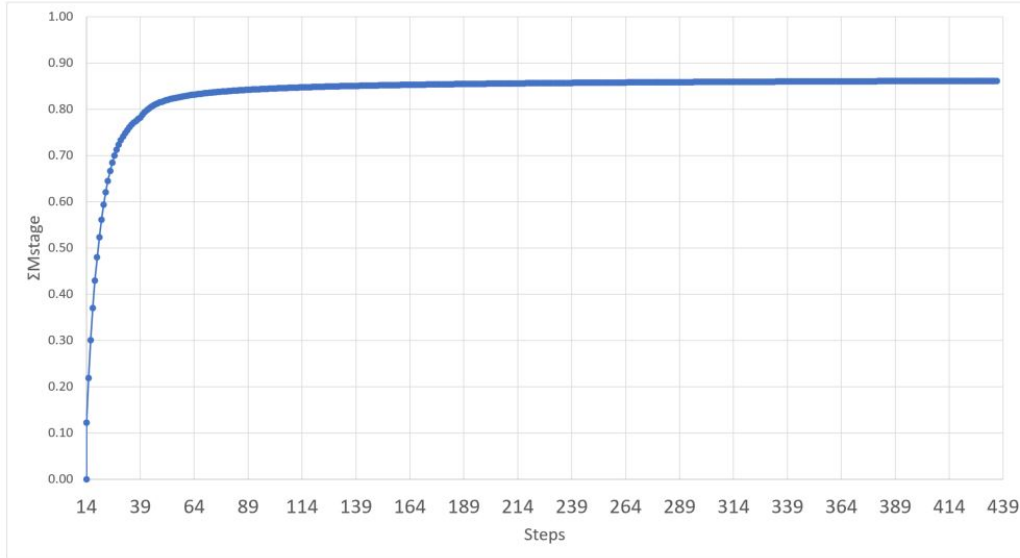


Figure C.52: Ultimate moment loading in y direction having $V_{max}/2$ & $H_{y,max}/2$ applied

The ΣM_{stage} is 0.5445 and the primarily moment load applied is 1500 kN.m for the condition that half of the maximum possible vertical and horizontal load in y direction is also assigned to the structure. Therefore:

$$\text{For } \frac{V_{max}}{2} + \frac{H_{y,max}}{2} + M_y \rightarrow M_{y,max} = 0.5445 * 1500 = 816.75 kN.m \quad (C.12)$$

C.1.4 Torsion Loading Results

Torsional loading has been only done using FEM software as an extra check. The results show that further analysis would be an interesting project to work on. Following shows the maximum torsion load in different load combination and the failure mechanism due to them.

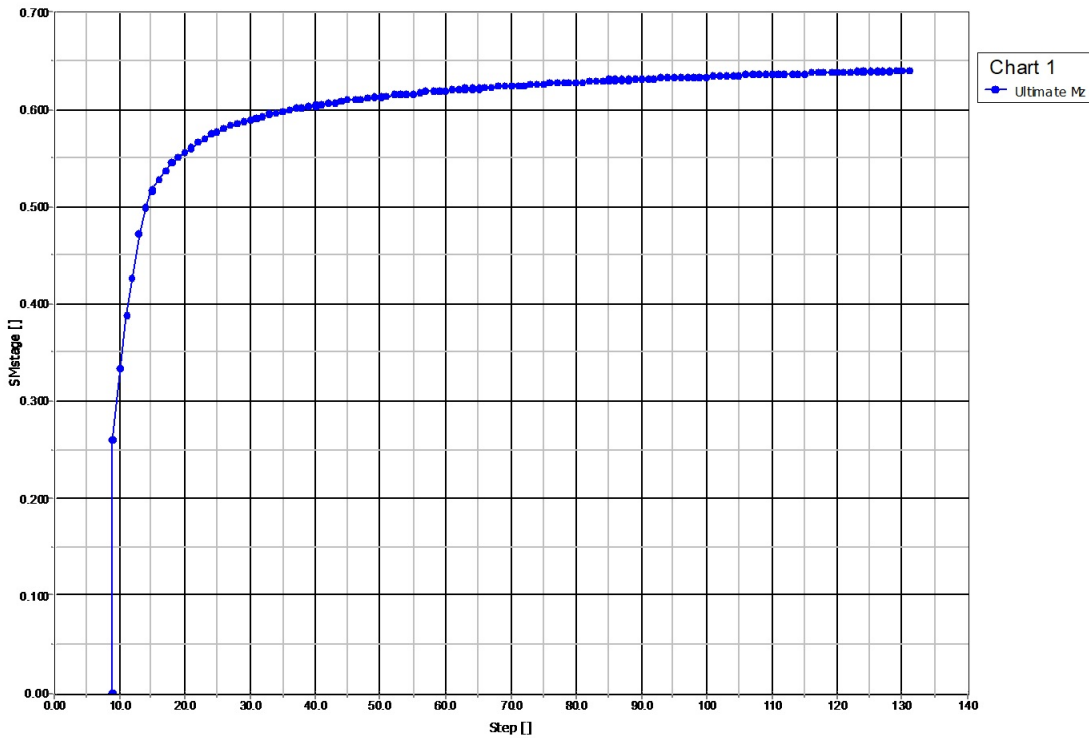


Figure C.53: Ultimate torsional loading possible

The ΣM_{stage} is 0.6397 and the primarily horizontal load applied is 1000 kN.m. Therefore:

$$\text{Pure moment load} \rightarrow M_{z,max} = 0.6397 * 1000 = 639.70 \text{ kN.m} \quad (\text{C.13})$$

Knowing more load on the foundation makes rotating it on its plane harder, is providing a logical reason for the increase observed in torsional capacity when the foundation is loaded with $V_{max}/2$. For the condition that half of the maximum possible vertical load is also assigned to the structure following statement is resulted:

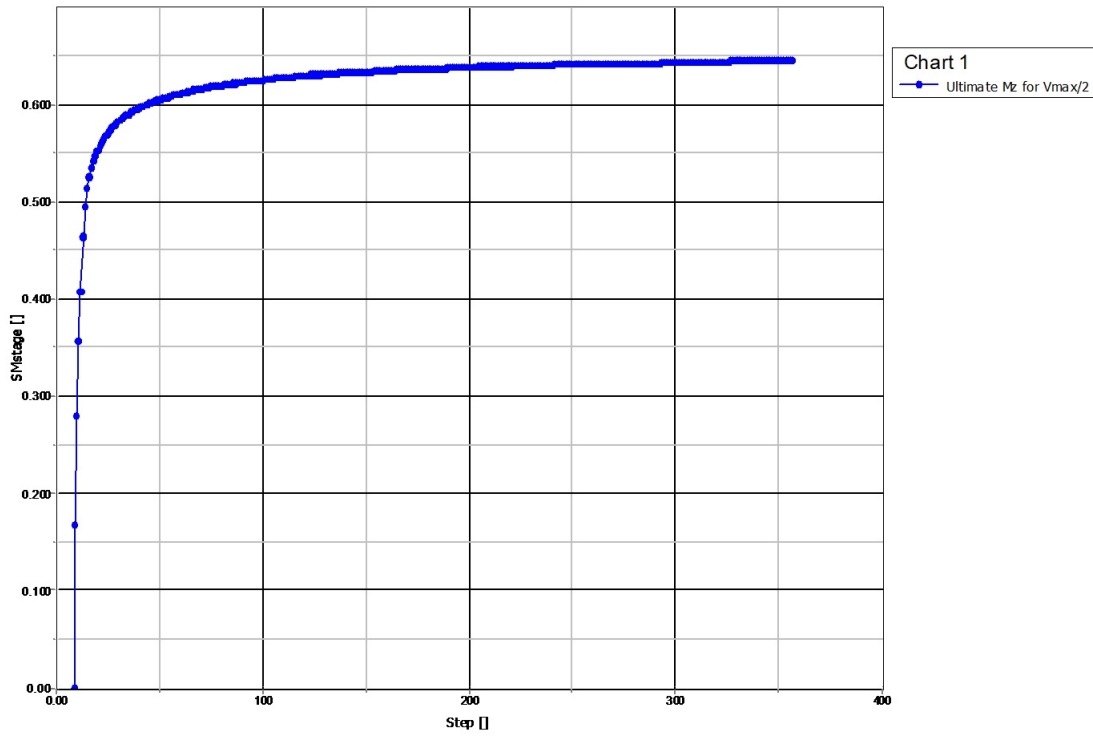


Figure C.54: Ultimate torsional loading possible

Knowing the primarily moment load assigned is 1000 kN.m. then:

$$\text{For } V_{max}/2 + M_z \rightarrow M_{z,max} = 0.6446 * 1000 = 644.60 \text{ kN.m} \quad (C.14)$$

The failure mechanisms for pure moment in z direction (torsion) is illustrated following:

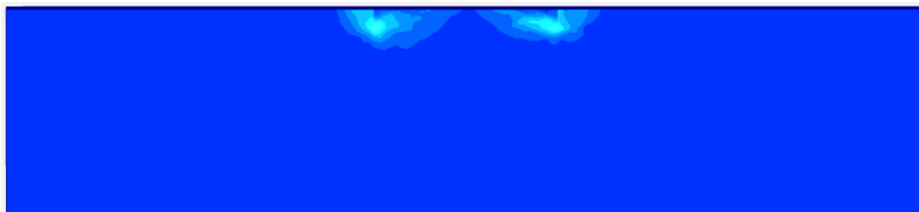


Figure C.55: Failure mechanism for pure moment loading in the z direction on the longer edge



Figure C.56: Failure mechanism for pure moment loading in the z direction on the smaller edge

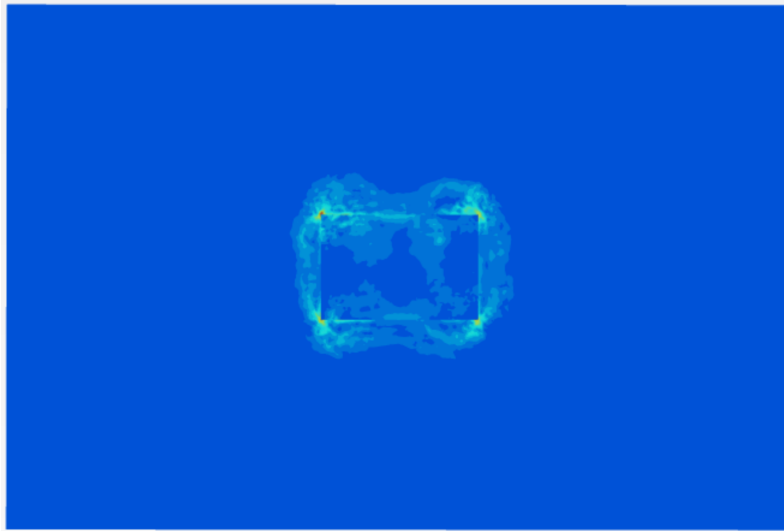


Figure C.57: Failure mechanism for pure moment loading in the z direction on the surface

Having vertical loading increases slightly the torsional capacity to some point and probably it is reduced afterwards and checking it would be a good topic for further works. Here is failure mechanism for torsional loading and having $V_{max}/2$ load.

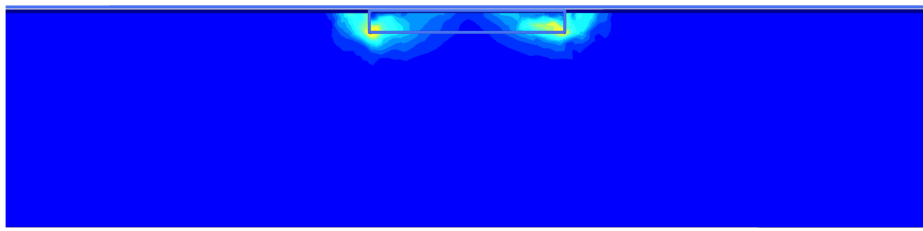


Figure C.58: Failure mechanism for ultimate moment loading in the z direction on the longer edge while having $\frac{V_{max}}{2}$ applied

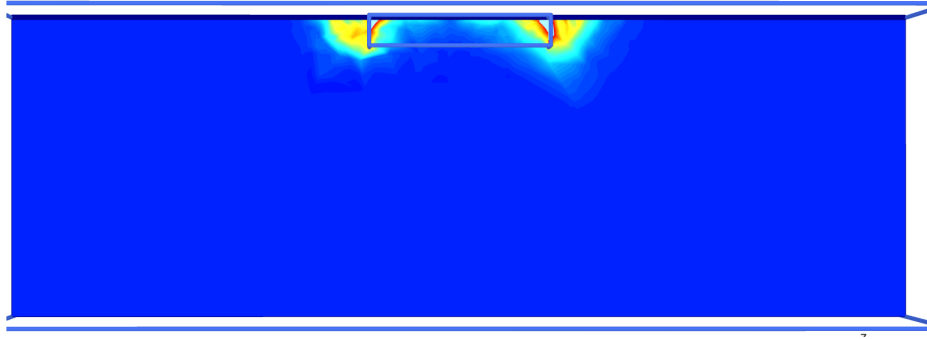


Figure C.59: Failure mechanism for ultimate moment loading in the z direction on the smaller edge while having $\frac{V_{max}}{2}$ applied

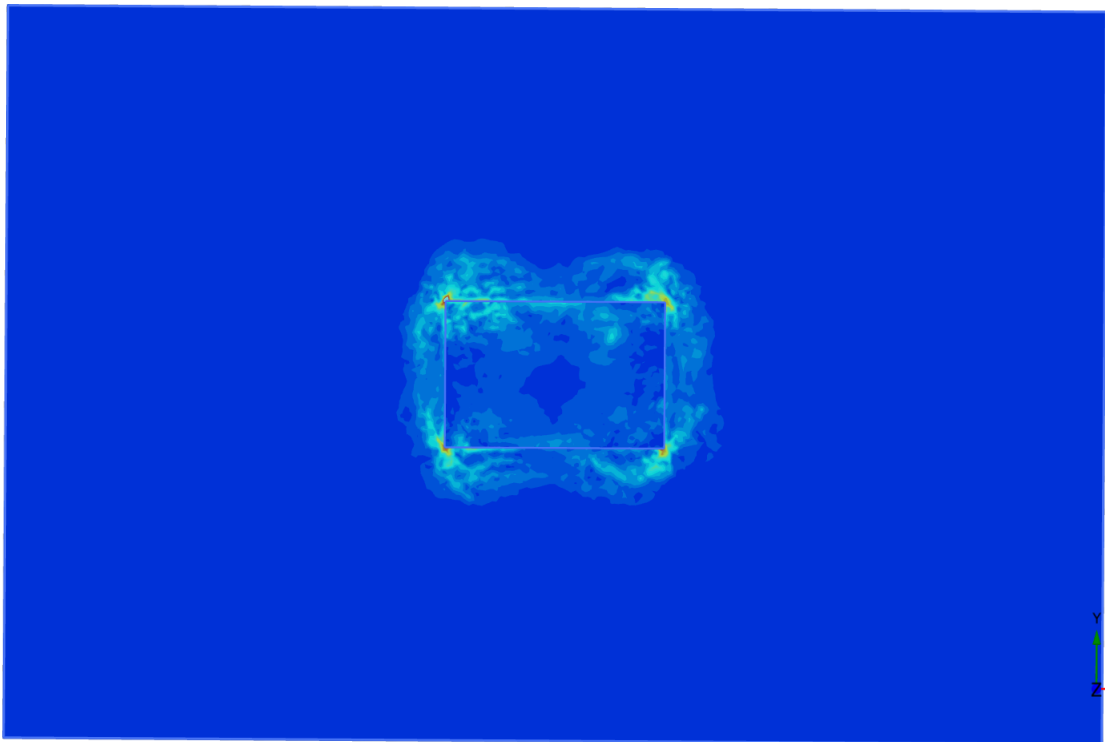


Figure C.60: Failure mechanism for ultimate moment loading in the z direction on the surface while having $\frac{V_{max}}{2}$ applied

Of course the amount of the horizontal loading and the direction of it could be effective which is advised for further works.

List of Figures

2.1	Shear modulus varying by depth patterns (Gazetas, 1991)	11
2.2	Stress Field Different Zones	13
2.3	General Shear Failure	13
2.4	Local Shear Failure	13
2.5	Punching Shear Failure	13
2.6	Effective dimensions	14
2.7	Comparing the failure mechanism of skirted shallow and solid foundations under pure vertical and horizontal loading (Mana et al., 2012a)	18
2.8	Failure mechanism (Kramer, 2014)	20
2.9	Beam Element with 3 nodes	22
2.10	Wedge Element with 6 nodes	22
2.11	Tetrahedrons Element with 10 nodes	22
3.1	A 3D model of the foundation by Autocad 3D	24
3.2	A 3D model of the foundation on the soil by Autocad 3D	25
4.1	Different shear strength	29
4.2	Correction factor F given for rough mooth footing (Davis et al., 1985)	29
4.3	Shape factor given in Table 4.2 shown in a graph	30
4.4	Parameters involved in $Su1$ calculation	30
4.5	Loads applied to the foundation in a 3D environment modeled by AutoCAD 3D	33
5.1	The location of the model	35
5.2	Mesh density on the model	36
5.3	Mesh elements on illustrated on one of the skirts	37

5.4	Failure mechanism for pure vertical loading in the longer edge	37
5.5	Failure mechanism for pure vertical loading in the smaller edge	38
5.6	Failure mechanism (Mana et al., 2012a)	38
5.7	Loading steps in pure vertical loading condition up to failure point	39
6.1	Comparison of PLAXIS 3D and hand calculation in $V-H_x$ normalised load space . .	41
6.2	Comparison of PLAXIS 3D and hand calculation in $V-H_y$ normalised load space . .	41
6.3	Deformation pattern and load assumption in hand calculation	42
6.4	Deformation pattern and load assumption in a 3D environment	42
6.5	Comparison of PLAXIS 3D and hand calculation in $V-M_x$ normalised load space .	43
6.6	Comparison of PLAXIS 3D and hand calculation in $V-M_y$ normalised load space .	43
6.7	Comparison of PLAXIS 3D and hand calculation in H_x-M_x normalised load space having $V_{max}/2$ constantly applied	44
6.8	Comparison of PLAXIS 3D and hand calculation in H_x-M_y normalised load space having $V_{max}/2$ constantly applied	45
6.9	Comparison of PLAXIS 3D and hand calculation in H_y-M_x normalised load space having $V_{max}/2$ constantly applied	46
6.10	Comparison of PLAXIS 3D and hand calculation in H_y-M_y normalised load space having $V_{max}/2$ constantly applied	46
7.1	Comparing results from hand calculation and PLAXIS 3D	48
B.1	The normalized vertical versus horizontal loading in x direction graph for hand calculation	59
B.2	The normalized vertical versus horizontal loading in y direction graph for hand calculation	59
B.3	The normalized vertical versus moment loading in x direction graph for hand cal- culation	60
B.4	The normalized vertical versus moment loading in y direction graph for hand cal- culation	61
B.5	The normalized horizontal versus moment loading in x direction graph for hand calculation	62

B.6	The normalized x directed horizontal load versus moment loading in y direction graph for hand calculation	63
B.7	The normalized y directed horizontal load versus moment loading in x direction graph for hand calculation	64
B.8	The normalized horizontal versus moment loading in y direction graph for hand calculation	65
C.1	The normalized vertical versus horizontal loading in x direction graph resulted by PLAXIS 3D	67
C.2	The normalized vertical versus horizontal loading in y direction graph resulted by PLAXIS 3D	67
C.3	The normalized vertical versus moment loading in x direction graph resulted by PLAXIS 3D	68
C.4	The normalized vertical versus moment loading in y direction graph resulted by PLAXIS 3D	68
C.5	The normalized horizontal versus moment loading in x direction graph for hand calculation	69
C.6	The normalized horizontal versus moment loading in y direction graph for hand calculation	69
C.7	The normalized horizontal versus moment loading in x direction graph for hand calculation	70
C.8	The normalized horizontal versus moment loading in y direction graph for hand calculation	70
C.9	Failure mechanism for pure horizontal loading in the x direction on the longer edge	71
C.10	Failure mechanism for pure horizontal loading in the x direction on the smaller edge	71
C.11	Failure mechanism for pure horizontal loading in the y direction on the longer edge	71
C.12	Failure mechanism for pure horizontal loading in the y direction on the smaller edge	72
C.13	Failure mechanism for pure moment loading in the x direction on the longer edge	72
C.14	Failure mechanism for pure moment loading in the x direction on the smaller edge	72
C.15	Failure mechanism for pure moment loading in the x direction on the surface . . .	73
C.16	Failure mechanism for pure moment loading in the y direction on the longer edge	73
C.17	Failure mechanism for pure moment loading in the y direction on the smaller edge	73

C.18 Failure mechanism for pure moment loading in the y direction on the surface . . .	74
C.19 Failure mechanism for ultimate horizontal loading in the x direction on the longer edge while having $\frac{V_{max}}{2}$ applied	74
C.20 Failure mechanism for ultimate horizontal loading in the x direction on the smaller edge while having $\frac{V_{max}}{2}$ applied	74
C.21 Failure mechanism for ultimate horizontal loading in the y direction on the longer edge while having $\frac{V_{max}}{2}$ applied	75
C.22 Failure mechanism for ultimate horizontal loading in the y direction on the smaller edge while having $\frac{V_{max}}{2}$ applied	75
C.23 Failure mechanism for ultimate moment loading in the x direction on the longer edge while having $\frac{V_{max}}{2}$ applied	75
C.24 Failure mechanism for ultimate moment loading in the x direction on the smaller edge while having $\frac{V_{max}}{2}$ applied	75
C.25 Failure mechanism for ultimate moment loading in the x direction on the surface while having $\frac{V_{max}}{2}$ applied	76
C.26 Failure mechanism for ultimate moment loading in the y direction on the longer edge while having $\frac{V_{max}}{2}$ applied	76
C.27 Failure mechanism for ultimate moment loading in the y direction on the smaller edge while having $\frac{V_{max}}{2}$ applied	76
C.28 Failure mechanism for ultimate moment loading in the y direction on the surface while having $\frac{V_{max}}{2}$ applied	77
C.29 Failure mechanism for ultimate moment loading in the x direction on the longer edge while having $\frac{V_{max}}{2}$ and $\frac{H_{x,max}}{2}$ applied	77
C.30 Failure mechanism for ultimate moment loading in the x direction on the smaller edge while having $\frac{V_{max}}{2}$ and $\frac{H_{x,max}}{2}$ applied	77
C.31 Failure mechanism for ultimate moment loading in the x direction on the surface while having $\frac{V_{max}}{2}$ and $\frac{H_{x,max}}{2}$ applied	78
C.32 Failure mechanism for ultimate moment loading in the y direction on the longer edge while having $\frac{V_{max}}{2}$ and $\frac{H_{x,max}}{2}$ applied	78
C.33 Failure mechanism for ultimate moment loading in the y direction on the smaller edge while having $\frac{V_{max}}{2}$ and $\frac{H_{x,max}}{2}$ applied	78

C.34 Failure mechanism for ultimate moment loading in the y direction on the surface while having $\frac{V_{max}}{2}$ and $\frac{H_{x,max}}{2}$ applied	79
C.35 Failure mechanism for ultimate moment loading in the x direction on the longer edge while having $\frac{V_{max}}{2}$ and $\frac{H_{y,max}}{2}$ applied	79
C.36 Failure mechanism for ultimate moment loading in the x direction on the smaller edge while having $\frac{V_{max}}{2}$ and $\frac{H_{y,max}}{2}$ applied	79
C.37 Failure mechanism for ultimate moment loading in the x direction on the surface while having $\frac{V_{max}}{2}$ and $\frac{H_{y,max}}{2}$ applied	80
C.38 Failure mechanism for ultimate moment loading in the y direction on the longer edge while having $\frac{V_{max}}{2}$ and $\frac{H_{y,max}}{2}$ applied	80
C.39 Failure mechanism for ultimate moment loading in the y direction on the smaller edge while having $\frac{V_{max}}{2}$ and $\frac{H_{y,max}}{2}$ applied	80
C.40 Failure mechanism for ultimate moment loading in the y direction on the surface while having $\frac{V_{max}}{2}$ and $\frac{H_{y,max}}{2}$ applied	81
C.41 Ultimate horizontal loading in x direction	82
C.42 Ultimate horizontal loading in y direction	82
C.43 Ultimate moment loading in x direction	83
C.44 Ultimate moment loading in y direction	83
C.45 Ultimate horizontal loading in x direction having $V_{max}/2$ applied	84
C.46 Ultimate horizontal loading in y direction having $V_{max}/2$ applied	84
C.47 Ultimate moment loading in x direction having $V_{max}/2$ applied	85
C.48 Ultimate moment loading in y direction having $V_{max}/2$ applied	85
C.49 Ultimate moment loading in x direction having $V_{max}/2$ & $H_{x,max}/2$ applied	86
C.50 Ultimate moment loading in y direction having $V_{max}/2$ & $H_{x,max}/2$ applied	87
C.51 Ultimate moment loading in x direction having $V_{max}/2$ & $H_{y,max}/2$ applied	87
C.52 Ultimate moment loading in y direction having $V_{max}/2$ & $H_{y,max}/2$ applied	88
C.53 Ultimate torsional loading possible	89
C.54 Ultimate torsional loading possible	90
C.55 Failure mechanism for pure moment loading in the z direction on the longer edge	90
C.56 Failure mechanism for pure moment loading in the z direction on the smaller edge	91
C.57 Failure mechanism for pure moment loading in the z direction on the surface	91

C.58 Failure mechanism for ultimate moment loading in the z direction on the longer edge while having $\frac{V_{max}}{2}$ applied	91
C.59 Failure mechanism for ultimate moment loading in the z direction on the smaller edge while having $\frac{V_{max}}{2}$ applied	92
C.60 Failure mechanism for ultimate moment loading in the z direction on the surface while having $\frac{V_{max}}{2}$ applied	92

List of Tables

2.1	Shape Factors for Terzaghi method	15
2.2	Methods and their usage (Bowles et al., 1996)	18
2.3	Different meshing types by default of <i>PLAXIS 3D</i> for the model discussed in this thesis	23
3.1	Dimension for soil and foundation models	25
3.2	Plate assigned to mudmat foundation	25
3.3	Soil parameters considered for hand calculation and FE analysis	26
4.1	Presumptive bearing capacity values as per IS1904-1978	28
4.2	Shape factor for pure vertical loading & circular foundations	30
4.3	Different load combination considered in this thesis	34
5.1	Number of elements and nodes after meshing with different coarseness	36
6.1	Loads and used factors for normalising	40
B.1	Vertical and horizontal loading in <i>x</i> direction ratio	59
B.2	Vertical and horizontal loading in <i>y</i> direction ratio	59
B.3	Vertical and moment loading in <i>x</i> direction ratio	60
B.4	Vertical and moment loading in <i>y</i> direction ratio	61
B.5	Horizontal and moment loading in <i>x</i> direction ratio while the vertical loading is kept constant as half of its maximum	62
B.6	Horizontal load in the <i>x</i> direction and moment loading in <i>y</i> direction ratio while the vertical loading is kept constant as half of its maximum	63

B.7	Horizontal load in the y direction and moment loading in x direction ratio while the vertical loading is kept constant as half of its maximum	64
B.8	Horizontal and moment loading in y direction ratio while the vertical loading is kept constant as half of its maximum	65
C.1	Vertical and horizontal loading in x direction ratio	67
C.2	Vertical and horizontal loading in y direction ratio	67
C.3	Vertical and moment loading in x direction ratio	68
C.4	Vertical and moment loading in y direction ratio	68
C.5	Horizontal and moment loading in x direction ratio while the vertical loading is kept constant as half of its maximum	69
C.6	Horizontal and moment loading in y direction ratio while the vertical loading is kept constant as half of its maximum	69
C.7	Horizontal and moment loading in x direction ratio while the vertical loading is kept constant as half of its maximum	70
C.8	Horizontal and moment loading in y direction ratio while the vertical loading is kept constant as half of its maximum	70